Dynamic Aspects of Boiling-Heavy Water Nuclear Reactors. Part II

Kjær-Pedersen, N.

Publication date:
1966

Document Version
Publisher's PDF, also known as Version of record

Risö Report No. 129

Danish Atomic Energy Commission

Research Establishment Risö

Dynamic Aspects of Boiling-Heavy-Water Nuclear Reactors

Part II

by Niels Kjær-Pedersen

August, 1966

Sales distributors: Jul. Gjellerup, 87, Sölvgade, Copenhagen K, Denmark

Available on exchange from: Library, Danish Atomic Energy Commission, Risö, Roskilde, Denmark

August, 1966 Risö Report No. 129

Dynamic Aspects of Boiling-Heavy-Water Nuclear Reactors

Part II

by

Niels Kjær-Pedersen

The Danish Atomic Energy Commission
Research Establishment Risö
Reactor Physics Department

Abstract

This report contains a description and a discussion of the digital-computer code BRENDA, prepared for the Danish digital computer GIER.

This code is an attempt to simulate some of the major physical effects which determine the dynamic behaviour of a cooling channel of a boiling-heavy-water reactor.

Preface

The present report, together with Risö Report No. 128, constitutes a thesis aimed at fulfilling part of the requirements for obtaining the degree of lic. techn. in reactor physics at the Technical University of Denmark.

The studies have been carried out at the Danish Atomic Energy Commission Research Establishment Risö on a fellowship granted by the Technical University of Denmark.

My thanks are due to both institutions and are directed especially to Professor of Reactor Physics, Dr. O. Kofoed-Hansen, for his gentle inspiration and encouragement. I also want to thank P. L. Ølgaard, head of the Reactor Physics Department at Risö, who kindly allowed me to use the facilities of his department, especially the GIER digital computer. Several members of the staff of the department are gratefully borne in mind for the help they rendered through valuable discussions, especially Aksel Olsen, leader of the theoretical dynamics group.

The author

Contents

CHAPTER I

DESCRIPTION OF BRENDA

1. Introduction

The name BRENDA stands for Boiling Reactor Non-linear Dynamic Analysis.

The aim of the work invested in this programme has been to provide a means of studying large, space-dependent transients in a cooling channel of a boiling-heavy-water reactor.

Hence the feedback effects from neighbouring channels and from the circulation loop outside the core are not dealt with.

The input quantities necessary to define a transient run are the time variations of

(a) Coolant inlet velocity

(b) Coolant inlet temperature

(c) System pressure

(d) Spatial distribution of moderator temperature

(e) Control-rod position.

From the beginning of the development, strong emphasis has been laid on the term non-linear. Therefore, many simplifications ordinarily used in reactor dynamics have not been permissible here, which has contributed greatly to reducing the computing speed.

The geometry considered is cylindrical, the fuel element being assumed to be composed of a cluster of rods contained in a shroud through which the coolant is circulated. The outer boundary of the channel is a hypothetical cylinder shell obtained by arranging the amount of moderator available per element symmetrically around the shroud. At both ends of the element a layer of moderator is assumed to be present. To define a radial buckling for use in the neutron-flux calculations it is assumed that the reactor consists of a sufficient number of parallel channels to make up a cylinder of a certain radius.

The physical effects considered in the model are

(1) Neutron physics

(2) Heat transfer from fuel rods to coolant

(3) Hydraulics of the coolant.

The calculations are performed by intensive use of the iteration technique in accordance with the scheme presented in fig. 1. Here reference is made to the above three categories, and the sequence of the calculations is shown by arrows. It appears that two main iteration loops are established: the inner one, coupling hydraulic and heat-transfer calculations, and the outer one, coupling the neutron-physics calculations to the inner iteration loop. Convergence criteria are built in at the marked positions in the two loops.

The code always starts with a steady-state calculation and goes on immediately with the transient description, taking in current information on outer-loop conditions and control-rod positions at the beginning of each time step.

In the following the different parts of the code will be described separately.

2. Neutron Physics

The neutron-flux calculations are based on the method developed by Nahavandi and von Hollen[1]. This method requires the derivation of two-group diffusion parameters for the lattice structure considered. This is done in accordance with the recipe for treating low-enrichment, uranium-fuelled, heavy-water-moderated cylindrical lattices developed at Risö[2] and represented by the digital-computer code TATAR[3]. A detailed description of this calculational method is given in appendix 1. Below, a description of the flux calculational method is given. On certain points it will appear to differ from that of ref. 1.

a. Mathemetical formulation of the theory

The basis of the theory is the neutron-balance diagram shown in fig. 2.

The scheme leads to the following three equations for the fast and thermal fluxes and the concentrations of delayed neutron precursors:

$$D_1 \nabla^2 \phi_1 - \Sigma_{r1} \phi_1 + (1-\beta)\varepsilon\nu \Sigma_f \phi + \sum_i \lambda_i C_i = \frac{1}{v_1} \frac{\partial \phi_1}{\partial t} \qquad (1)$$

$$D \nabla^2 \phi - \Sigma_a \phi + p \Sigma_{r1} \phi_1 = \frac{1}{v} \frac{\partial \phi}{\partial t} \qquad (2)$$

$$-\lambda_i C_i + \beta_i \varepsilon \nu \Sigma_f \phi = \frac{\partial C_i}{\partial t} \quad . \tag{3}$$

Here ϕ_1 and ϕ are the fast and the thermal flux respectively, D_1 and D fast and thermal diffusion constants respectively, Σ_{r1} the slowing-down cross section of the fast group, Σ_a and Σ_f the absorption and fission cross sections of the thermal group, ε the fast-fission factor, p the resonance escape probability, ν the number of neutrons released per fission, and β_i, λ_i and C_i the relative occurrence, decay constant and concentration of the i'th delayed-neutron precursor.

Elimination of ϕ_1 between eqs. (1) and (2) yields

$$D \nabla^2 \phi - \Sigma_a \phi + p(1-\beta) \varepsilon \nu \Sigma_f \phi + p D_1 \nabla^2 \left(\frac{\Sigma_a \phi}{p \Sigma_{r1}}\right) + p \sum_i \lambda_i C_i$$

$$= \frac{1}{v} \frac{\partial \phi}{\partial t} + p D_1 \nabla^2 \left(\frac{D}{p \Sigma_{r1}} \nabla^2 \phi\right) + \frac{p}{v_1} \frac{\partial}{\partial t} \left\{ \frac{1}{p \Sigma_{r1}} \left(\frac{1}{v} \frac{\partial \phi}{\partial t} + \Sigma_a \phi - D \nabla^2 \phi\right) \right\}$$

$$- p D_1 \nabla^2 \left\{ \frac{1}{p \Sigma_{r1}} \left(\frac{1}{v} \frac{\partial \phi}{\partial t} \right) \right\} \quad . \tag{4}$$

Neglecting of the three last terms on the right-hand side of eq. (4) leads to

$$D \nabla^2 \phi - \Sigma_a \phi + p(1-\beta) \varepsilon \nu \Sigma_f \phi + p D_1 \nabla^2 \left(\frac{\Sigma_a \phi}{p \Sigma_{r1}}\right) + p \sum_i \lambda_i C_i = \frac{1}{v} \frac{\partial \phi}{\partial t} \quad . \tag{5}$$

The approximation contained in eq. (5) is valid under the following assumptions:

(1) The order of magnitude of $\nabla^2 \phi$ is equal to $B^2 \phi$, where B is the geometrical buckling.

(2) The fast-neutron speed v_1 is much higher than the thermal-neutron speed v.

(3) The 4th-order operator $\nabla^4 \phi$ is negligible.

It is noticed that these assumptions can always be controlled after a machine calculation of $\emptyset$ has been carried out.

Eq. (5) can be modified to a well-known expression if it is assumed that Σ_a, p and Σ_{r1} are not space-dependent:

$$D \nabla^2 \emptyset - \Sigma_a \emptyset + p(1-\beta) \varepsilon \nu \Sigma_f \emptyset + D_1 \frac{\Sigma_a}{\Sigma_{r1}} \nabla^2 \emptyset + p \sum_i \lambda_i C_i = \frac{1}{v} \frac{\partial \emptyset}{\partial t}$$

$$D(1+ \frac{\tau}{L^2}) \nabla^2 \emptyset - \Sigma_a \emptyset + p(1-\beta) \varepsilon \nu \Sigma_f \emptyset + p \sum_i \lambda_i C_i = \frac{1}{v} \frac{\partial \emptyset}{\partial t} \quad . \qquad (5)^x$$

Eq. $(5)^x$ is the equation resulting from an ordinary one-group treatment where the fast-neutron leakage is accounted for by the addition of the Fermi age τ to the thermal diffusion length squared, L^2.

Thus the advantage of (5) compared with $(5)^x$ is a more exact representation of the fast-neutron leakage obtained by considering the spatial variation of the group constants p, Σ_a and Σ_{r1}.

So far the development has paid no regard to boundary conditions, i. e. reflected or bare reactor. In a practical case, appropriate boundary conditions must be chosen. In the present work it is assumed that the thermal flux goes to zero at some extrapolated boundary which must be precalculated and is kept fixed throughout the transient calculations.

The radial finiteness of the reactor is taken into account by increasing the thermal absorption cross section Σ_a by a factor of $1+B^2(L^2+\tau)$, where $B = 2.405/R$, $L^2 = D/\Sigma_a$, and $\tau = D_1/\Sigma_{r1}$, R being the extrapolated radius of the core.

b. Numerical treatment of the steady-state case

Elimination of the term $\sum_i \lambda_i C_i$ from eq. (5) by means of eq. (3) yields for the steady state

$$D \nabla^2 \emptyset - \Sigma_a \emptyset + p(\varepsilon \nu \Sigma_f \emptyset + D_1 \nabla^2 (\frac{\Sigma_a \emptyset}{p \Sigma_{r1}})) = 0 \quad . \qquad (6)$$

This equation is expressed by finite differences, the axial step length dx being introduced:

$$\frac{D_j}{dx^2}\left\{ \phi_{j+1} - 2\phi_j + \phi_{j-1}\right\} - \Sigma_{aj}\,\phi_j$$

$$+ p_j\left\{ \nu\Sigma_{fj}\,\varepsilon_j\phi_j + \frac{D_{1j}}{dx^2}\left(\frac{\Sigma_{a(j+1)}}{p_{j+1}\,\Sigma_{r1(j+1)}}\phi_{j+1} - 2\frac{\Sigma_{aj}}{p_j\,\Sigma_{r1j}}\right)\phi_j\right.$$

$$\left. + \frac{\Sigma_{a(j-1)}}{p_{j-1}\,\Sigma_{r1(j-1)}}\phi_{j-1}\right)\Big\} = 0, \qquad 2 \le j \le n-1 \tag{7}$$

where n is the number of mesh points along the axis.

The n-2 equations (7) together with two boundary equations constitute n linear equations for the determination of the axial flux distribution.

The boundary equations which indicate that the flux is zero at either extrapolated boundary are

$$-\left(\frac{3}{2dx} + \frac{1}{H_1}\right)\phi_1 + \frac{2}{dx}\phi_2 - \frac{1}{2dx}\phi_3 = 0 \tag{8}$$

$$\frac{1}{2dx}\phi_{n-2} - \frac{2}{dx}\phi_{n-1} + \left(\frac{3}{2dx} + \frac{1}{H_n}\right)\phi_n = 0. \tag{9}$$

Here H_1 and H_n are the lower and the upper extrapolation length respectively. The equations express a parabolic extrapolation.

As (7), (8) and (9) constitute a homogeneous system of linear equations, the condition for the existence of a non-trivial solution is that the determinant is zero, or, physically, that the reactor is critical.

Guided by physical intuition, we make an attempt to fulfil this condition by adjusting the physical parameters through an iterative process based on the concept of an eigenvalue, μ .

The latter is defined as the ratio between the actual value of ν and the hypothetical value which would secure criticality. Thus

$$\mu_{crit} = \frac{\nu}{\nu_{crit}} \,. \tag{10}$$

Eq. (7) is rearranged:

$$\phi_j = \left\{ \frac{\nu\Sigma_{fj}}{\mu} \epsilon_j p_j \phi_j^o + \left(\frac{D_j}{dx^2} + p_j \frac{D_{1j}}{dx^2} \frac{\Sigma_{a(j+1)}}{p_{j+1} \Sigma_{r1(j+1)}} \right) \phi_{j+1} \right. \tag{11}$$

$$\left. + \left(\frac{D_j}{dx^2} + p_j \frac{D_{1j}}{dx^2} \frac{\Sigma_{a(j-1)}}{p_{j-1} \Sigma_{r1(j-1)}} \right) \phi_{j-1} \right\} / \left(2\frac{D_j}{dx^2} + \Sigma_{aj} + 2p_j \frac{D_{1j}}{dx^2} \frac{\Sigma_{aj}}{p_j \Sigma_{r1j}} \right) .$$

The first term in the numerator on the right-hand side of (11) is called the source term.

The iteration process is started with an initial guess of ϕ_j^o. On the basis of this function we calculate the corresponding source function, putting $\mu = \mu^o = 1$. By means of eq. (11) we calculate a new function ϕ_j, putting $\phi_j = \phi_j^o$ on the right-hand side. Without changing the source function, we recalculate ϕ_j on the basis of the preceding ϕ_j-function until convergence. This procedure is called the inner iteration loop.

Now an attempt is made to choose an eigenvalue μ such that the integrated source function, calculated with this μ and the most recent ϕ_j function, is nearly unaltered (picturing the physical condition of criticality).

This trial value is selected as

$$\mu = \mu^o \frac{\sum_j \epsilon_j \nu\Sigma_{fj} p_j \phi_j^o}{\sum_j \epsilon_j \nu\Sigma_{fj} p_j \phi_j} . \tag{12}$$

Next, the new source function is calculated and an inner iteration performed. Then a new estimate of μ is made according to (12), and so on until μ has converged. This procedure is called the outer iteration loop.

As the eigenvalue μ is a purely mathematical tool, it is desirable to introduce a physical control in the form of a thermal absorption cross section in order to adjust μ_{crit} to unity.

This is achieved by introducing a function Σ_{cj} which contributes a control cross section to each core element. A multiplier c is determined so that the absorption function $\Sigma'_{aj} = \Sigma_{aj} + c \times \Sigma_{cj}$ yields a critical reactor with $\mu = 1$. The multiplier c is determined by an iterative process:

When criticality is obtained by putting $c = c'$, the next guess of a better c is made by putting

$$(c-c') \sum_j \Sigma_{cj} \phi_j^2 = \frac{\mu-1}{\mu} \sum_j (\Sigma_{aj} \phi_j^2 + c' \Sigma_{cj} \phi_j^2) \quad . \tag{13}$$

In this way the statistical weight of the different core elements is utilized in order to accelerate the convergence. This procedure is called the control iteration loop.

The resulting values of c and μ are conserved throughout the transient calculations.

A pure reactivity change can now be introduced by adding a small quantity to c, corresponding to a movement of the control-rod system.

It is noticed that through specification of the function Σ_{cj} any axial distribution of the control cross section can be achieved. However, extreme variations should be avoided because they would cause the conditions for the modified two-group treatment to be violated (for instance the ∇^4-operator may become important, see subsection (a)).

Finally the concentration function of the steady-state precursors can be calculated from eq. (3):

$$C_{ij} = \frac{\beta_i}{\lambda_i} \epsilon_j \frac{\nu}{\mu} \Sigma_{fj} \phi_j \quad . \tag{14}$$

So far the treatment has been concerned with an arbitrary number of delayed-neutron groups. However, the programme works with only one lumped group in order to simplify the transient calculations.

c. Numerical treatment of the transient case

The transient flux variation is also treated by means of a finite difference method.

The first decision to be made in this connection is whether forward or backward time steps should be used. Forward time steps lead to simple expressions which can be directly solved without any reduction of the system of equations. Backward time steps, however, provide a much more stable system from a numerical point of view. For this reason backward time steps were chosen although the system of equations is a little more complicated, being of the Clapeyron type.

Thus eqs. (5) and (3) lead to

$$\phi_j^n - \phi_j^{n-1} = A_o\ \phi_{j+1}^n + B_o\ \phi_j^n + C_o\ \phi_{j-1}^n + D_o\ C_j^n \qquad (15)$$

$$C_j^n - C_j^{n-1} = B_1\ \phi_j^n + D_1\ C_j^n\ , \qquad (16)$$

where

$$\left.\begin{aligned} A_o &= \frac{vdt}{dx^2}\left(D_j + p_j D_{1j}\ \frac{\Sigma_{a(j+1)}}{p_{j+1}\ \Sigma_{r1(j+1)}}\right) \\ B_o &= \frac{vdt}{dx^2}\left(2\left(D_j + D_{1j}\ \frac{\Sigma_{aj}}{\Sigma_{r1j}}\right) + dx^2\left(\Sigma_{aj} - p_j\ \epsilon_j \nu (1-\beta)\Sigma_{fj}\right)\right) \\ C_o &= \frac{vdt}{dx^2}\left(D_j + p_j D_{1j}\ \frac{\Sigma_{a(j-1)}}{p_{j-1}\ \Sigma_{r1(j-1)}}\right) \\ D_o &= p_j\ \lambda\ vdt \\ B_1 &= \beta\ \ \epsilon_j\ \ \nu \Sigma_{fj}\ dt \\ D_1 &= -\lambda\ dt\ . \end{aligned}\right\} \qquad (17)$$

Here the index n refers to the time mesh points, while dt denotes the size of the time step.

Note: in this treatment ν and Σ_{aj} should be interpreted as $\frac{\nu}{\mu}$ and $\Sigma_{aj} + c\ \Sigma_{cj}$ respectively, in accordance with section 3.

Elimination of C_j^n between (15) and (16) yields

$$A_o(D_1-1)\phi_{j+1}^n + ((B_o-1)(D_1-1) - D_o B_1)\phi_j^n + C_o(D_1-1)\phi_{j-1}^n = D_o C_j^{n-1} - (D_1-1)\phi_j^{n-1}$$

$$2 \leq j \leq n-1\ . \qquad (18)$$

Together with the boundary equations, which are quite similar to (8) and (9), eq. (18) constitutes a system of linear equations for the determination of $\emptyset_j^n$.

By two very simple row operations (first and last row) this system is transformed into one of the Clapeyron type, i.e. one in which the coefficient matrix is a band matrix with three terms in each row grouped around the diagonal. Such a system is quickly reduced by applying one row operation to each row except the first, beginning with the second row. The reduced system is immediately solved, beginning at the bottom of the diagonal.

When the $\emptyset^n$ function has been determined, the C_j^n function is readily obtained from eq. (16).

To save computing time, the physical parameters, which are in principle functions of flux through temperature mechanisms, are only recalculated at certain points on the time axis, marking so-called macrosteps. At these points new information about the different temperatures and densities of the reactor is taken in through the data input. Each macrostep is divided into a number of microsteps to secure a sufficiently accurate calculation of the flux variation. While the size of the macrostep is fixed by the user, the microstep size is determined automatically by the code in the following way:

Starting from the steady-state situation, a step size equal to a macrostep is chosen and a flux calculation performed. Afterwards two successive flux calculations corresponding to half a macrostep are performed and the result compared with that of the one-step calculation. If the divergence is greater than a prescribed error, the step size is halved once more, and so on until the error criterion is fulfilled. Then the smallest but one step size applied is accepted for a successive run throughout the macrostep. Thus each trial takes three flux calculations, which is a waste of time. However, as the number of microsteps in the final run increases as 2^{sub}, where sub denotes the number of subdivisions, the search time is smaller than the total effective computing time per macrostep when sub is greater than 3. Otherwise the sum of the total effective computing time and the search time will appear to be small compared with the time it takes to compute the physical parameters at the beginning of the macrostep.

Starting on a new macrostep, we choose the initial value of sub as one lower than the accepted value from the preceding macrostep to provide a chance to save time in case the flux variations become smoother. Also the mean search time should be shorter than that of the first macrostep.

d. Calculational pattern

The pattern according to which the calculations are effected depends on three error quantities named errorphi, errormy and erfeul.

In the steady-state calculations errorphi and errormy express the permissible relative errors in flux and eigenvalue (see subsection (b)) respectively. However, in some cases the iterations are not carried through to full accuracy, namely in the (frequent) cases where the iteration loop considered constitutes a part of an exterior iteration loop which at that stage of the calculations is far from convergence. Actually the rules followed by the code are:

The control iteration loop is broken after one circulation more than that which gives an eigenvalue diverging less than 1 per cent from unity.

The outer iteration loop is carried through to full accuracy only in the last circulation in the control iteration loop. In the last but one circulation an error of 100 x errormy is permitted, in the others one of 0.001.

The inner iteration loop is carried through to full accuracy only in the last circulation in the control iteration loop and only if the eigenvalue is nearer to convergence than 10 x errormy. Otherwise an error of 0.0001 times the flux at the centre of the reactor is permitted.

The error in flux is calculated as the root mean square of the deviations in the axial mesh points corresponding to two successive flux calculations.

During the transient calculations the quantity erfeul is decisive for both accuracy and computing time.

A microscopic step length is accepted if the difference between the flux distribution calculated by taking a step of this size and the corresponding flux distribution calculated by taking two successive steps of half the size (in both cases starting from the beginning of a macrostep) is less than erfeul. In this case the flux deviation is calculated simply as the numerical value of the mean deviation in the axial mesh points.

e. Manual control during operation

During the steady-state calculations the convergence of the different iteration loops may be followed by setting kbon. Then all values of the eigenvalue μ and the control parameter c will be printed out by the typewriter.

During the transient calculations the automatic step-size mechanism may be controlled or replaced by a manual control by means of the KB button.

The effect of kbon will always be the printing of a message to the operator, followed by a stop of the calculations. The calculations proceed when the operator has made a choice according to the message. The diagram in fig. 3 shows the details of this control system.

If a fixed value of sub has been chosen in accordance with message C, the automatic control of the step size still functions from the next macrostep. Only if the automatic stepsize control has been abandoned through messages A and B will the fixed value of sub be retained through the following macrosteps, i.e. until the automatic control has been re-established through messages A and B or the fixed value is altered through message C.

3. Heat Transfer from Fuel Rods to Coolant

The heat transfer from the cluster of fuel rods to the coolant is calculated by considering the heat transfer from a single fuel rod to a proper amount of coolant assigned to it by equal distribution of all the coolant in the shroud among the rods of the cluster.

Here the assumption is made that all the rods behave in exactly the same manner independently of each other.

a. Mathematical formulation of the physical situation

The geometry considered is a single, cylindrical fuel rod contained in a cladding tube and surrounded by a certain amount of coolant, forming a cylinder shell.

The following assumptions are made:

(1) The power-production density P within the fuel rod is uniform.

(2) There is no heat conduction along the fuel-rod axis.

(3) There is no heat transport through the outer surface of the coolant shell assigned to the fuel rod.

The heat-balance equations for the fuel and cladding regions respectively may be written

$$\varrho_u c_u \frac{\partial T_u}{\partial t}(r,t) = P(t) + \frac{1}{r}\frac{\partial}{\partial r}\left\{ r \varkappa_u \frac{\partial T_u}{\partial r}(r,t)\right\} \qquad (1)$$

$$\varrho_c c_c \frac{\partial T_c}{\partial t}(r,t) = \frac{\varkappa_c}{r} \frac{\partial}{\partial r}\left\{ r \frac{\partial T_c}{\partial r}(r,t)\right\} \quad , \tag{2}$$

where ϱ denotes the density, c the specific heat, T the temperature, t the time, r the radial co-ordinate, and $\varkappa$ the heat conductivity, while index u refers to the fuel, c to the cladding.

The equations for the gap between fuel and cladding are

$$r_a \varkappa_u \frac{\partial T_u}{\partial r}(r_a,t) = r_b \varkappa_c \frac{\partial T_c}{\partial r}(r_b,t) \tag{3}$$

$$- \varkappa_u \frac{\partial T_u}{\partial r}(r_a,t) = \frac{1}{\eta}\left\{ T_u(r_a,t) - T_c(r_b,t)\right\} \quad , \tag{4}$$

where r_a and r_b are the fuel-rod radius and the inner radius of the cladding respectively, while η is the thermal resistance of the gap.

The boundary condition of the centre of the rod is

$$\frac{\partial T_u}{\partial r}(0,t) = 0 \quad . \tag{5}$$

At the boundary between cladding and fuel the following equation is valid:

$$T_c(r_c,t) - T \text{ coolant} = \sqrt[4]{\frac{qh}{khl}} \quad , \tag{6}$$

where r_c is the outer radius of the cladding tube and qh the heat flux through the cladding surface. khl is considered to be a constant.

On the assumption that the heat transferred to the coolant is uniformly distributed (through turbulence) and on assumption (3) above, the following relation exists between qh, which has the dimension of energy per unit area per unit time, and a quantity Q, the heat inflow into the coolant, having the dimension of energy per unit volume per unit time:

$$qh = Q \frac{r_{ch}^2 - r_c^2}{2r_c} \quad , \tag{7}$$

where r_{ch} is the outer radius of the coolant shell.

Further qh is given by the expression

$$qh = - \varkappa_c \frac{\partial T_c}{\partial r} (r_c, t) . \tag{8}$$

b. Numerical technique

We replace eqs. (1) - (5) and (8) by finite difference representations, using backward time steps for stability reasons(cf. section 4 of this chapter) and a parabolic approximation for the spatial derivatives.

The thermal conductivity of the fuel, $\varkappa_u$, is regarded as temperature dependent, while all other physical characteristics concerning the heat conduction are regarded as constants.

If we assign numbers from 1 to p to the radial mesh points from the centre to the surface of the rod and numbers from p + 1 to p + q to the mesh points from the inner to the outer surface of the cladding and denote the running index of the time steps by n, eqs. (1) - (5) and (8) become

Eq. (1):

$$\frac{y_j^n - y_j^{n-1}}{dt} - \frac{1}{\varrho_u c_u dr^2} \left\{ \frac{j-\frac{1}{2}}{j-1} \varkappa_{u,j} y_{j+1}^n - \frac{(j-\frac{1}{2}) \varkappa_{u,j} + (j-\frac{3}{2}) \varkappa_{u,j-1}}{j-1} y_j^n \right. \tag{9}$$

$$\left. + \frac{j-\frac{3}{2}}{j-1} \varkappa_{u,j-1} y_{j-1}^n \right\} = \frac{P^n}{\varrho_u c_u} , \quad j = 2, 3, \ldots , p-1 ;$$

Eq. (2):

$$\frac{y_j^n - y_j^{n-1}}{dt} - \frac{\varkappa_c}{\varrho_c c_c drc^2} \left\{ \frac{\frac{r_b}{drc} + j - p - \frac{3}{2}}{\frac{r_b}{drc} + j - p - 2} y_{j+1}^n - 2y_j^n \right. \tag{10}$$

$$\left. + \frac{\frac{r_b}{drc} + j - p - \frac{5}{2}}{\frac{r_b}{drc} + j - p - 2} y_{j-1}^n \right\} = 0, j = p+2, \ldots , p+q-1 ;$$

(this equation vanishes for q = 0, 1, 2)

Eq. (3):

$$\frac{p-2}{p-1}\,\frac{\varkappa_{u,p-1}}{2dr}\,y^n_{p-2} - \frac{p-\frac{3}{2}}{p-1}\,\frac{\varrho_u c_u\,dr}{2dt}\,y^n_{p-1}$$

$$-\left\{\frac{p-\frac{3}{2}}{p-1}\,\frac{\varrho_u c_u\,dr}{2dt} + \frac{p-2}{p-1}\,\frac{\varkappa_{u,p-1}}{2dr}\right\} y^n_p$$

$$-\left\{\frac{\frac{r_b}{drc}+\frac{1}{2}}{\frac{r_a}{drc}}\,\frac{\varrho_c c_c}{2dt} + \frac{\frac{r_b}{drc}+1}{\frac{r_a}{drc}}\,\frac{\varkappa_c}{2drc}\right\} y^n_{p+1}$$

$$-\frac{\frac{r_b}{drc}+\frac{1}{2}}{\frac{r_a}{drc}}\,\frac{\varrho_c c_c\,drc}{2dt}\,y^n_{p+2} + \frac{\frac{r_b}{drc}+1}{\frac{r_a}{drc}}\,\frac{\varkappa_c}{2drc}\,y^n_{p+3} \qquad (11)$$

$$= -\frac{p-\frac{3}{2}}{p-1}\,dr\left\{P + \frac{\varrho_u c_u}{2dt}\,(y^{n-1}_p + y^{n-1}_{p-1})\right\}$$

$$+\frac{\frac{r_b}{drc}+\frac{1}{2}}{\frac{r_a}{drc}}\,\frac{\varrho_c c_c\,drc}{2dt}\,(y^{n-1}_{p+1} + y^{n-1}_{p+2}) \quad ;$$

(this equation vanishes for q = 0, 1, while for q = 2

$$\frac{3}{2dr}\,y^n_p - \frac{2}{dr}\,y^n_{p-1} + \frac{1}{2dr}\,y^n_{p-2} = \frac{\varkappa_c}{\varkappa_{u,p}}\,\frac{r_b+r_c}{2r_a}\left\{\frac{1}{drc}\,y^n_{p+2} - \frac{1}{drc}\,y^n_{p+1}\right\}); \qquad (11)^x$$

Eq. (4):

$$\frac{3}{2dr}\,y^n_p - \frac{2}{dr}\,y^n_{p-1} + \frac{1}{2dr}\,y^n_{p-2} = -\frac{1}{\eta\varkappa_{u,p}}\,(y^n_p - y^n_{p+1}) \quad ; \qquad (12)$$

(this equation vanishes for q = 0)

Eq. (5):

$$\frac{3}{4dr}\, y_1^n - \frac{1}{dr}\, y_2^n + \frac{1}{4dr}\, y_3^n = 0 \quad ; \tag{13}$$

Eq. (8):

$$qh = - \frac{\frac{r_c}{drc} - \frac{1}{2}}{\frac{r_a}{drc}} \quad \frac{\varrho_c\, c_c\, drc}{2dt} \left(y^n_{p+q} - y^n_{p+q-1} - y^{n-1}_{p+q} - y^{n-1}_{p+q-1}\right)$$

$$- \frac{\frac{r_c}{drc} - 1}{\frac{r_a}{drc}} \quad \frac{\varkappa_c}{2drc} \left(y^n_{p+q} - y^n_{p+q-2}\right) \quad ; \tag{14}$$

(for $q < 3$ this equation is modified to

$$qh = - \frac{r_a}{r_c} \left\{ \frac{p - \frac{3}{2}}{p - 1} \quad \frac{\varrho_u c_u dr}{2dt} \left(y^n_p + y^n_{p-1} - y^{n-1}_p - y^{n-1}_{p-1}\right) \right.$$

$$\left. - \frac{p - \frac{3}{2}}{p-1}\, dr\, P + \frac{p-2}{p-1} \quad \frac{\varkappa_{u,p-1}}{2dr} \left(y^n_p - y^n_{p-2}\right) \right\} \Big) \; . \tag{14}^x$$

By means of a few very simple row operations the system of linear equations constituted by eqs. (9) - (14) together with eqs. (6) and (7) is transformed into a system of the Clapeyron type. This system is immediately reduced and solved as indicated in subsection 2.c of this chapter.

4. Hydraulics

The treatment of the hydraulic effects in the channel pays regard to bulk boiling only and not to subcooled boiling.

The water is supposed to enter the channel at the bottom, from which the space variable x is measured positive upwards. The inlet temperature is kr own. As the water receives heat from the fuel rods, the

temperature increases and at a certain level, the boiling boundary, exceeds that of saturated steam at the pressure given. From this point the temperature follows that of saturated steam, while the void, i.e. the volume fraction occupied by saturated steam, begins to develop. In special cases the boiling zone may be split up into several minor zones. These cases are also handled by the programme, though with reduced accuracy.

a. Development of the mathematical model

Two major equations for the description of the system can be established:

(1) The mass flow balance.

(2) The enthalpy balance.

Re (1). The equation is

$$\frac{\delta}{\delta x}\left\{M_s(x,t)v_s(x,t)+M_w(x,t)v_w(x,t)\right\}+\frac{\delta}{\delta t}\left\{M_s(x,t)+M_w(x,t)\right\}=0\,. \tag{1}$$

Here M_s and M_w are the total masses of steam and water respectively in a certain volume Vt, while v_s and v_w are the steam and water velocities measured positive upwards.

This equation is exact and requires no further comments.

Re (2). The equation is

$$\frac{\delta}{\delta x}\left\{M_s(x,t)v_s(x,t)h_s(x,t)+M_w(x,t)v_w(x,t)h_w(x,t)\right\} + \frac{\delta}{\delta t}\left\{M_s(x,t)h_s(x,t)+M_w(x,t)h_w(x,t)\right\}=Q(x,t)\,. \tag{2}$$

Here h_s and h_w are the enthalpy per unit mass of steam and water respectively, while Q is the heat inflow into the volume Vt. Q has the dimension of energy per unit time.

The conditions for this relation are

(a) $vdp \sim 0$: $dQ \sim dh$.

(b) The steam, if any, is saturated.

Eqs. (1) and (2) can be combined to give

$$\frac{\partial}{\partial x}\left\{M_s v_s\right\}(h_s-h_w)+\frac{\partial}{\partial t}M_s(h_s-h_w)+\frac{\partial h_w}{\partial x}M_w v_w+\frac{\partial h_w}{\partial t}M_w=Q, \tag{3}^1$$

the quantities $\frac{\partial h_s}{\partial t}$ and $\frac{\partial h_s}{\partial x}$ being supposed to be negligible.

Upon the substitutions

$$M_s=a\cdot\varrho_s\cdot V_t,\quad M_w=(1-a)\varrho_w\cdot V_t,\quad Q=q\cdot V_t,$$

where a denotes the void fraction, ϱ_s and ϱ_w the densities of steam and water respectively, and q the specific heat inflow, which has the dimension of energy per unit time per unit volume, $(3)^1$ is reduced to

$$\frac{\partial}{\partial x}\left\{a\varrho_s v_s\right\}(h_s-h_w)+\frac{\partial}{\partial t}\left\{a\varrho_s\right\}(h_s-h_w)$$

$$+\frac{\partial h_w}{\partial x}(1-a)\varrho_w v_w+\frac{\partial h_w}{\partial t}(1-a)\varrho_w=q;$$

$$\frac{\partial a}{\partial t}+\frac{\partial}{\partial x}\left\{a v_s\right\}=-\frac{(1-a)\varrho_w}{(h_s-h_w)\varrho_s}\left(\frac{\partial h_w}{\partial t}+v_w\frac{\partial h_w}{\partial x}\right)+\frac{q}{(h_s-h_w)\varrho_s};$$

Further, with $h_s - h_w = r(x,t)$ and $\partial h_w = c(T)\ \partial T$, where r is obviously the vaporization enthalpy, c the specific heat of water and T the absolute temperature of the water, we have

$$\frac{\partial a}{\partial t}+\frac{\partial}{\partial x}\left\{a v_s\right\}=-\frac{(1-a)\varrho_w\cdot c}{r\cdot\varrho_s}\left(\frac{\partial T}{\partial t}+v_w\frac{\partial T}{\partial x}\right)+\frac{q}{r\cdot\varrho_s}. \tag{3}$$

It should be noted that the equation $\partial h_w = c(T)\ \partial T$ implies the condition that the heat exchange develops in a quasistatic manner.

Eq. (3) is true over the whole length of the channel; therefore, by putting $a = 0$, the equation

$$\frac{\partial T}{\partial t}+v_w\frac{\partial T}{\partial x}=\frac{q}{c\cdot\varrho_w} \tag{4}$$

for the determination of the temperature distribution in regions without steam formation is immediately derived.

Eqs. (3) and (4), with appropriate boundary conditions, constitute the basis of the calculations.

In the boiling region another temperature equation is necessary, namely the relationship between the temperature and pressure of saturated steam.

The quantities c, r, ϱ_s, and ϱ_w are considered to be functions of temperature/pressure.

The pressure variation in the channel is calculated simply by means of the gravitation law, no regard being paid to steam voids.

The water velocity $v_w(x)$ is calculated from the inlet value, which is specified through the data input, by paying regard to the water supersession caused by the steam and by taking the slip ratio, s, defined as the ratio v_s/v_w, equal to a constant.

Thus we write the equation

$$v_w(x) = v_{inlet}/(1-a(1-s\,\frac{\varrho_s}{\varrho_w}))\,, \qquad (5)$$

the approximate validity of which is readily verified.

The slip ratio is put equal to 2.

The direct introduction of the above velocity representation into the coefficients of eq. (3) can be shown, from a mathematical argumentation, to spoil the convergence of the iterative method described in subsection b. Hence eqs. (3) and (5) are combined to give

$$\frac{\partial}{\partial t}(\frac{z}{v_s}) + \frac{\partial}{\partial x}(z) = -\frac{(1-\frac{z}{v_s})\,\varrho_w \cdot c}{r \cdot \varrho_s}\,(\frac{\partial T}{\partial t} + v_w\,\frac{\partial T}{\partial x}) + \frac{q}{r \cdot \varrho_s}\,, \qquad (6)$$

with

$$v_s = v_{inlet}\,s + (1-s\,\frac{\varrho_s}{\varrho_w})z\;; \qquad z = a \cdot v_s\;;$$

In this way the numerical technique of subsection b is usuable without convergence problems. This has not been proved theoretically, but has been shown by computer experiments.

b. The integration technique

The differential equations (6) and (4) are both of the general form

$$\frac{\partial}{\partial t}\{ay\} + g\frac{\partial}{\partial x}\{by\} = f \quad , \tag{7}$$

where the coefficients a, b, g, and f can be thought of as functions of x, t and y.

An integration technique has been constructed which seems to honour the requirements of the present application. This technique is based on an iterative method: where y occurs in the functions a, b, g, and f, it is put equal to the appropriate value from the preceding iteration. Of course this implies bonds on the permissible form of the functions a, b, g, and f due to the absolute requirement that the iteration must converge. These bonds have not been investigated in general.

(7) can be written as a difference equation in the following way:

$$\frac{a_j^n y_j^n + a_{j-1}^n y_{j-1}^n}{2\,dt} - \frac{a_j^{n-1} y_j^{n-1} + a_{j-1}^{n-1} y_{j-1}^{n-1}}{2\,dt} + gm\frac{b_j^n y_j^n - b_{j-1}^n y_{j-1}^n}{dx} = fm. \tag{8}$$

Here j and n refer to mesh points in the x and t directions respectively; gm and fm are values of g and f referring to the point halfway between the x mesh points j and j-1 and the t mesh point n.

It is seen that a backward difference is used in the t-direction, while a parabolic approximation is used in the x-direction. This choice was necessitated by stability considerations, cf. subsection c.

Eq. (8) is transformed by the substitutions

$$y_j^n - y_j^{n-1} = \Delta_j \,, \quad y_{j-1}^n - y_{j-1}^{n-1} = \Delta_{j-1} \,,$$

$$a_{j-1}^n/2dt - gm \cdot b_{j-1}^n/dx = c_m \,, \quad a_j^n/2dt + gm \cdot b_j^n/dx = c_p \quad ,$$

giving

$$\Delta_j = fm/c_p - \Delta_{j-1}\, c_m/c_p - (y_j^{n-1} - y_{j-1}^{n-1})\, b_j^n\, gm/dx \cdot c_p$$

$$- y_{j-1}^{n-1} (b_j^n - b_{j-1}^n)\, gm/dx \cdot c_p - y_j^{n-1} (a_j^n - a_j^{n-1})/2\,dt \cdot c_p$$

$$- y_{j-1}^{n-1} (a_{j-1}^n - a_{j-1}^{n-1})/2\,dt \cdot c_p \quad . \tag{9}$$

Eq. (9) is a recursion formula which gives the value of Δ_j when the value of Δ_{j-1}, y_{j-1}^{n-1}, y_j^{n-1} and the system parameters are known; in other words, y_j^n is given when y_{j-1}^n, y_{j-1}^{n-1}, y_j^{n-1} and the system parameters are known.

The reason for choosing the special form of (9) is that by espressing the small increment Δ_j in terms of a sum of other small increments we reduce the influence of rounding-off errors.

c. Numerical stability of the difference equation

If in eq. (8) an arbitrary function δy is added to the correct solution y, the resulting function $y1 = y + \delta y$ will represent a false solution to the difference equation if δy is a solution to the homogeneous equation developing from (8) when the right-hand side is put equal to zero.

The condition for numerical stability is that such false solutions, once introduced, should be damped out after a few time steps, that is, the homogeneous difference equation should be "self-quenching".

For simplicity the investigation is carried out for a system with constant a's and b's:

$$\frac{y_j^n + y_{j-1}^n}{2\,dt} - \frac{y_j^{n-1} + y_{j-1}^{n-1}}{2\,dt} + gm\,\frac{y_j^n - y_{j-1}^n}{dx} = 0 \,. \tag{10}$$

Putting $y_j^n = \sum_m a_m (\xi_m)^n e^{i\frac{j}{m}\pi}$,

we obtain after reduction

$$\xi_m = \frac{1}{1 + i \cdot 2gm\,\frac{dt}{dx} \cdot tg\,(\frac{\pi}{2m})} \quad . \tag{11}$$

Since $|\xi_m|$, which is the damping factor for the amplitude of the m'th harmonic in the false increment δy corresponding to one time step, is always smaller than unity, it can be concluded that the system is always numerically stable.

It is supposed that the actual equation (6), which has constant or only slightly varying a's and b's, will also show numerical stability.

It is a general observation that the use of backward time steps normally ensures numerical stability.

The problem of the proper choice of step lengths dx and dt from a convergence point of view is treated in the next chapter.

5. Instructions for Use of the Code

a. General explanation of the iteration scheme

With reference to fig. 1, an explanation of the time sequence of the calculation is given below:

The code starts at the dashed line on the assumption of certain fuel and coolant temperature distributions and certain moderator and coolant density distributions. On these assumptions a neutron-flux calculation is performed. As the neutron level is arbitrary, the maximum flux is specified through the data input.

Next, using the calculated neutron flux by which the axial power-production distribution in the rods is given, we perform a heat-transfer calculation to determine the heat inflow into the coolant and the radial and axial temperature distribution in the rods. Now a hydraulic calculation is performed to give a better coolant-temperature distribution, which in turn is utilized for a better heat-transfer calculation, and so on until convergence. Then the hydraulic calculations are completed with a steam-void calculation.

According to the latest calculations of coolant temperature and void distribution together with the axial fuel-temperature distribution, averaged radially, circulation in the outer iteration loop goes on until convergence of the neutron-flux distribution.

Having finished the steady-state calculation, the code immediately starts on the transient calculation, which follows the same iteration scheme.

To provide a means of supervising the described iteration sequence the code prints out an "s" on the on-line typewriter at the start of the steady-state calculation and at the start of each time step of the transient calculation. Further, a line shift indicates the start of an outer-loop circulation, while a "1" is printed for each circulation in the heat-transfer - hydraulics iteration loop.

Without describing in detail how the different convergence criteria work, it is important to point out how the converged state of the calculations,

as accepted by the code after the steady-state calculation or after each time step, is characterized. This acceptance occurs when the following error quantities have become smaller than specified values:

epsP = root mean square relative difference between the last two neutron-flux distributions of the outer iteration loop.

errorphi = r.m.s. relative difference between the last two flux distributions of the local inner loop of the steady-state neutron-flux calculation (see section 2).

errormy = numerical difference between the last two eigenvalues of the local outer loop of the steady-state neutron-flux calculation (see section 2).

erfeul = numerical mean relative difference between one-step and two-step transient neutron-flux calculations (see section 2).

error T = r.m.s. difference between the last two coolant temperature distributions of the local iteration loop within the hydraulics calculation (see section 4).

error Q = r.m.s. relative difference between the last two heat-inflow-to-coolant calculations of the heat-transfer - hydraulics iteration loop.

error Teff = r.m.s. relative difference between the last two radially averaged axial fuel-temperature distributions of the heat-transfer - hydraulics iteration loop.

error v = r.m.s. difference between the last two void distributions of the local iteration loop within the hydraulics calculation.

b. Library system

Physical data are necessary for the calculations described in sections 2, 3 and 4. These are neutron-physics cross sections and constants for a number of materials, thermodynamic data for heavy water and heat-conduction data for fuel and cladding materials. Some of the data are temperature or pressure dependent, and in these cases tables are stored in the computer and a parabolic interpolation routine used for calculating actual values during the run. The physical data are contained in three library tapes named "Library for CROSS", "Library for CHANNEL" and "Library for HEAT", corresponding to the above-mentioned three groups of physical

data. These tapes must be supplied to the computer at the beginning of each run.

No details on this library system will be given here, but for practical reasons reference numbers for certain materials and their weight percentages in some compounds are suggested below because they have been used in existing library tapes for CROSS and reference must be made to them from the data tape (see subsection c):

Material	U^{238}	U^{235}	O	Al	U	D	Zircaloy-2
Reference number	1	2	3	4	5	6	7

Content of	Any material	U	O	H	O	D	O	Al	O
in compound	itself	UO_2	UO_2	H_2O	H_2O	D_2O	D_2O	Al_2O_3	Al_2O_3
Reference number	1	2	3	4	5	6	7	8	9

The first quantity on each library tape is an identification number. The existing tapes have been identified by number 1. To avoid mistakes the code checks that the tape supplied has the intended identification number, which must also be specified on the data tape.

c. Preparation of data

Before going through the data sheet it is practical to comment on the way of describing the geometry and composition of the lattice cell.

The cell is thought to consist of five homogeneous regions, numbered from 1 to 5:

(1) fuel material, (2) cladding, (3) coolant, (4) shroud, and (5) moderator.

To define the composition, all materials represented in each of the five regions are listed by means of their reference numbers, beginning with the first region. These materials may be present either pure or in a compound or mixture. Hence it is necessary to specify for each material the density of the region, the weight fraction of the material or compound in question and the compound reference number.

During the computations the different regions are treated differently according to whether they contain solids, coolant or moderator. Hence for each material also the region number and another indicator of the region

type are to be specified. Thus, solid regions are indicated by "0", coolant by "1" and moderator by "2".

In section 4 it was mentioned that the system pressure is to be specified. If the value given refers to the upper end of the channel, a parameter called "pressure index" must be assigned the value 1, otherwise 0.

If output of results is desired after each time step, a parameter called "printing index" must be assigned the value 1. In general, if it is assigned the value p, output will be obtained after every p'th time step.

Now the data sheet presented in appendix 2 can be immediately understood and employed.

d. Output and treatment of results

The amount of results produced by BRENDA is often very comprehensive. Therefore a separate code has been written for the purpose of sorting the output and present in a convenient form the exact amount of information desired by the user.

This code, named BRENDAPLOT, makes use of the digital plotter Calcomp, model 507, which is permanently coupled to the GIER computer at the Risö establishment.

To use BRENDAPLOT it is necessary to prepare a small data tape to specify what information is wanted. After the insertion of this tape the total amount of output from BRENDA is supplied.

The preparation of data tapes for BRENDAPLOT appears from the scheme of appendix 3, which is immediately understandable. At the same time this scheme illustrates the latent possibilities of presentation of results.

CHAPTER II

DISCUSSION OF BRENDA

1. Introduction

A thorough numerical and theoretical testing of a computer code of the size of BRENDA is a huge task which would require endless series of computer runs. Further, in our particular case the lack of relevant experimental data has been a regrettable source of uncertainty as to the physical correctness of the mathematical representations.

An attempt to carry out a fairly sufficient numerical test has been made by parts, in the sense that the neutron physics, the hydraulics and

the heat-transfer calculations have been checked separately by minor codes.

These codes were established as steps on the way to the large code BRENDA and are in every detail similar to the respective parts of BRENDA.

The checking in each case consisted in running several examples which had an analytical solution for comparison.

The interaction of the different physical effects, i.e. the coupling between the individual parts of BRENDA, was checked by means of the equivalent linear point model of BRENDA, based on the transfer-function concept as derived in ref. 11. In this way, of course, the check is restricted to space-independent, small transients.

The above-mentioned checking operations revealed no deviations large enough to indicate errors in the numerical technique. However, a good deal of experience as to how to make proper choices of the mathematical quantities governing the integrative and iterative performance was gained. A summary of this experience is found at the end of the chapter.

2. Neutron Physics

(a) The group diffusion model

The role played by the neutron kinetics in the overall transient behaviour of the channel is not so important as to justify a very rigorous treatment. Thus it is generally accepted that two-group diffusion theory is sufficient.

However, it is very desirable to reduce the requirements of computer storage space and computing time imposed by a two-group treatment.

The method used in BRENDA imposes approximately the same space and time requirements as a one-group treatment, and yet it has some of the advantages of a two-group treatment in that it considers the individual space dependence of fast and thermal fluxes through the fast-neutron leakage representation, as pointed out in chapter I, section 2.

The assumptions on which this representation is valid are stated in chapter I, section 2. Roughly, what they express is that the axial flux variation should be smooth and without drastic variations.

(b) The control-rod simulation

A general and rigorous treatment of the control problem would require detailed specifications as to whether solid rods, soluble poisons, circulating fluid poisons, or other means are used to provide the necessary neutron absorption or leakage to control the chain reaction.

It has not been the intention to restrict this code to any specific control device. Further, the difficulties involved in a proper representation of just one of these several possibilities are so great as to necessitate a separate treatment. Hence, a very general and therefore very crude representation of the control system was chosen as described in chapter I, section 2. However, so long as it is meaningful to express the effect of the control system on a single element of the channel considered by a single quantity (reactivity), this effect may always be thought of as a consequence of an increase in thermal absorption in that element. Thus the deficiency of the method can to a great extent be considered as a question of calibration of the control system; the main disadvantage then lies in the restriction that the control system is supposed to act according to a fixed spatial distribution at all times.

(c) The one-delayed-group approximation

To estimate the validity of the one-delayed-group approximation to the neutron-kinetics treatment the problem will be discussed from two different points of view:

(1) Small reactivities. This case can be described in full detail by means of the transfer-function concept.

Schultz[5] has computed the exact transfer function for a U^{235}-fuelled reactor, using six groups of delayed neutrons, and compared it with the simple approximation corresponding to one group of delayed neutrons. Fig. 4 presents the plot, taken from ref. 5, by means of which this comparison is performed. It is evident from the general form of the transfer function

$$\frac{\bar{\delta n}(s)}{\bar{\varrho}(s)} = \frac{n_o}{ls} \frac{\prod_{i=1}^{p} (s + \lambda_i)}{\prod_{i=1}^{p} (s + r_i)} ,$$

where p is the number of delayed neutron groups, that the high frequency response depends only on l, the neutron life-time, and hence is the same for both functions. The low-frequency phase response tends to $-\frac{\pi}{2}$ for any number of groups. By varying λ and r for the one-group approximation a reasonable fit with both low-frequency amplitude response and medium-frequency phase response may be obtained, as in fig. 4, where $\lambda = 0.125\ \text{sec}^{-1}$ and $r = 50\ \text{sec}^{-1}$ are used.

(2) Step reactivities. Without loss of generality the kinetic equations can be lumped into the integro-differential equation

$$\Lambda \dot{n}(t) = K(t)\, n(t) - \int_0^t n'(\tau)\, f(t-\tau)\, d\tau + R(t) ,$$

where, by definition,

$$f(t) \equiv \sum_{i=1}^{p} a_i\, e^{-\lambda_i t}$$

$$\Lambda \equiv \frac{1}{\beta\, k_{eff}}$$

$$K \equiv \frac{\varrho}{\beta} \quad ;$$

R(t) denotes the initial source of neutrons, a_i the relative abundance of neutrons of the i'th delayed group.

A presentation of the above theory can be found in ref. 6, chapter 2.

If we put $R(t) \equiv 0$, $f(t) \equiv e^{-t/\tau}$ and $K(t) \equiv K$, we obtain by differentiation

$$\ddot{n}(t) - \left\{ \frac{K-1}{\Lambda} - \frac{1}{\tau} \right\} \dot{n}(t) - \frac{K}{\Lambda\tau}\, n(t) = 0$$

with the solution

$$n(t) = C_1\, e^{a_1 t} + C_2\, e^{a_2 t}$$

with

$$\left.\begin{matrix} a_1 \\ a_2 \end{matrix}\right\} = \frac{1}{2}\left\{ \frac{K-1}{\Lambda} - \frac{1}{\tau} \pm \sqrt{\left(\frac{K-1}{\Lambda} - \frac{1}{\tau}\right)^2 + \frac{4K}{\Lambda\tau}} \right\}$$

$$\left.\begin{matrix} C_1 \\ C_2 \end{matrix}\right\} = \frac{n(o)}{2} \left\{ 1 \pm \left(\frac{K+1}{\Lambda} + \frac{1}{\tau}\right) \frac{1}{\sqrt{\left(\frac{K-1}{\Lambda} - \frac{1}{\tau}\right)^2 + \frac{4K}{\Lambda\tau}}} \right\} .$$

For $|K| >> 1$ the solution is reduced to

$$\left.\begin{matrix} a_1 \\ a_2 \end{matrix}\right\} \sim \begin{cases} \frac{K}{\Lambda} \\ -\frac{1}{\tau} \end{cases}$$

$$\left.\begin{matrix} C_1 \\ C_2 \end{matrix}\right\} \sim \begin{cases} n(o)\,(1+\frac{1}{K}) \\ -n(o)\,\frac{1}{K} \end{cases} .$$

For positive reactivities this pictures a quickly rising exponential independent of τ .

For negative reactivities it shows a steep decrease (initial jump) independent of τ , followed by a decreasing exponential with the time constant τ .

For $|K| << 1$ the solution is reduced to

$$\left.\begin{matrix} a_1 \\ a_2 \end{matrix}\right\} \sim \begin{cases} -\frac{1}{\Lambda} \\ \frac{K}{\tau} \end{cases}$$

$$\left.\begin{matrix} C_1 \\ C_2 \end{matrix}\right\} \sim \begin{cases} -n(o)K \\ n(o)\,(1+K) \end{cases} .$$

For both positive and negative reactivities this pictures a steep initial jump independent of τ , followed by an exponential with the time constant $\frac{\tau}{K}$.

If $|K|$ is near to one, the approximation for $|K| >> 1$ applies provided $K < 0$. For $K > 0$ a special investigation shows:

For $2\sqrt{\frac{\Lambda}{\tau}} << |K - (1+\frac{\Lambda}{\tau})| << 1$:

$$\left.\begin{matrix} a_1 \\ a_2 \end{matrix}\right\} \sim \begin{cases} \dfrac{K - (1+\frac{\Lambda}{\tau})}{\Lambda} + \dfrac{1}{\left\{K - (1+\frac{\Lambda}{\tau})\right\}\tau} \sim \dfrac{K-1}{\Lambda} \\ - \dfrac{1}{\left\{K-(1+\frac{\Lambda}{\tau})\right\}\tau} \sim - \dfrac{1}{(K-1)\tau} \end{cases}$$

$$\left.\begin{matrix} C_1 \\ C_2 \end{matrix}\right\} \sim \frac{n(o)}{2}\left\{1 \pm \frac{2}{K-(1+\frac{\Lambda}{\tau})}\right\} \sim \frac{n(o)}{2}\left\{1 \pm \frac{2}{K-1}\right\} .$$

For $|K - (1 + \frac{\Lambda}{\tau})| \ll 2\sqrt{\frac{\Lambda}{\tau}}$:

$$\left.\begin{matrix} a_1 \\ a_2 \end{matrix}\right\} \sim \frac{K - (1+\frac{\Lambda}{\tau})}{2\Lambda} \pm \frac{1}{\sqrt{\Lambda\tau}} \sim \pm \frac{1}{\sqrt{\Lambda\tau}}$$

$$\left.\begin{matrix} C_1 \\ C_2 \end{matrix}\right\} \sim \frac{n(o)}{2}\left(1 \pm \sqrt{\frac{\tau}{\Lambda}}\right) .$$

In both cases this pictures a difference between two large exponentials, one increasing, the other decreasing. After some time the increasing one will dominate, but no destinct initial jump occurs. It should be noted that only when K is very close to or less than $1 + \frac{\Lambda}{\tau}$ is the dependence of τ extended over all times.

In conclusion of the discussion from the above two viewpoints it is first noted (from (1)) that small reactivity variations are fairly well treated by the one-group representation provided the constants are properly chosen. The accuracy is always better the higher the frequency. This fact is in accordance with (2), where it is concluded that τ for $|K| \ll 1$ is immaterial for short times.

Secondly (from (2)) it is noticed that for large positive reactivities, i.e. when K is a little greater than $1 + \frac{\Lambda}{\tau}$, the response is independent of τ, which indicates that the one-group representation suffices also in this case.

Thirdly (from (2)) it is noticed that for large negative reactivities, i.e. for $|K|$ not $\ll 1$, the initial jump, and hence the short-time response, is independent of τ and thus well described by the one-group representation.

However, the long-time response depends heavily on τ, i.e. in this case the one-group representation does not suffice.

Altogether it is seen that the one-group representation fails mainly in two cases:

Positive reactivities which are not small and up to a little over prompt critical, and

Negative reactivities which are not small and act for long times.

The conclusion indicates that for instance a reactor shut-down is not well represented unless the τ value is specified to correspond to the most delayed neutron group, which governs the transient response in this case. This, however, requires an alteration of the library tape for CROSS (see chapter I, section 5).

(d) Computer runs

In order to check the neutron-physics computations of BRENDA, a series of runs with a partial code named NEUPHTEST was performed.

This code is able to reproduce the case of a pure step reactivity on alteration of the control absorption cross section Σ_c mentioned in chapter I, section 2. Here it is assumed that the reactivity change obtained corresponds to an excess multiplication k_{ex} computed by means of

$$k_{ex} = k_{ex,o} \frac{\Delta \Sigma_c}{\Sigma_{co}} ,$$

where $k_{ex,o}$ is the excess multiplication corresponding to the insertion of the control absorption cross section Σ_{co}, and $\Delta\Sigma_c$ is the increase in the control absorption cross section introduced.

The following cases were considered and the results of the computations shown in figs. 5 and 6:

(1) $K = \pm 0.0257\ \not\$$ (fig. 5)

(2) $K = \pm 25.0\ \not\$$ (fig. 6)

(3) $K = -\ 2.52\ \$$ (fig. 6).

In each case the computed curve is compared with the exact solution obtained from subsection 2.c. It is concluded that the agreement is very fine and thus provides a check both on the coding technique for the kinetic equations and on the method of computing the reactivity as explained above.

Further, the case of K = + 2.52 $ was considered. The results of this computation have not been plotted because of the vast range of flux variation. Instead it was noted from the computer results that the increase in flux over a time step of 0.2 sec (for times long enough for the negative exponential to have died out) was very constantly equal to a factor of 299.83, corresponding to an a_1-value of 28.5 sec^{-1}. Similarly, an extrapolation of the computer results back to zero time using the above asymptotic multiplication per time step indicates a C_1-value of 1.666 · n(o).

According to the theory of the preceding subsection the exact solution is

$$\left.\begin{matrix} a_1 \\ a_2 \end{matrix}\right\} = \begin{cases} 28.8\ sec^{-1} \\ -0.11\ sec^{-1} \end{cases}$$

$$\left.\begin{matrix} C_1 \\ C_2 \end{matrix}\right\} = n(o) \begin{cases} 1.652 \\ -0.652 \end{cases}$$

with $\Lambda = 5.28\ 10^{-2}$ sec, $1/\tau = 0.076\ sec^{-1}$, $\beta = 0.00755$, which values correspond to the parameters computed during the NEUPHTEST run.

The difference between computer results and theory apparently amounts to -1 and +2 per cent for the quantities a_1 and C_1-1 respectively. This can be very satisfactorily explained by an uncertainty of 1 per cent in the reactivity, as may be seen from the approximate solution for $|K| >> 1$.

3. Heat Transfer from Fuel Rods to Coolant

(a) Heat release from cylindrical, cladded fuel rods

The rigorous analytical treatment of the heat release from cylindrical, cladded fuel rods is a rather involved problem.

In the following, Laplace-transformation theory is used together with the transfer-function concept to arrive at an exact solution.

Afterwards, an attempt is made to discuss these exact transfer functions and arrive at approximate expressions covering a sufficiently broad frequency domain for most applications.

The results are presented in the form of a general set of curves giving the amplitude and phase characteristics of the heat-release power-production transfer function. Some additional expressions are given to

make up a complete set of equations for general use in reactor-dynamics analysis.

Contrary to other treatments of this problem, e.g. that of ref. 9, this study, through an exact consideration of the properties of the cladding, gives a rather well-defined limit of the frequency range within which a first-order approximation is justified.

To provide an analytical representation of the results, the above-mentioned heat-release power-production transfer function has been approximated by a rational algebraic expression in the complex variable s.

Description of the system and basic equations. The system considered is a circular, cylindrical fuel rod of infinite length, surrounded by a cladding of annular cross section. The cladding is surrounded by some coolant. An air gap of finite thickness between fuel and cladding is provided. A cross section of the system is shown in fig. 7.

The fuel material has a uniform heat conductivity $\varkappa_1$, a uniform specific heat c_1 and a uniform density ϱ_1. Similar quantities, $\varkappa_2$, c_2 and ϱ_2, are introduced for the cladding material.

A heat source P, which is a function of time, is assumed to act uniformly in the fuel.

There is no heat source in the cladding, and the coolant is assumed to have a uniform temperature T_o, which is a function of time.

If we denote the temperature by T and the heat flux per unit area by Q and introduce the indices a, b and c for the outer surfaces of fuel, air gap and cladding, the heat-conduction equation with boundary conditions yields the following system of equations:

$$\varkappa_1 \nabla^2 T - \varrho_1 c_1 \frac{\partial T}{\partial t} + P = 0, \qquad 0 \leq r \leq r_a \tag{1}$$

$$\varkappa_2 \nabla^2 T - \varrho_2 c_2 \frac{\partial T}{\partial t} = 0, \qquad r_b \leq r \leq r_c \tag{2}$$

$$-r_a \varkappa_1 \left(\frac{\partial T}{\partial r}\right)_a = - r_b \varkappa_2 \left(\frac{\partial T}{\partial r}\right)_b \tag{3}$$

$$T_a - T_b = - \eta \varkappa_2 \left(\frac{\partial T}{\partial r}\right)_b \tag{4}$$

$$T_c - T_o = - \frac{1}{k} \varkappa_2 \left(\frac{\partial T}{\partial r}\right)_c \tag{5}$$

$$Q_c = - \varkappa_2 \left(\frac{\partial T}{\partial r}\right)_c \quad . \tag{6}$$

Here, η , the heat resistivity of the air gap, and k, the heat conductivity of the cladding-coolant interface, are introduced.

Exact solution by Laplace transformation. The step by step solution of the system of equations is recorded in appendix 4. Here only the final exact expressions will be presented.

The quantities of major interest to the reactor physicist are the mean fuel temperature, defined by

$$T_f \equiv \frac{1}{\pi r_a^2} \int_0^{r_a} 2\pi\, r\, T\, dr \,, \tag{7}$$

and the heat flux Q_c through the outer surface of the cladding, both considered as functions of the independent variables P and T_o.

If we denote the variation of a Laplace-transformed quantity A by $\overline{\delta A}(s)$, the resulting equations are

$$\overline{\delta T_f}(s) = (\eta^1 \alpha + \beta)\,\overline{\delta T_o}(s) + \left\{\eta^1 (X_{o1}^{bc} + \frac{a}{k}) + \frac{X_{oo}^{bc}}{\sqrt{-\varrho_2 c_2 \varkappa_2 s}} + \frac{\beta}{k}\right\} \overline{\delta Q_c}(s) \tag{8}$$

$$\frac{X_{o1}^{bc}\,\beta - \dfrac{X_{oo}^{bc}}{\sqrt{-\varrho_2 c_2 \varkappa_2 s}}\,a}{\eta^1 \alpha + \beta}\; \overline{\delta Q_c}(s) = \frac{1}{2}\,\frac{r_a^2}{r_b}\; \overline{\delta P}(s)$$

$$- \left\{\frac{1}{2}\,\frac{r_a^2}{r_b}\; \varrho_1 c_1 s + \frac{a}{\eta^1 \alpha + \beta}\right\} \overline{\delta T_f}(s) \quad . \tag{9}$$

Here the following definitions have been made:

$$X_{oo}^{bc} \equiv \frac{N_o^c J_o^b - N_o^b J_o^c}{N_o^c J_1^c - N_1^c J_o^c} \tag{10}$$

$$X_{o1}^{bc} \equiv \frac{N_o^c J_1^b - N_1^b J_o^c}{N_o^c J_1^c - N_1^c J_o^c} \tag{11}$$

$$\alpha \equiv -\sqrt{\varrho_2 c_2 \varkappa_2 s}\left\{\frac{J_1^b}{J_o^c} - \frac{J_1^c}{J_o^c} X_{o1}^{bc}\right\} \tag{12}$$

$$\beta \equiv \frac{J_o^b}{J_o^c} - \frac{J_1^c}{J_o^c} X_{oo}^{bc} \tag{13}$$

$$\eta^1 \equiv \eta + \frac{1}{4}\frac{r_b}{\varkappa_1}\bar{Z}(s) \tag{14}$$

$$\bar{Z}(s) \equiv -\frac{2}{x}\left\{1 - \sqrt{-x}\,\frac{J_o(2\sqrt{-x})}{J_1(2\sqrt{-x})}\right\}, \quad x \equiv \frac{1}{4}\frac{\varrho_1 c_1}{\varkappa_1} r_a^2 s \,. \tag{15}$$

J_ν and N_ν ($\nu = 0, 1$) denote Bessel functions of the first and second kind respectively. Where these symbols are provided with a superscript, b or c, the arguments

$$\sqrt{-\frac{\varrho_2 c_2}{\varkappa_2} s}\, r_b \quad \text{and} \quad \sqrt{-\frac{\varrho_2 c_2}{\varkappa_2} s}\, r_c \,,$$

respectively, apply.

A useful expression for $\overline{\delta Q_c}(s)$ is obtained by eliminating $\overline{\delta T_f}(s)$ between (8) and (9):

$$\overline{\delta Q_c}(s) = \bar{Y}_p(s)\left\{\overline{\delta P}(s) - \varrho_1 c_1 s \cdot \bar{C}(s) \cdot \overline{\delta T_o}(s)\right\} , \tag{16}$$

where

$$\bar{Y}_p(s) \equiv \frac{\frac{1}{2}\frac{r_a^2}{r_b}}{X_{o1}^{bc} + \frac{a}{k} + \frac{1}{2}\frac{r_a^2}{r_b}\,\varrho_1 c_1 s\left\{\eta^1\left(X_{o1}^{bc} + \frac{a}{k}\right) + \frac{X_{oo}^{bc}}{\sqrt{-\varrho_2 c_2 \varkappa_2 s}} + \frac{\beta}{k}\right\}} \tag{17}$$

and

$$\bar{C}(s) \equiv \beta + \left\{ \eta^1 + \frac{2r_b}{\varrho_1 c_1 r_a^2 s} \right\} \alpha \quad . \tag{18}$$

Approximation of $\bar{Z}(s)$. The first step in attacking the complicated expressions that have now been established is to approximate the function $\bar{Z}(s)$ of eq. (15).

This has been done by working out tables of the amplitude and phase of the quantity $(\bar{Z}(x))^2$, where x is assumed purely imaginary. For this task, performed by means of a desk calculator, Bessel-function values from ref. 7 were used. Fig. 8 shows a plot of the results. It is noted that the phase tends to $-\frac{\pi}{2}$ and the amplitude to zero as $|x|$ tends to infinity. In fact a very good approximation to this function is $(\bar{Z}(x))^2 \sim \frac{1}{1+\frac{1}{3}x}$, as demonstrated in fig. 8.

Hence, for all the following applications, the approximation

$$\bar{Z}(s) \sim \frac{1}{\sqrt{1 + \frac{1}{12} \frac{\varrho_1 c_1}{\varkappa_1} r_a^2 s}} \tag{19}$$

will be adopted.

First-order approximations. By means of elementary rules of differentiation of Bessel functions (ref. 8) the following first-order approximations can be established:

$$X_{oo}^{bc} \sim \sqrt{-\frac{\varrho_2 c_2}{\varkappa_2} s \Delta r}, \qquad \Delta r \equiv r_c - r_b$$

$$\frac{X_{oo}^{bc}}{\sqrt{-\varrho_2 c_2 \varkappa_2 s}} \sim \frac{\Delta r}{\varkappa_2}$$

$$X_{o1}^{bc} \sim 1 + \frac{\Delta r}{r_c} \sim \frac{r_c}{r_b}$$

$$\frac{J_1^b}{J_o^c} \sim \frac{J_1^c}{J_o^c}\left(1 + \frac{\Delta r}{r_c}\right) - \sqrt{-\frac{\varrho_2 c_2}{\varkappa_2}\, s}\,\Delta r$$

$$\frac{J_o^b}{J_o^c} \sim 1 + \frac{J_1^c}{J_o^c}\sqrt{-\frac{\varrho_2 c_2}{\varkappa_2}\, s}\,\Delta r$$

$$\frac{J_1^b}{J_o^c} - \frac{J_1^c}{J_o^c}\, X_{o1}^{bc} \sim - \sqrt{-\frac{\varrho_2 c_2}{\varkappa_2}\, s}\,\Delta r$$

$$\frac{J_o^b}{J_o^c} - \frac{J_1^c}{J_o^c}\, X_{oo}^{bc} \sim 1$$

$$\alpha \sim s\ \varrho_2 c_2\ \Delta r$$

$$\beta \sim 1\ .$$

By insertion of these results into the exact equations (9), (17) and (18) the following expressions are obtained:

$$\frac{\frac{r_c}{r_b} - s\ \varrho_2 c_2 \frac{\Delta r^2}{\varkappa_2}}{1 + s\ \varrho_2 c_2\ \Delta r\ \eta^1}\ \overline{\delta Q}_c(s) \sim \frac{1}{2}\frac{r_a^2}{r_b}\ \overline{\delta P}(s) - \left\{\frac{1}{2}\frac{r_a^2}{r_b}\ \varrho_1 c_1\, s + \frac{s\ \varrho_2 c_2\ \Delta r}{1 + s\ \varrho_2 c_2 \Delta r\ \eta^1}\right\}\overline{\delta T}_f(s) \tag{20}$$

$$\overline{Y}_p(s) \sim \frac{\frac{1}{2}\frac{r_a^2}{r_c}}{1 + s\,\varrho_2 c_2 \frac{\Delta r}{k}\frac{r_b}{r_c} + \frac{1}{2}\frac{r_a^2}{r_b}\,\varrho_1 c_1 s\left\{\frac{1}{k} + \frac{\Delta r}{\varkappa_2} + \eta^1 \frac{r_c}{r_b}\left(1 + s\varrho_2 c_2 \frac{\Delta r}{k}\frac{r_b}{r_c}\right)\right\}} \tag{21}$$

$$\overline{C}(s) \sim 1 + \frac{2r_b}{r_a^2}\frac{\varrho_2 c_2 \Delta r}{\varrho_1 c_1} + s\,\varrho_2 c_2 \Delta r\,\eta^1 \quad . \tag{22}$$

Introduction of η^1 from (14) and (19) into (20), (21) and (22) yields

$$\frac{1 - s\,\varrho_2 c_2 \frac{r_b}{r_c}\frac{\Delta r^2}{\varkappa_2}}{1 + s\,\varrho_2 c_2 \Delta r\left(\eta + \frac{1}{4}\frac{r_c}{\varkappa_1}\frac{1}{\sqrt{1+\frac{1}{12}\frac{\varrho_1 c_1}{\varkappa_1} r_a^2 s}}\right)} \overline{\delta Q_c}(s) \sim \frac{1}{2}\frac{r_a^2}{r_c}\overline{\delta P}(s) \tag{24}$$

$$-\left\{\frac{1}{2}\frac{r_a^2}{r_c}\varrho_1 c_1 s + \frac{s\,\varrho_2 c_2 \Delta r \frac{r_b}{r_c}}{1+ s\,\varrho_2 c_2 \Delta r\left(\eta + \frac{1}{4}\frac{r_b}{\varkappa_1}\frac{1}{\sqrt{1+\frac{1}{12}\frac{\varrho_1 c_1}{\varkappa_1} r_a^2 s}}\right)}\right\}\overline{\delta T_f}(s)$$

$$\overline{Y}_p(s) \sim \frac{1}{2}\frac{r_a^2}{r_c} \Big/$$

(25)

$$1+\frac{1}{8}\frac{r_a^2}{\varkappa_1}\varrho_1 c_1 \frac{s\left(1+\varrho_2 c_2 \frac{\Delta r}{k}\frac{r_b}{r_c} s\right)}{\sqrt{1+\frac{1}{12}\frac{\varrho_1 c_1}{\varkappa_1} r_a^2 s}} + \left\{\varrho_2 c_2 \frac{r_b}{r_c}\frac{\Delta r}{k} + \frac{1}{2}\frac{r_a^2}{r_c}\varrho_1 c_1\left(\frac{1}{k}+\frac{\Delta r}{\varkappa_2}+\eta\frac{r_c}{r_b}\left(1+\varrho_2 c_2 \frac{r_b}{r_c}\frac{\Delta r}{k}\right.\right.\right.$$

$$\overline{C}(s) \sim 1 + \frac{2r_b}{r_a^2}\frac{\varrho_2 c_2}{\varrho_1 c_1}\Delta r + \frac{1}{4}\frac{r_b}{\varkappa_1}\frac{\varrho_2 c_2 \Delta r\, s}{\sqrt{1+\frac{1}{12}\frac{\varrho_1 c_1}{\varkappa_1} r_a^2 s}} + \varrho_2 c_2 \Delta r \eta\, s \quad . \tag{26}$$

The third term in $\overline{C}(s)$ can be rewritten

$$\frac{1}{4}\,\frac{r_b}{\varkappa_1}\,\frac{\varrho_2 c_2\,\Delta r\, s}{\sqrt{1+\frac{1}{12}\,\frac{\varrho_1 c_1}{\varkappa_1}\,r_a^{\,2}\,s}}$$

$$= \frac{\sqrt{3}}{2}\,\frac{r_b}{r_a}\,\sqrt{\frac{\varrho_2 c_2\,\varkappa_2}{\varrho_1 c_1\,\varkappa_1}}\,\sqrt{\frac{\frac{1}{12}\,\frac{\varrho_1 c_1}{\varkappa_1}\,r_a^{\,2}\,s}{1+\frac{1}{12}\,\frac{\varrho_1 c_1}{\varkappa_1}\,r_a^{\,2}\,s}}\,\sqrt{\frac{\varrho_2 c_2}{\varkappa_2}\,s\,\Delta r}\quad . \tag{27}$$

Now a series of further approximations can be made from (24), (25) and (26):

$$\overline{\delta T_f}(s) \sim \frac{1}{\varrho_1 c_1 s\left(1+\frac{2 r_b\,\varrho_2 c_2}{r_a^{\,2}\,\varrho_1 c_1}\,\Delta r\right)}\left\{\overline{\delta P}(s)-\frac{2 r_c}{r_a^{\,2}}\;\overline{\delta Q_c}(s)\right\}, \tag{28}$$

which is valid for

$$\left.\begin{aligned}
&\varrho_2 c_2\,\frac{r_b}{r_c}\,\frac{\Delta r^2}{\varkappa_2}\;|s| \ll \frac{\frac{1}{2}\,\frac{r_a^{\,2}}{r_c}}{|\overline{Y}_p(s)|}\\
&\varrho_2 c_2\,\Delta r\,\eta\;|s| \ll \frac{\frac{1}{2}\,\frac{r_a^{\,2}}{r_c}}{\overline{Y}_p(s)}\\
&\frac{\sqrt{3}}{2}\,\frac{r_b}{r_a}\,\sqrt{\frac{\varrho_2 c_2\,\varkappa_2}{\varrho_1 c_1\,\varkappa_1}}\,\sqrt{\frac{\varrho_2 c_2}{\varkappa_2}}\;|s|\,\Delta r \ll \frac{\frac{1}{2}\,\frac{r_a^{\,2}}{r_c}}{|\overline{Y}_p(s)|}\quad ;
\end{aligned}\right\} \tag{29}$$

$$\overline{Y}_p(s) \sim$$

$$\frac{\frac{1}{2}\,\frac{r_a^2}{r_c}}{1+\frac{1}{8}\,\frac{r_a^2}{\varkappa_1}\,\varrho_1 c_1\,\frac{s}{\sqrt{1+\frac{1}{12}\,\frac{\varrho_1 c_1}{\varkappa_1}\,r_a^2 s}}+\left\{\varrho_2 c_2\,\frac{r_b}{r_c}+\frac{\Delta r}{k}+\frac{r_a^2}{r_c}\,\varrho_1 c_1\left(\frac{1}{k}+\frac{\Delta r}{\varkappa_2}+\eta\,\frac{r_c}{r_b}\right)\right\} s} \quad , \tag{30}$$

which is valid for

$$\varrho_2 c_2\,\frac{r_b}{r_c}\,\frac{\Delta r}{k}\,|s| \ll 1 \quad ; \tag{31}$$

$$\overline{C}(s) \sim 1 + \frac{2 r_b}{r_a^2}\,\frac{\varrho_2 c_2}{\varrho_1 c_1}\,\Delta r \quad , \tag{32}$$

which is valid for

$$\left.\begin{aligned} &\varrho_2 c_2 \Delta r \eta \quad |s| \ll 1 \\ &\frac{\sqrt{3}}{2}\,\frac{r_b}{r_a}\,\sqrt{\frac{\varrho_2 c_2\,\varkappa_2}{\varrho_1 c_1\,\varkappa_1}}\,\sqrt{\frac{\varrho_2 c_2}{2}}\quad |s|\ \Delta r \ll 1 \quad . \end{aligned}\right\} \tag{33}$$

Frequency range of validity of first-order approximations. To evaluate the range of validity of the first-order expressions of the preceding subsection, the following asymptotic expressions are introduced:

$$J_\nu\ (Z) \sim \frac{\cos\left(Z - \frac{\pi}{2}\left(\nu + \frac{1}{2}\right)\right)}{\sqrt{\frac{\pi}{2}\ Z}} \tag{34}$$

$$N_\nu\ (Z) \sim \frac{\sin\left(Z - \frac{\pi}{2}\left(\nu + \frac{1}{2}\right)\right)}{\sqrt{\frac{\pi}{2}\ Z}} \tag{35}$$

(see e.g. ref. 8).

These expressions lead to

$$X_{oo}^{bc} \sim \sqrt{\frac{r_c}{r_b}} \sin\left(\sqrt{-\frac{\varrho_2 c_2}{\varkappa_2}}\, s\, \Delta r\right)$$

$$X_{o1}^{bc} \sim \sqrt{\frac{r_c}{r_b}} \cos\left(\sqrt{-\frac{\varrho_2 c_2}{\varkappa_2}}\, s\, \Delta r\right)$$

$$\alpha \sim -\sqrt{\frac{r_c}{r_b}} \sqrt{-\varrho_2 c_2 \varkappa_2}\, s \sin\left(\sqrt{-\frac{\varrho_2 c_2}{\varkappa_2}}\, s\, \Delta r\right)$$

$$\beta \sim \sqrt{\frac{r_c}{r_b}} \cos\left(\sqrt{-\frac{\varrho_2 c_2}{\varkappa_2}}\, s\, \Delta r\right) .$$

Further, by means of the general relations sin (i Z) = i sinh (Z), cos (i Z) = cosh (Z):

$$\frac{\alpha}{X_{o1}^{bc}} \sim \sqrt{\varrho_2 c_2 \varkappa_2 s}\, \tanh\left(\sqrt{\frac{\varrho_2 c_2}{\varkappa_2}}\, s\, \Delta r\right) \tag{36}$$

$$\frac{X_{oo}^{bc}}{X_{o1}^{bc}} \sim \frac{1}{\sqrt{-\varrho_2 c_2 \varkappa_2 s}} \frac{\tanh\left(\sqrt{\frac{\varrho_2 c_2}{\varkappa_2}}\, s\, \Delta r\right)}{\sqrt{\frac{\varrho_2 c_2}{\varkappa_2}}\, s\, \Delta r} \frac{\Delta r}{\varkappa_2} \tag{37}$$

$$\frac{\beta}{X_{o1}^{bc}} \sim 1 \tag{38}$$

$$X_{o1}^{bc} \sim \sqrt{\frac{r_c}{r_b}} \quad \cosh\left(\sqrt{\frac{\varrho_2 c_2}{\varkappa_2}}\, s\, \Delta r\right) \quad . \tag{39}$$

The above asymptotic formulae are applicable provided

$$\sqrt{\frac{\varrho_2 c_2}{\varkappa_2}}\, |s|\, r_b \gg 1 \quad . \tag{40}$$

It is noted that, for small Δr, (36) - (39) become identical with the first-order expressions of the last subsection. Hence the range of validity of these can be deduced from the condition

$$\sqrt{\frac{\varrho_2 c_2}{\varkappa_2}}\, |s|\, \Delta r \lesssim 1 \quad . \tag{41}$$

The value 1 on the right side is reasonable because for an argument $|Z| = 1$ the terms $|\cosh(Z)|$, $|\tanh(Z)|$ and $\left|\frac{\tanh(Z)}{Z}\right|$ diverge less than 50% from their first-order expansions while the divergence for larger arguments is quickly increasing.

At this stage it should be assured that the asymptotic formulae are applicable at the frequency limit determined by (41). This is obviously the case according to (40) because $r_b \gg \Delta r$ will always be fulfilled.

Conclusion. The following equations have been obtained as a first-order approximation to the exact ones derived in appendix 4:

$$\overline{\delta Q_c}(s) \sim \overline{Y}_p(s) \left\{ \overline{\delta P}(s) - \varrho_1 c_1 s \left(1 + \frac{2 r_b}{r_a^2} \frac{\varrho_2 c_2}{\varrho_1 c_1} \Delta r\right) \overline{\delta T}_o(s) \right\} \tag{42}$$

$$\overline{\delta T}_f(s) \sim \frac{1}{\varrho_1 c_1 s \left(1 + \frac{2 r_b}{r_a^2} \frac{\varrho_2 c_2}{\varrho_1 c_1} \Delta r\right)} \left\{ \overline{\delta P}(s) - \frac{2 r_c}{r_a^2} \overline{\delta Q_c}(s) \right\} \tag{43}$$

$$\overline{Y}_p(s) \sim \frac{\frac{1}{2} \frac{r_a^2}{r_c}}{1 + \frac{1}{2} \frac{x}{\sqrt{1 + \frac{1}{3} x}} + \epsilon x} \tag{44}$$

$$x = \frac{1}{4} \frac{r_a^2}{\varkappa_1} \varrho_1 c_1 s \tag{45}$$

$$\epsilon = \frac{4 \varkappa_1}{r_a^2 \varrho_1 c_1} \left\{ \varrho_2 c_2 \frac{r_b}{r_c} \frac{\Delta r}{k} + \frac{1}{2} \frac{r_a^2}{r_c} \varrho_1 c_1 \left(\frac{1}{k} + \frac{\Delta r}{\varkappa_2} + \eta \frac{r_c}{r_b} \right) \right\}. \tag{46}$$

Plots of the amplitude and phase of the function $\overline{Y}_p(x)$ are given in fig. 9 for a series of values of the parameter ϵ .

By the means of (41) and (45) the range of validity of the first-order approximation can be expressed as

$$|x| \lesssim \left(\frac{r_a}{\Delta r}\right)^2 \frac{\varrho_1 c_1 \varkappa_2}{4 \varrho_2 c_2 \varkappa_1} = |x_o| \ . \tag{47}$$

From (29) and (45) the bi-conditions for the validity of (43) are, when we use

$$\frac{|\overline{Y}_p(s)|}{\frac{1}{2} \frac{r_a^2}{r_c}} \ll 1 \text{ for } |x| \gtrsim \left(\frac{r_a}{\Delta r}\right)^2 \frac{\varrho_1 c_1 \varkappa_2}{4 \varrho_2 c_2 \varkappa_1} \ ,$$

as is generally true (see fig. 3 and assume $\frac{\varrho_1 c_1 \varkappa_2}{4 \varrho_2 c_2 \varkappa_1} \gtrsim 1$):

$$\left.\begin{aligned} &\frac{\sqrt{3}}{2} \frac{r_b}{r_a} \sqrt{\frac{\varrho_2 c_2 \varkappa_2}{\varrho_1 c_1 \varkappa_1}} \lesssim 1 \\ &|x| \lesssim \frac{1}{\eta} \frac{\Delta r}{\varkappa_2} |x_o| \ . \end{aligned}\right\} \tag{48}$$

The bi-condition for (44) is, by (31) and (45),

$$|x| \ll k \frac{\Delta r}{\varkappa_2} \cdot |x_o| \quad . \tag{49}$$

The bi-conditions so far introduced will often mean no serious restrictions beyond the requirement of (47).

The bi-conditions applying to (42) are somewhat more serious. By (33) and (45) they are

$$\left.\begin{aligned} &|x| \ll \frac{1}{\eta} \frac{\Delta r}{\varkappa_2} |x_o| \\ &\frac{\sqrt{3}}{2} \frac{r_b}{r_a} \sqrt{\frac{\varrho_2 c_2 \varkappa_2}{\varrho_1 c_1 \varkappa_1}} \sqrt{|x|} \ll \sqrt{|x_o|} \end{aligned}\right\} \tag{50}$$

Thus, in general (42) is only fully applicable up to a frequency limit that is an order of magnitude lower than that permitted by other restrictions. However, if the variation in T_o is small, as is the case in boiling-water reactors, condition (50) is without importance.

For practical applications of the results obtained it is desirable to express the function $\overline{Y}_p(x)$ by an analytical approximation. An attempt at this has been made by means of the rational algebraic function

$$\overline{Y}_p(x) \sim \frac{1}{2} \frac{r_a^2}{r_c} \frac{1 + a_1 x + a_2 x^2 + \ldots + a_p x^p}{1 + b_1 x + b_2 x^2 + \ldots + b_q x^q} \quad . \tag{51}$$

The fitting was performed by means of the digital computer GIER for a series of values of the parameter ε with a ready-made algorithm, COMPFIT[10].

Proper values of p and q were chosen to obtain a reasonable accuracy within the range $0 < |x| < 1000$. The coefficients of (51) thus obtained are plotted in fig. 10 as functions of ε. Also an error quantity, defined as the numerical value of the relative complex difference between the fitting expression and $\overline{Y}_p(x)$ (averaged over the x-domain considered), is plotted in fig. 4. It appears that the choices of $p = 1$, $q = 2$ when $\varepsilon \gtrsim 0.5$, and $p = 2$, $q = 3$ when $0.05 \lesssim \varepsilon \lesssim 0.5$, lead to average errors below 8%. Actually, the main contribution to the error originates from the range $|x| \gtrsim 10$. For

$|x| \lesssim 10$, which is the most important domain, the accuracy is comparable to the drawing accuracy of fig. 9.

For very small values of ϵ the fitting by (51) requires increasingly high values of p and q. No effort has been made to cover this range, which is of minor practical interest.

(b) Computer runs

In order to check the heat-transfer calculations of BRENDA, a series of runs with a partial code named CHANNELHEAT were performed.

These runs can be referred to two main groups as follows:

(1) Simple analytical examples. Constant heat flux. From eq. (1) of subsection (a) by subtraction of $\varrho_1 c_1 \frac{\partial T_c}{\partial t}$, where T_c denotes the coolant temperature, the following equation is obtained for the case of a fuel rod without cladding:

$$\varrho_1 c_1 \frac{\partial}{\partial t}(T-T_c) = P(t) - \varrho_1 c_1 \frac{\partial T_c}{\partial t} + \varkappa_1 \nabla^2 (T-T_c) \ .$$

This equation, applied to the surface of the rod, shows that a constant temperature difference between surface and coolant, and hence a constant heat flux, occurs when and only when $P(t) - \varrho_1 c_1 \frac{\partial T_c}{\partial t}$ is equal to a constant.

Thus, assuming

$$P(t) \equiv P(o)\, e^{t/\tau} \ ,$$

we obtain the coolant temperature variation

$$T_c(t) = T_c(o) + \frac{P(o)}{\varrho_1 c_1} \left\{ \tau \left(e^{t/\tau} - 1 \right) - t \right\}$$

$$\sim T_c(o) + \frac{P(o)}{2 \varrho_1 c_1 \tau} \ t^2 \ .$$

Using the values

$P(o) = 3 \cdot 10^5$ kwatt/m^3

$\tau = 31.13$ sec

$T_c(o) = 550^{\circ}$K

$\varrho_1 = 10900\ \mathrm{kg/m^3}$

$c_1 = 0.238\ \mathrm{kJoule/kg/^oK}$,

we calculated the heat flux by means of CHANNELHEAT as a function ot time. The plot in fig. 11 shows how well the results fit a constant heat flux as expected.

Steady-state temperature distribution for non-constant $\varkappa_1$. Although the results of the preceding example apply for both constant and non-constant heat conductivity of the fuel, the proper form of eq. (1) of subsection (a) in the latter case is

$$\varrho_1 c_1 \frac{\partial T}{\partial t} = P(t) + \frac{1}{r} \frac{\partial}{\partial r} \left(\varkappa_1 r \frac{\partial T}{\partial r} \right) .$$

On substitution of the expression $\frac{a}{b+T}$ for $\varkappa_1$ and of y for $\ln \frac{T+b}{T_o+b}$, T_o being the surface temperature, the equation is transformed to

$$\varrho_1 c_1 (T+b) \frac{\partial y}{\partial t} = P(t) + \frac{a}{r} \frac{\partial}{\partial r} \left(r \frac{\partial y}{\partial r} \right) .$$

Putting $\frac{\partial y}{\partial t} = 0$, we obtain the steady-state distribution

$$y(r) = \frac{1}{4} \frac{P(o)}{a} r_a^2 \left(1 - \left(\frac{r}{r_a}\right)^2\right)$$

and hence

$$T(r) = (T_o+b)\, e^{\frac{1}{4} \frac{P(o)}{a} r_a^2 \left(1 - \left(\frac{r}{r_a}\right)^2\right)} - b .$$

The library tape used in BRENDA assumes a $\varkappa_1$-variation as above with a = 4.5 kwatt/m and b = 100°K.

A calculation was performed with CHANNELHEAT with the values

$T_o = 689.5^oK$

$P(o) = 3.82o7 \cdot 10^5\ \mathrm{kwatt/m^3}$

$r_a = 0.006\ \mathrm{m}$.

A centre temperature of 1602°K was obtained as compared with the theoretical value according to the above considerations of 1598°K. The temperature distribution is plotted in fig. 12 for comparison with the expected one and that corresponding to a constant $\varkappa_1$-value (a parabola).

Temperature distribution with exponential power variation and constant $\varkappa_1$. Equation (1) of subsection (a) has a solution which is separable in space and time for the special case of an exponential power variation and times long enough for $T-T_o$ to follow this variation.

Defining $T-T_o = \theta(r)\ \tau(t)$, we obtain

$$\varrho_1 c_1\, \theta\, \frac{\partial \tau}{\partial t} - P(t) - \frac{\varkappa_1}{r}\left\{\tau \frac{\partial \theta}{\partial r} + \tau r \frac{\partial^2 \theta}{\partial r^2}\right\} = 0$$

$$\varrho_1 c_1 \frac{1}{\tau}\frac{\partial \tau}{\partial t} - \frac{P(t)}{\theta \tau} = \frac{\varkappa_1}{r}\frac{1}{\theta}\frac{\partial \theta}{\partial r} + \frac{\varkappa_1}{\theta}\frac{\partial^2 \theta}{\partial r^2} \quad .$$

$\tau(t) = \frac{P(t)}{P(o)} = e^{\frac{C}{\varrho_1 c_1} t}$ yields

$$\frac{\partial^2 \theta}{\partial r^2} + \frac{1}{r}\frac{\partial \theta}{\partial r} + \frac{P(o)}{\varkappa_1} - C\frac{\theta}{\varkappa_1} = 0 \quad .$$

If we put $\theta = a_o + a_1 r + a_2 r^2 + \ldots + a_p r^p + \ldots$,

this equation can be solved in a straightforward manner.

We arrive at the result

$$\theta(r) = \theta(o)\left\{1 + \left(1 - \frac{P(o)}{C\,\theta(o)}\right) \sum_{p=1}^{\infty} \frac{\left(\frac{C}{\varkappa_1} r^2\right)^p}{\prod_{i=1}^{p} (2i)^2}\right\} .$$

The boundary condition $\theta(r_a) = 0$ yields

$$\theta(o) = \frac{P(o)}{C} \quad \frac{\sum_{p=1}^{\infty} \frac{\left(\frac{C}{\varkappa_1} r_a^2\right)^p}{\prod_{i=1}^{p} (2i)^2}}{1 + \sum_{p=1}^{\infty} \frac{\left(\frac{C}{\varkappa_1} r_a^2\right)^p}{\prod_{i=1}^{p} (2i)^2}} \quad .$$

Hence, defining

$$L(Z) \equiv \sum_{p=1}^{\infty} \frac{Z^p}{\prod_{i=1}^{p} (2i)^2} \quad , \quad Z \equiv \frac{C}{\varkappa_1} r^2 \quad , \quad Z_a \equiv \frac{C}{\varkappa_1} r_a^2 \quad ,$$

we have

$$\theta(Z) = \theta(o) \left(1 - \frac{L(Z)}{L(Z_a)}\right)$$

$$\theta(o) = \frac{P(o)}{C} \quad \frac{L(Z_a)}{1+L(Z_a)} \quad .$$

For $C \to 0$ it can easily be shown that the expression for $\theta(Z)/\theta(o)$ converges towards the parabolic expression $1 - \left(\frac{r}{r_a}\right)^2$, valid for the steady-state case.

The series expansion for $L(Z)$ is quickly converging and has been calculated by means of GIER. Thus $\theta(Z)/\theta(o)$ and $\theta(r)/\theta(o)$ have been calculated for some different values of Z_a.

The results are shown in fig. 13.

With the values

ϱ_1 = 10900 kg/m^3

c_1 = 0.238 kJoule/kg/^{o}K

$\varkappa_1$ = 0.003 kwatt/m/^{o}K (special library tape)

r_a = 0.006 m

τ = 6.226 sec,

a computation was performed with CHANNELHEAT to simulate the above case. The Z_a-value corresponding to the given quantities is $Z_a = 5$. Fig. 14 shows a comparison between the distribution obtained and that expected, both at zero time (steady state) and at a time sufficient for the exponential increase to have manifested itself in the temperature of the fuel, in this particular case 15 sec.

Actually some further studies have been made of the time delay between the power increase and the heat-flux and fuel-temperature responses. The theory is a very simple extension of that developed above, but has been omitted here for simplicity. The main results, showing how the heat flux and fuel centre temperature gradually assume an exponential form, following the power increase with certain time delays, are given briefly in fig. 15.

(2) Determination of the transfer functions. From the results of subsection (a) the approximate transfer functions for a given fuel rod and their frequency range of validity can easily be determined.

If we use the values

$r_a = 0.006$ m

$r_b = 0.006$ m

$r_c = 0.0065$ m

$\varkappa_1 = 0.003$ kwatt/m/°K

$\varrho_1 = 10900$ kg/m^3

$c_1 = 0.238$ k Joule/kg/°K

$\varkappa_2 = 0.0125$ kwatt/m/°K

$\varrho_2 = 6570$ kg/m^3

$c_2 = 0.297$ k Joule/kg/°K

$k = 50$ kwatt/m^2/°K

$y = 0.05$ (kwatt/m^2/°K)$^{-1}$,

eq. (46) of subsection (a) yields

$\varepsilon = 0.108$,

while eq. (45) gives

$x = 7.79 \cdot s$.

Now, by means of eq. (44) or fig. 9, the transfer function $\overline{Y}_p(s) \cdot \frac{2r_c}{r_a^2}$ is obtained as shown in fig. 16.

The frequency limit of validity is determined by (47):

$$|x| \leq |x_o| = 200 \text{ sec}^{-1} ,$$

corresponding to

$$\omega \leq \omega_o = 26 \text{ sec}^{-1} .$$

However, this result has to be somewhat modified by reference to (49), say

$$\omega < 5 \text{ sec}^{-1} .$$

For comparison, a series of runs with CHANNELHEAT was performed to determine the transfer function for the above case. The coolant temperature was kept fixed, and the power density was given a small sinusoidal variation in time. After a few periods the amplitude and phase of the computed heat-flux response were determined. Thus, for each run a point of the transfer function corresponding to the frequency of the power oscillation was obtained.

It is evident that the time-step size as well as the radial-step size in fuel and cladding are very important for these calculations. Further it may be important whether the $\varkappa_1$-value is considered constant or not. As will be remembered, the theory of subsection (a) assumes a constant $\varkappa_1$-value.

For the basic series of runs a time-step size of 1/20 of the power oscillation period was used. The radial-step size in the cladding was made equal to the cladding thickness, and in the fuel a "sufficiently" small value was used, varying from 1/6 to 1/12 of the fuel radius. The results from this basic series are shown in fig. 16. The series was performed both with constant (special library tape) and non-constant $\varkappa_1$-value. It appears from fig. 16 that (so long as only small variations are considered) a properly chosen constant $\varkappa_1$-value represents a very usable approximation if only the heat-flux response is of interest. The centre temperature, however, is strongly influenced by the $\varkappa_1$-variation.

As to the general agreement with theory, it appears that the amplitude response fits well while there is a phase deviation increasing to some 10 degrees at $\omega \sim 3 \text{ sec}^{-1}$.

From the theory of subsection (a) it is evident that the phase response is the more dependent on the properties of the cladding the higher the frequency. Hence, two extra runs were performed, at the frequencies $\omega \sim 0.3$ sec^{-1} and $\omega \sim 3$ sec^{-1}, in which the number of mesh points in the cladding was increased from 2 to 5. The points obtained by these runs are marked in fig. 16. The effect of the alteration is apparently small at the lower frequency while a considerable decrease of the deviation from the theoretical curve is obtained at the higher frequency. However, it may be concluded that for most applications two mesh points in the cladding will be sufficient as frequencies higher than a few sec^{-1} are usually not dominating.

To study the effect of the step size in the fuel, the number of mesh points in the cladding was fixed at 2, and two additional runs were performed at each of the frequencies $\omega \sim 0.3$ sec^{-1} and $\omega \sim 1$ sec^{-1}. For these runs the number of mesh points in the fuel was varied upwards and downwards from the value of the basic series run. The variations in amplitude and phase as functions of the number of mesh points in the fuel are plotted in fig. 17 for each of the two frequencies.

The use of finite difference equations for the solution of the heat-conduction equation corresponds to a second-order Taylor expansion of the fuel-temperature distribution around each mesh point. Hence it seems natural to assume that the condition for a good performance is that the second-order term in this expansion is small. As this term contains the step size in the second power and the frequency in the first power (see e.g. the theory of subsection (a)), it may be required that $\omega/(p-1)^2$, where p is the number of mesh points, is small as compared with some constant that is independent of the physical system.

Application of these considerations to the results of fig. 17 suggests that the condition $(p-1)^2 > 150\ \omega$ may be used to determine a proper value of the number of mesh points in the fuel as a function of frequency.

Finally, an attempt was made to determine the proper size of the time step. This was done simply by performing two extra runs at one frequency, $\omega \sim 0.3$ sec^{-1}, keeping the same radial step sizes as in the basic series run, but with half and double time-step size.

The results, shown in fig. 17, indicate that a time step of 1/20 power oscillation period is a suitable choice.

4. Hydraulics

The differential equation used for the mathematical treatment of the thermodynamic effects in the cooling channel has the form

$$\frac{\delta y}{\delta t} + g \frac{\delta y}{\delta x} = f(x, t) \quad .$$

How this equation has been transformed to a finite difference equation is described in chapter I, section 4.

In the following a discussion is given of the convergence of the solution obtained towards the solution of the differential equation in terms of the step sizes in the directions of the two co-ordinate axes.

The discussion concludes in a method for determining proper values of these step sizes.

(a) Convergence properties of the difference equation

Introduction. The aim of the present analysis is to provide a means of determining proper step sizes in the two co-ordinate directions when applying the finite difference approximation

$$\frac{y_j^n - y_j^{n-1}}{2dt} + \frac{y_{j-1}^n - y_{j-1}^{n-1}}{2dt} + g \frac{y_j^n - y_{j-1}^n}{dx} = \frac{q_j^n + q_{j-1}^n}{2ro \cdot ce} \qquad (1)$$

to the differential equation

$$\frac{dy}{dt} + g \frac{dy}{dx} = \frac{q(x, t)}{ro \cdot ce} \quad . \qquad (2)$$

The form of the right side of eq. (2) has been chosen to make the results directly applicable in connection with BRENDA.

The investigation is carried out as follows:

First the complete solution to the differential equation is provided. It appears to be composed of two different types of functions, the "particular" and the "homogeneous" solution. Next, the corresponding "particular" and "homogeneous" solutions to the difference equation are obtained. At last, the errors introduced into these finite difference solutions are evaluated and discussed.

Complete solution of the differential equation. The differential equation (2) has the complete solution

$$y = F(u) + \sum_{p,\omega} Y_p^{\omega} \quad , \tag{3}$$

where u denotes an arbitrary solution to the homogeneous equation and f is an arbitrary function of u. $\sum_{p,\omega} Y_p^{\omega}$ represents a particular solution to (2) according to a forcing function of the type

$$q = \sum_{p,\omega} q_{o,p}^{\omega} \exp(i(\frac{p\pi}{L} x + \omega t + \phi_o^{\omega})) \quad . \tag{4}$$

In the following we shall discuss the constituents of (3), keeping an eye on the special application in BRENDA.

The simple form of u

$$u = \omega (t - \frac{x}{g}) \tag{5}$$

can be adopted without any loss of generality.

On the assumption, as in BRENDA, that the value of y at x = 0 is given as a function of t while $\sum_{p,\omega} Y_p^{\omega}(x=0) = 0$ for all t, F(u) can be determined:

$$F(u) = \sum_{\omega} a_{\omega} \exp(i (u + \phi_1^{\omega})) \tag{6}$$

when

$$y(x=0) = \sum_{\omega} a_{\omega} \exp (i (\omega t + \phi_1^{\omega})) \quad . \tag{7}$$

The terms Y_p^{ω} of the particular solution corresponding to the forcing function (4) can, as is readily verified, be expressed as

$$Y_p^{\omega} = \frac{q_{o,p}^{\omega}}{ro \cdot ce} \cdot \frac{L}{gp\pi + \omega L} \exp(i (\frac{p\pi}{L} x + \omega t + \phi_o^{\omega} - \frac{\pi}{2})). \tag{8}$$

For the above-mentioned condition, $\sum_{p,\omega} Y_p^{\omega}(x=0) = 0$ for all t, to be fulfilled, a term that is a function of u alone must be added to the right side of (8). This has been omitted for simplicity.

Particular solution to the difference equation. Corresponding to eq. (4), the following forcing function is adopted:

$$q_j^n = q_o \exp(i(\omega ndt + \frac{p\pi}{L} jdx + \phi_o^\omega)). \tag{9}$$

The particular solution to (1) can be written in the form

$$y_j^n = \frac{q_o}{ro \cdot ce} \cdot \frac{L}{gp\pi + \omega L} \beta_p^\omega \exp(i(\omega ndt + \frac{p\pi}{L} jdx + \phi_o^\omega - \frac{\pi}{2})) , \tag{10}$$

where β_p^ω is a complex number to be determined through substitution:

$$\frac{q_o}{ro \cdot ce} \cdot \frac{L}{gp\pi + \omega L} \frac{\beta_p^\omega}{2idt} \left\{ 1 - \exp(-i\omega dt) + \exp(-i\frac{p\pi}{L} dx) - \exp(-i\omega dt - i\frac{p\pi}{L} dx) \right.$$

$$\left. + 2g\frac{dt}{dx}(1 - \exp(-i\frac{p\pi}{L} dx)) \right\} = \frac{q_o}{ro \cdot ce} \cdot \frac{1}{2}(1 + \exp(-i\frac{p\pi}{L} dx)) .$$

With the substitutions

$a \equiv \omega dt$ and $c \equiv 2g\frac{dt}{dx}$ this gives

$$\beta_p^\omega = \frac{gp\pi + \omega L}{\omega L} \frac{a}{\sin a + c\, tg(\frac{gp\pi}{\omega L} \frac{a}{c}) - i(1 - \cos a)} . \tag{11}$$

Splitting into amplitude and phase, we have

$$|\beta_p^\omega| = \frac{gp\pi + \omega L}{\omega L} a / \sqrt{(\sin a + c\, tg(\frac{gp\pi}{\omega L} \frac{a}{c}))^2 + (1 - \cos a)^2} ; \tag{12}$$

$$v = \text{Arctg} \frac{1 - \cos a}{\sin a + c\, tg \frac{gp\pi}{\omega L} \frac{a}{c}} . \tag{13}$$

Special cases:

I: $\omega = 0$:

$$|\beta_p^o| = \frac{\frac{p\pi}{2L}dx}{tg(\frac{p\pi}{2L}dx)} \sim 1 - \frac{1}{3}(\frac{p\pi}{2L}dx)^2 \quad \text{for } \frac{p\pi}{2L}dx << 1; \quad v=0; \tag{14}$$

II: $p = 0$:

$$|\beta_o^\omega| = \frac{a/2}{\sin a/2} \sim 1 + \frac{1}{24}a^2 \text{ for } a << 1; \quad v = \frac{a}{2} \; . \tag{15}$$

Homogeneous solution to the difference equation. Corresponding to eqs. (5) and (6), the solution to eq. (1) (the homogeneous part) is written

$$y_j^n = a_\omega (\xi_\omega)^j \exp(i(u + \phi_1^{(\omega)})) \; , \quad u = \alpha n - \frac{2a}{c} j \; , \tag{16}$$

where the quantities a and c, defined in the preceding subsection, have been introduced, and the complex number ξ_ω is interpreted as the amplification per step in the x-direction.

ξ_ω is determined by substitution:

$$1-\exp(-ia)+(\xi_\omega)^{-1}\exp(i\tfrac{2a}{c})-(\xi_\omega)^{-1}\exp(-ia+i\tfrac{2a}{c})+c(1-(\xi_\omega)^{-1}\exp(i\tfrac{2a}{c})) = 0$$

$$\xi_\omega = -\frac{1 - c - \exp(-ia)}{1 + c - \exp(-ia)} \exp(i\frac{2a}{c}) \; . \tag{17}$$

Splitting into amplitude and phase, we have

$$|\xi_\omega| = \sqrt{\frac{c^2 + (1-c)\varkappa^2}{c^2 + (1+c)\varkappa^2}} \; , \qquad \varkappa = 2\sin\frac{a}{2} \; ; \tag{18}$$

$$\gamma_\omega = \text{Arctg}\frac{\sin a}{1-c-\cos a} - \text{Arctg}\frac{\sin a}{1+c-\cos a} + \frac{2a}{c} - (1-\text{sign}(c-\frac{\varkappa^2}{2}))\frac{\pi}{2} \; . \tag{19}$$

In the limit of $a << 1$, $\left|\frac{a}{c}\right| << 1$, (18) and (19) lead to the approximations

$$|\xi_\omega| \simeq 1 - \frac{a^2}{c}$$

$$\gamma_\omega \simeq \frac{1}{3}\frac{a^3}{c} + \frac{2}{3}\frac{a^3}{c^3} \quad . \tag{20}$$

It is noticed that, while (17) and (18) are applicable for all values of a, (19) is restricted to $0 \leq a \leq \pi$.

Convergence of the particular solution. Examination of eqs. (14) and (15) yields the general result that for harmonics of a high order in the x-direction no important phase error is introduced, while the amplitude may be considerably reduced.

For rapid oscillations in the time direction, however, the amplitude is only slightly altered while the main effect is a phase deviation.

Thus for the determination of suitable step sizes in either direction eq. (14) should be used to control the amplitude while for the phase eq. (15) should be applied.

Hence the conditions to be fulfilled are

$\frac{p\pi}{2L}$ dx/tg($\frac{p\pi}{2L}$ dx) near to unity for all relevant p's. (21)

$\frac{a}{2} = \frac{\omega dt}{2}$ near to zero for all relevants ω 's . (22)

The function of condition (21) is plotted in fig. 18.

Convergence of the homogeneous solution. According to eqs. (16), (18) and (19), the total amplitude amplification and phase deviation at x = 1 are

$$|\xi_\omega^1| = \sqrt{\frac{c^2 + (1-c)\varkappa^2}{c^2 + (1+c)\varkappa^2}}^{\frac{1}{dx}} \tag{23}$$

$$\gamma_\omega^1 = \frac{1}{dx}\left\{\operatorname{Arctg}\frac{\sin\alpha}{1-c-\cos\alpha} - \operatorname{Arctg}\frac{\sin\alpha}{1+c-\cos\alpha} + \frac{2\alpha}{c} - (1-\operatorname{sign}(c-\frac{\varkappa^2}{2}))\frac{\pi}{2}\right\}. \quad (24)$$

If we introduce the quantities

$$|\xi_\omega^0| = \sqrt{\frac{c^2 + (1-c)\,\varkappa^2}{c^2 + (1+c)\,\varkappa^2}}^{\frac{c}{2\alpha}}, \quad (25)$$

$$\gamma_\omega^0 = 1 + \frac{c}{2\alpha}\left\{\operatorname{Arctg}\frac{\sin\alpha}{1-c-\cos\alpha} - \operatorname{Arctg}\frac{\sin\alpha}{1+c-\cos\alpha} - (1-\operatorname{sign}(c-\frac{\varkappa^2}{2}))\frac{\pi}{2}\right\}, \quad (26)$$

eqs. (23) and (24) are reduced to

$$|\xi_\omega^1| = |\xi_\omega^0|\,\frac{1\omega}{g}, \quad (27)$$

$$\gamma_\omega^1 = \frac{1\omega}{g}\cdot\gamma_\omega^0. \quad (28)$$

$|\xi_\omega^0|$ and γ_ω^0 can be interpreted as amplitude amplification and phase deviation at $x = \frac{g}{\omega}$. Fig. 20 shows a diagram presenting curves of constant ξ_ω^0 and γ_ω^0 in the c-$\varkappa$ -plane, computed by the GIER computer on the basis of eqs. (25) and (26).

It appears that $\alpha = \omega dt$ should be as small as possible, while it is not immediately clear what value should be assigned to c. Of course a smaller c (for given α) means a larger step size dx and hence a shorter computing time for the problem given. However, there is apparently a prohibitive increase in γ_ω^0 when c goes to zero for fixed $\varkappa$.

As a suitable criterion for the choice of c it may be required that the quadratic sum of relative amplitude decrease and phase deviation is at a minimum, $\varkappa$ being kept constant:

$$\frac{d}{dc}\left\{(|\xi_\omega^0| - 1)^2 + (\gamma_\omega^0)^2\right\} = 0.$$

From eqs. (25) and (26) we may obtain

$$\frac{d}{dc}\,|\xi_\omega^o| = \frac{c}{2a}\,|\xi_\omega^o|^{\frac{c-4a}{c}}\,\frac{\varkappa^2(c^2-\varkappa^2)}{(c^2+(1+c)\varkappa^2)^2}\;; \tag{30}$$

$$\frac{d}{dc}\,\gamma_\omega^o = \frac{\gamma_\omega^o - 1}{c} + \frac{c}{a}\cdot\frac{\sin a(c^2+\varkappa^2)}{(c^2+(1+c)\varkappa^2)(c^2+(1-c)\varkappa^2)}\;. \tag{31}$$

Eq. (29) leads to

$$2(|\xi_\omega^o| - 1)\,\frac{d}{dc}\,|\xi_\omega^o| + 2\,\gamma_\omega^o\,\frac{d}{dc}\,\gamma_\omega^o = 0\;. \tag{32}$$

Solving eq. (32), using (30) and (31), by means of the GIER computer, we have obtained a series of corresponding values of $\varkappa$ and c and plotted them in the diagram of fig. 20 (the curve labelled "optimum"). As the combined quadratic error increases rapidly to the left of this curve, while only a slight variation is noticed to the right, it is concluded that c may be chosen at any (not exorbitantly large) value to the right of "optimum" without spoiling the convergence of the desired solution to (1). To keep the computing time at a minimum, c should be chosen as near to "optimum" as allowed by the condition (21).

For practical reasons the minor (most frequently applied) part of the diagram in fig. 20 has been transferred to fig. 19 on a larger scale.

Conclusion. The error introduced on application of (1) instead of (2) is described in terms of an amplitude amplification and a phase deviation for the actual Fourier components involved, considered as functions of the step sizes dx and dt.

The investigations have been carried out separately for the "particular" solution and the "homogeneous" solution. Applied to the code BRENDA, the former corresponds to the heat inflow considered as a forcing function, while the latter corresponds to the inlet temperature as a function of time considered as a boundary condition.

Once acquainted with the method, the user may apply it very easily through the diagrams of figs. 18-20 in connection with the conditions (21) and (22).

(b) Computer runs

Calculation of boiling boundary in a cooling channel. Assume the forcing function

$$q = q_o \sin(\frac{\pi}{L} x)(1 + \frac{dq}{q_o} \sin(\omega_o t))$$

and the boundary condition

$$T_{inlet} = T_o + dT \sin(\omega t) \quad .$$

Using the complex formulation

$$q=q_o \exp(i(\frac{\pi}{L}x - \frac{\pi}{2})) - \frac{dq}{2}(\exp(i(\frac{\pi}{L}x + \omega_o t)) - \exp(i(\frac{\pi}{L}x - \omega_o t)))$$

and applying eq. (8), paying regard to the comment below it, we obtain the particular solution

$$T_p(x,t) = \frac{L}{ro \cdot ce \cdot g \cdot \pi} \Big\{ (1-\cos(\frac{\pi}{L}x))\,(q_o + dq \sin(\omega_o t))$$

$$+ dq(-\sin(\omega_o t) + \frac{1}{2}\frac{\omega_o L}{\omega_o L + g\pi}(\sin(\omega_o t + \frac{\pi}{L}x)$$

$$+ \frac{g\pi}{\omega_o L}\sin(\omega_o t - \frac{\omega o}{g}x)) - \frac{1}{2}\frac{\omega_o L}{-\omega_o L + g\pi}(\sin(\omega_o t - \frac{\pi}{L}x)$$

$$- \frac{g\pi}{\omega_o L}\sin(\omega_o t - \frac{\omega_o}{g}x))) \Big\} \quad .$$

The homogeneous solution corresponding to the boundary condition is

$$T_h(x,t) = T_o + dT \sin(\omega t - \frac{\omega}{g}x), \quad \text{using (6).}$$

The boiling boundary, denoted BB, is determined by intersecting the temperature surface over the x-t-plane with the plane $T_s(x) = T_{so} + \frac{dT_s}{dx}(BB-x_o)$, picturing the saturation temperature, a constant external pressure assumed:

$$T_s(BB) = T_p(BB, t) + T_h(BB, t) \quad . \tag{33}$$

From this equation BB is determined as a function of t.

A calculation according to (33) has been performed by means of the GIER computer, with the values

$L = 1.5$ m

$q_o = 42000$ kwatt/m^3

$dq = 4200$ kwatt/m^3

$\omega_o = \frac{2\pi}{5}$

$T_o = 504.6^oK$

$dT = 1\ ^oK$

$\omega = 2\pi$

$ro = 10^3$ kg/m^3

$ce = 1.121$ cal/g $^oK = 4.700$ kJoule/kg ^oK

$g = 1$ m/sek

$T_{so} = 505.915\ ^oK$ (corresponding to a pressure of 30 ata)

$\frac{dT_s}{dx} = -0.178440\ ^oK/m$ (fitted value from table)

$x_o = 0$.

The curve obtained is plotted in the diagram of fig. 21, labelled "Exact solution, differential eq.".

Modifying (33) by introducing the quantities β_p^ω and ξ_ω^{BB}, we can obtain the exact solution to the difference equation.

Choosing dx = 0.1 m and dt = 0.025 seconds, we performed this work by means of GIER, with the very permissible approximation $\beta_p^\omega = 1$, thus using only eqs. (25)-(28). The resulting curve is shown in the diagram, labelled "Exact solution, difference eq.".

Finally the solution to the difference equation was obtained by application of the programme CHANNELHEAT. The boiling-boundary values according to this calculation are plotted in the diagram by circled points. The small discrepancies noticed at some of the upper peaks of the "exact" solution may be due to the approximation $\beta_p^\omega = 1$ in connection with the fact that

CHANNELHEAT uses values of the saturation temperature obtained by interpolation in a table, contrary to the approximation of a linear dependence used above.

The main conclusion of the example is that the agreement is quite satisfactory.

5. Transient Runs with BRENDA

In the foregoing it has been described how a numerical and mathematical testing of the different parts of BRENDA has been carried through.

In order to find out whether or not these parts of the total code have been coupled together in the right way and co-operate satisfactorily, transient runs with BRENDA have been performed. In these runs a sinusoidal variation was applied to one of the independent variables, and the response of some of the most important dependent variables was measured by amplitude and phase after the initial response had been damped out (i. e. after five periods had elapsed). The amplitude of the perturbation was chosen sufficiently small to justify a comparison with the linear transfer function model of the channel described in ref. 11.

Because of time and space limitations connected with the use of BRENDA, it was only possible to obtain a set of linear response measurements at one frequency, $\omega = 1.57\ \text{sec}^{-1}$, corresponding to a period of 4 seconds.

The number of mesh points along the channel was chosen to be 16 while 7 radial mesh points were used in the fuel and 2 in the cladding. The calculations were carried out in the IBM 7090 facility at NEUCC with the ILLINOIS ALGOL version mentioned in the next section.

The computing time for each problem was about 40 minutes.

The table below lists the results obtained with BRENDA and the corresponding results of the linear model, read from the curves of ref. 11.

It is seen that the agreement is generally within 2.5 dB for the amplitudes and about 20 degrees for the phases. Considering the many approximations necessary to carry through the analytical calculations of the linear model, this must be said to be satisfactory and indicates no errors in the performance of BRENDA.

	BRENDA		Linear model	
	Amplitude/ dB	Phase/deg.	Amplitude/dB	Phase/deg.
$\delta Tf/\delta k_i$	77.0	-68	75.5	-74
$\delta P/\delta k_i$	152.8	9	151.9	6
$\delta Q/\delta k_i$	130.8	-36	129.9	-48
$\delta \alpha/\delta k_i$	17.6	-50	18.1	-68
$\delta BB/\delta k_i$	~20	117	17.1	109
$\delta Tf/\delta p$	2.9	-54	2.9	-41
$\delta P/\delta p$	77.5	27	78.1	40
$\delta Q/\delta p$	53.6	-63	53.9	-53
$\delta \alpha/\delta p$	-38.2	217	-37.5	216
$\delta BB/\delta p$	-28.0	0	-28.8	1
$\delta Tf/\delta T_{inlet}$	0.4	40	-0.5	26
$\delta P/\delta T_{inlet}$	76.4	126	75.9	106
$\delta Q/\delta T_{inlet}$	54.4	90	53.5	53
$\delta \alpha/\delta T_{inlet}$	-43.1	-72	-40.6	-75
$\delta BB/\delta T_{inlet}$	-28.0	126	-28.2	125
$\delta Tf/\delta V_{inlet}$	27.5	-90	29.4	-94
$\delta P/\delta V_{inlet}$	103.3	-14	105.8	-14
$\delta Q/\delta V_{inlet}$	81.5	-59	83.8	-68
$\delta \alpha/\delta V_{inlet}$	-11.9	166	-10.5	167
$\delta BB/\delta V_{inlet}$	-8.0	-18	-11.5	-16

The testing method referred to above is clearly rather unsatisfactory because BRENDA has many aspects beyond those considered in the linear model. Especially the space-dependent and non-linear properties of the code have still not been properly investigated. However, because of the immense amount of computing time required, further testing has to be carried out alongside with the use of the code within the tested domain. As mentioned earlier, a very valuable part of the testing programme has to be postponed until relevant experimental results are available for comparison.

6. Concluding Remarks

The first conclusion to be drawn from the preceding discussion is that the computer model seems to be in accordance with the intended mathematical model.

Next, several important restrictions have to be mentioned:

(a) Physical restrictions

The model assumes that variations in coolant inlet velocity and inlet temperature as well as in system pressure and moderator temperature are controlled from outside. This means that the model is restricted to cases of forced circulation. Inclusion of the case of natural circulation would imply the introduction of a pressure-drop representation within the cooling channel and a detailed description of the rest of the circulation loop, including the moderator. Hence it would mean a considerable extension of the code and of the computing time, which is absolutely prohibitive as long as the code is to run in the GIER computer.

The simulated control system has the major deficiency that the control absorption is assumed to retain its spatial distribution during the time variations.

Further it should be noted that only bulk boiling in the channel is considered, i. e. there is assumed to be no void in the subcooled region. It should also be remembered that the assumption of a constant slip ratio between the velocities of steam and water in the channel is an approximation, although probably not a serious one.

Because of the one-delayed-group approximation used in the description of the neutron kinetics the code is not fit for simulating shut-down conditions or other conditions with large negative reactivities of long duration.

(b) Numerical restrictions

The coding technique used for solving the differential equations of course means a restriction of the applicability of the code.

As appears from the discussion, care must be taken to choose proper values of axial, radial and time-step lengths, regard being paid to the frequency range of the variations of the physical quantities in question. For rapid oscillations it may be necessary to introduce a very fine network in space and time to secure a reliable performance.

This, in turn, will increase the requirements of storage room in the computer and of computing time. Hence an upper frequency limit will always exist in practical problems.

(c) Time restrictions

As the code makes extensive use of the iteration technique, it is very difficult to give a general estimate of the computing time. However, in one case, with 8 axial and 6 radial mesh points and a time step of 0.2 seconds, 9 seconds of real time was simulated by 6 hours of computing time. In this case the control-system reactivity was given a sinusoidal variation of a period of 4 seconds and an amplitude of about 100 p.c.m. Thus the ratio of computing time to real time was approximately 2500. The reason for this large ratio is, partly, that the GIER computer has a very small fast memory, requiring extensive use of the drum store, which has a very long access time.

To overcome this handicap the code has been given a form (ILLINOIS ALGOL language) that permits the use of an IBM 7090 facility. This has reduced the computing time by a factor of approximately 25. However, there are still some problems to be solved in connection with the use of the 7090 version at the Northern Europe University Computing Centre (NEUCC), Lyngby, Denmark. These problems mainly concern the proper presentation of the results since a plotter facility similar to that used in connection with the GIER computer is not yet available.

Nevertheless, the reduction in computing time obtained indicates that it will be meaningful to extend the code to represent the total circulation loop and hence to include the case of natural circulation.

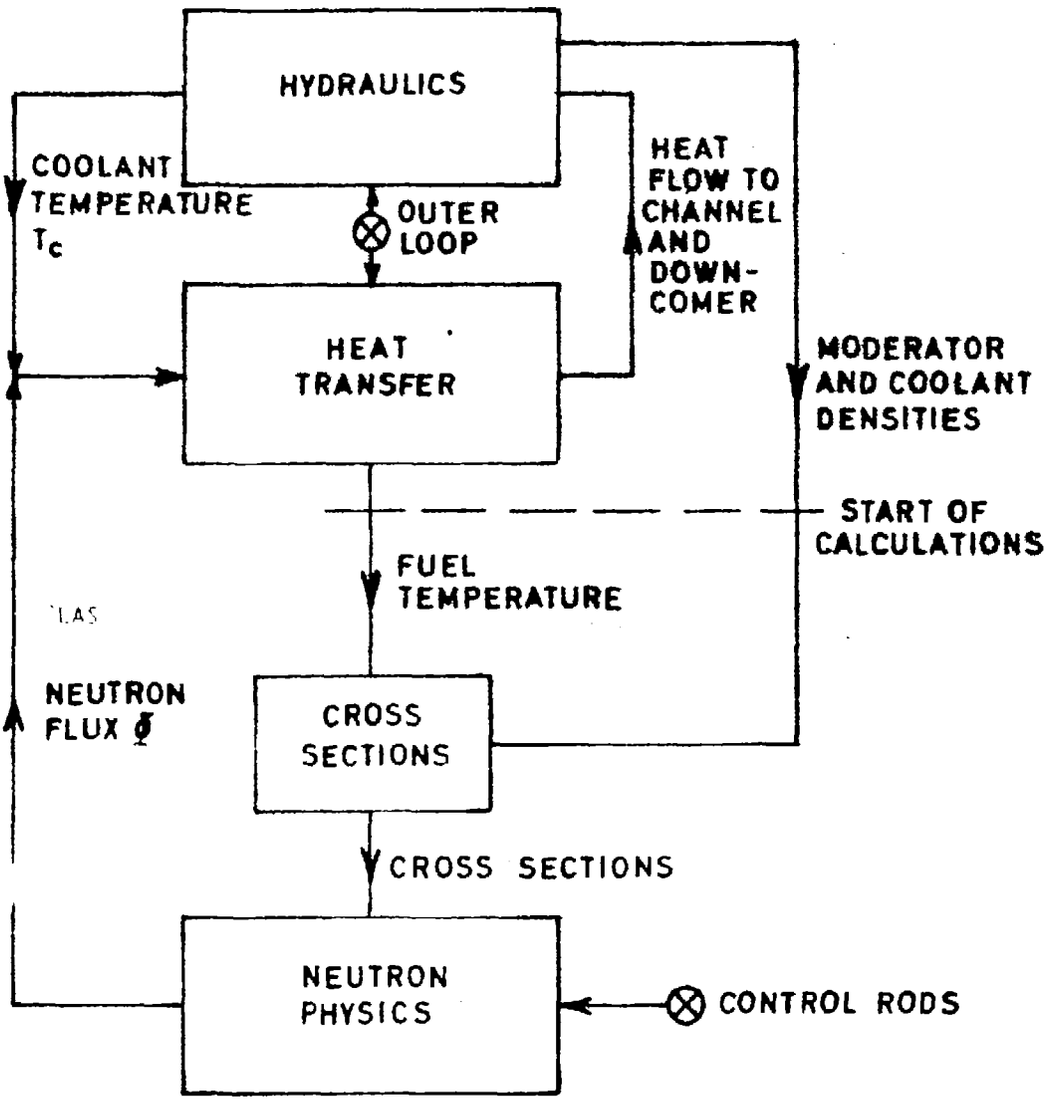

SCHEME OF DYNAMIC MODEL

Fig.1

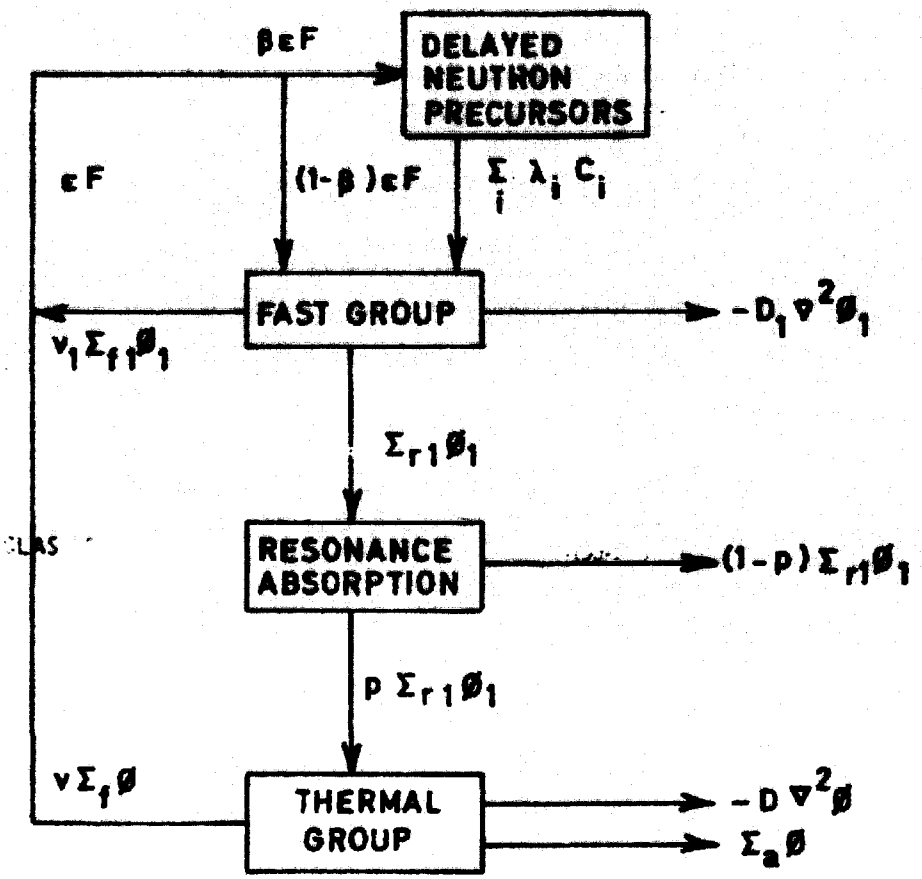

NEUTRON BALANCE SCHEME

Fig. 2

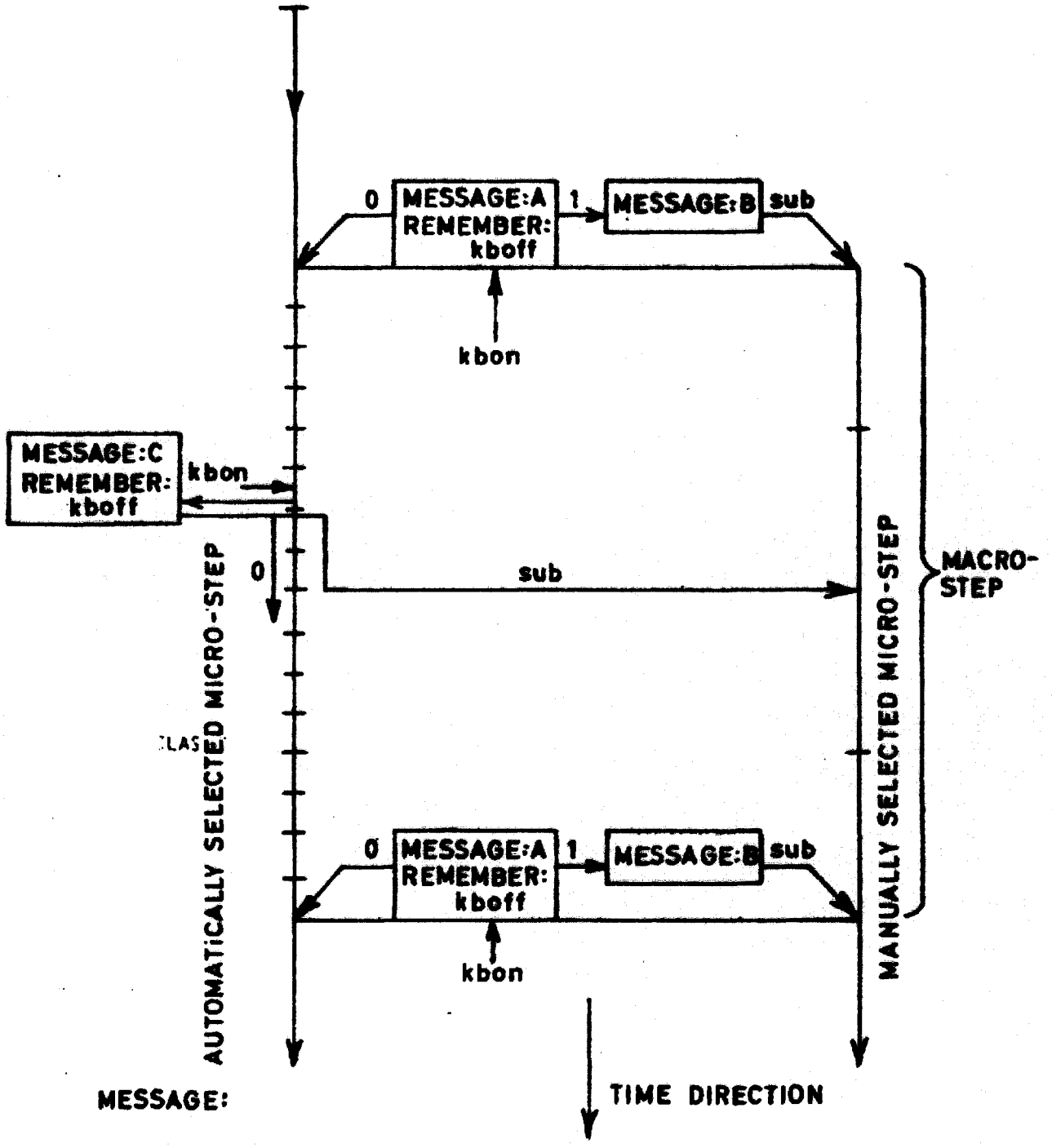

A: sub = xx

FOR AUTOMATIC STEP SIZE TYPE 0, ELSE 1:

B: TYPE VALUE OF SUB:

C: VALUE OF SUB SELECTED: XX
[OR: VALUE OF SUB NOT SELECTED. TEMPORARY VALUE = XX]

TO CONTINUE TYPE 0, ELSE SPECIFY FIXED VALUE OF SUB:

Fig.3

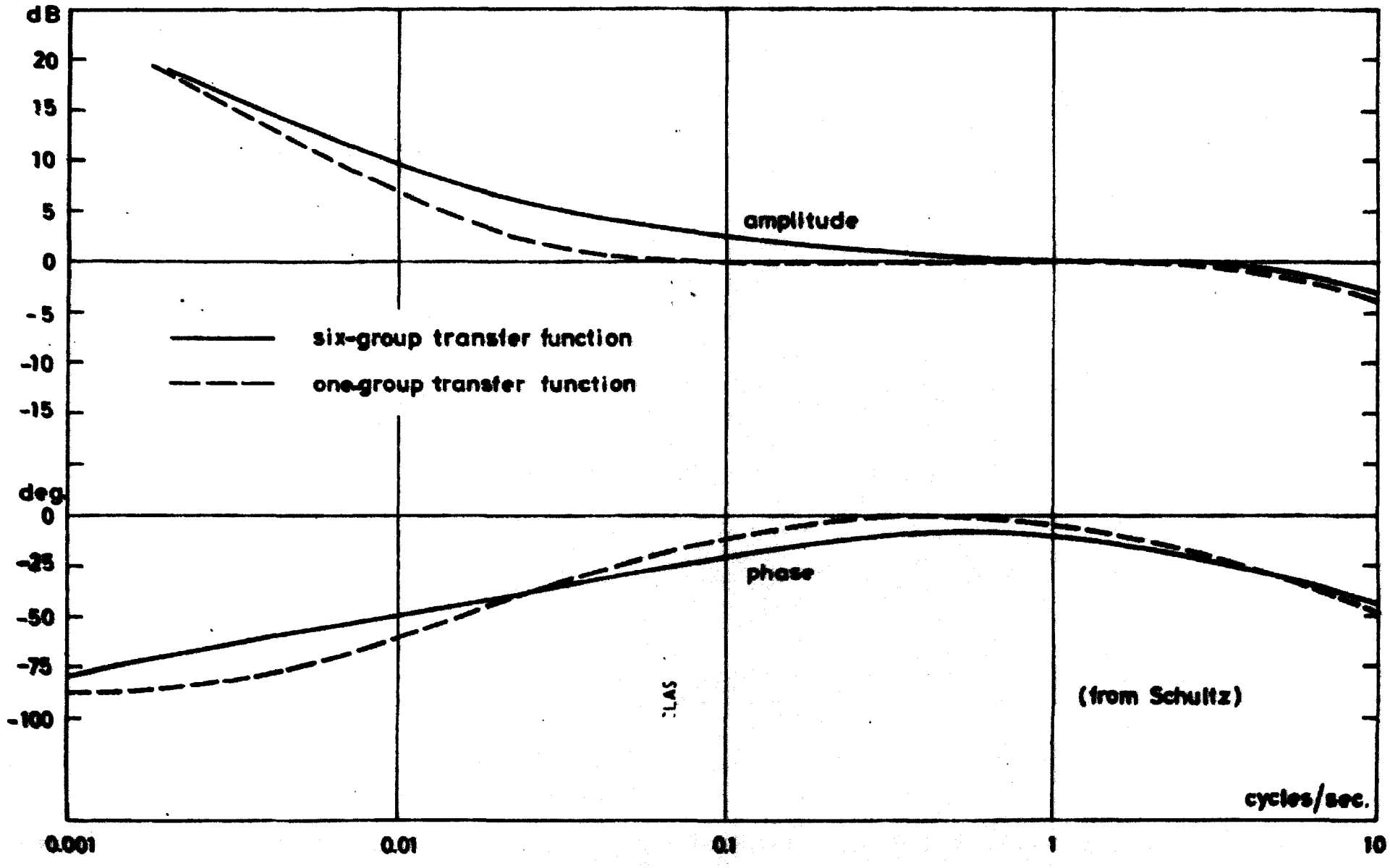
dB
20
15
10
5
0
-5
-10
-15
amplitude
six-group transfer function
one-group transfer function
deg.
0
-25
-50
-75
-100
phase
(from Schultz)
cycles/sec.
0.001
0.01
0.1
1
10

Fig.4

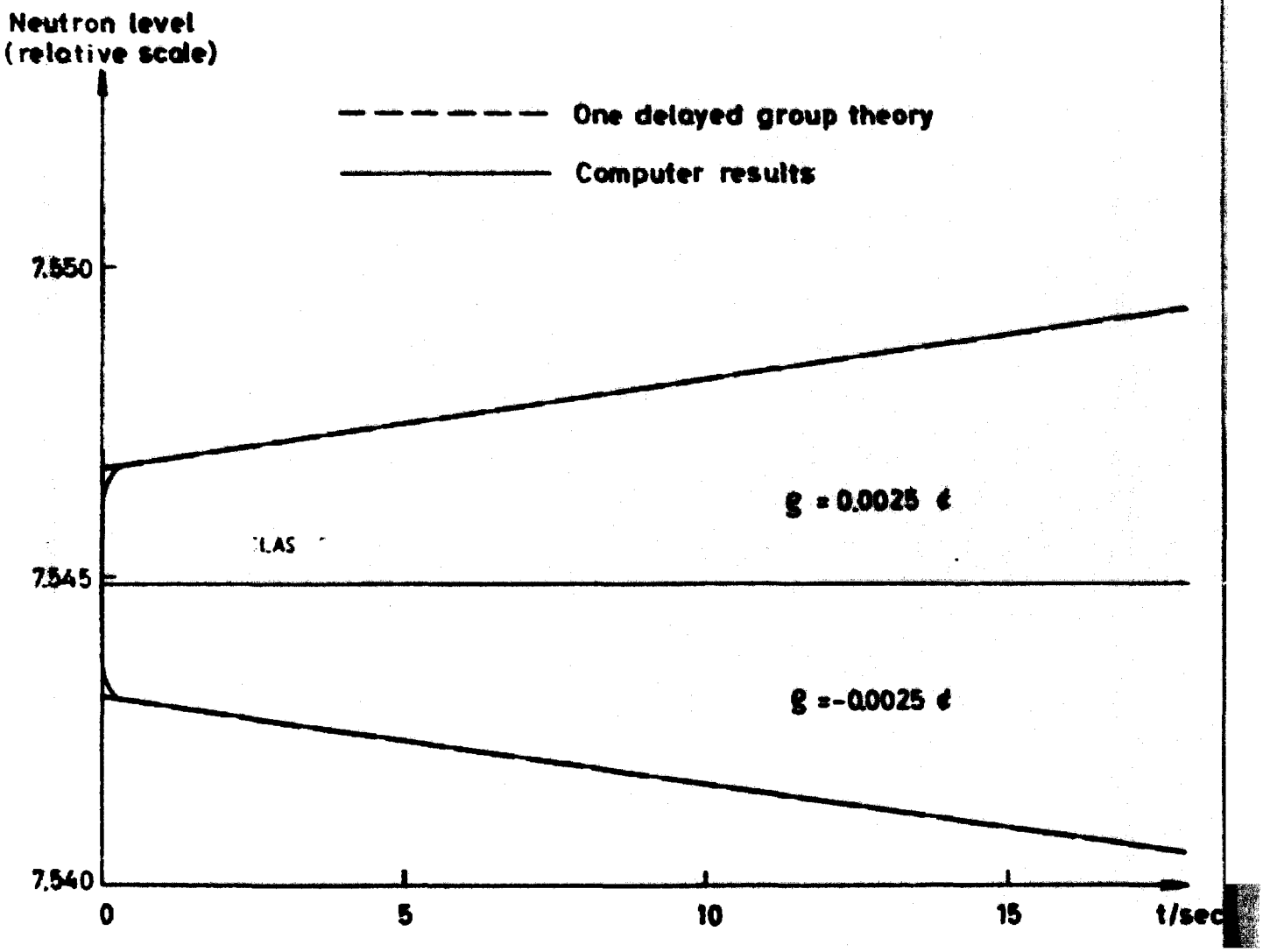
Neutron level
(relative scale)
One delayed group theory
Computer results
7.550
7.545
7.540
ρ = 0.0025 ¢
ρ = -0.0025 ¢
0
5
10
15
t/sec

Fig.5

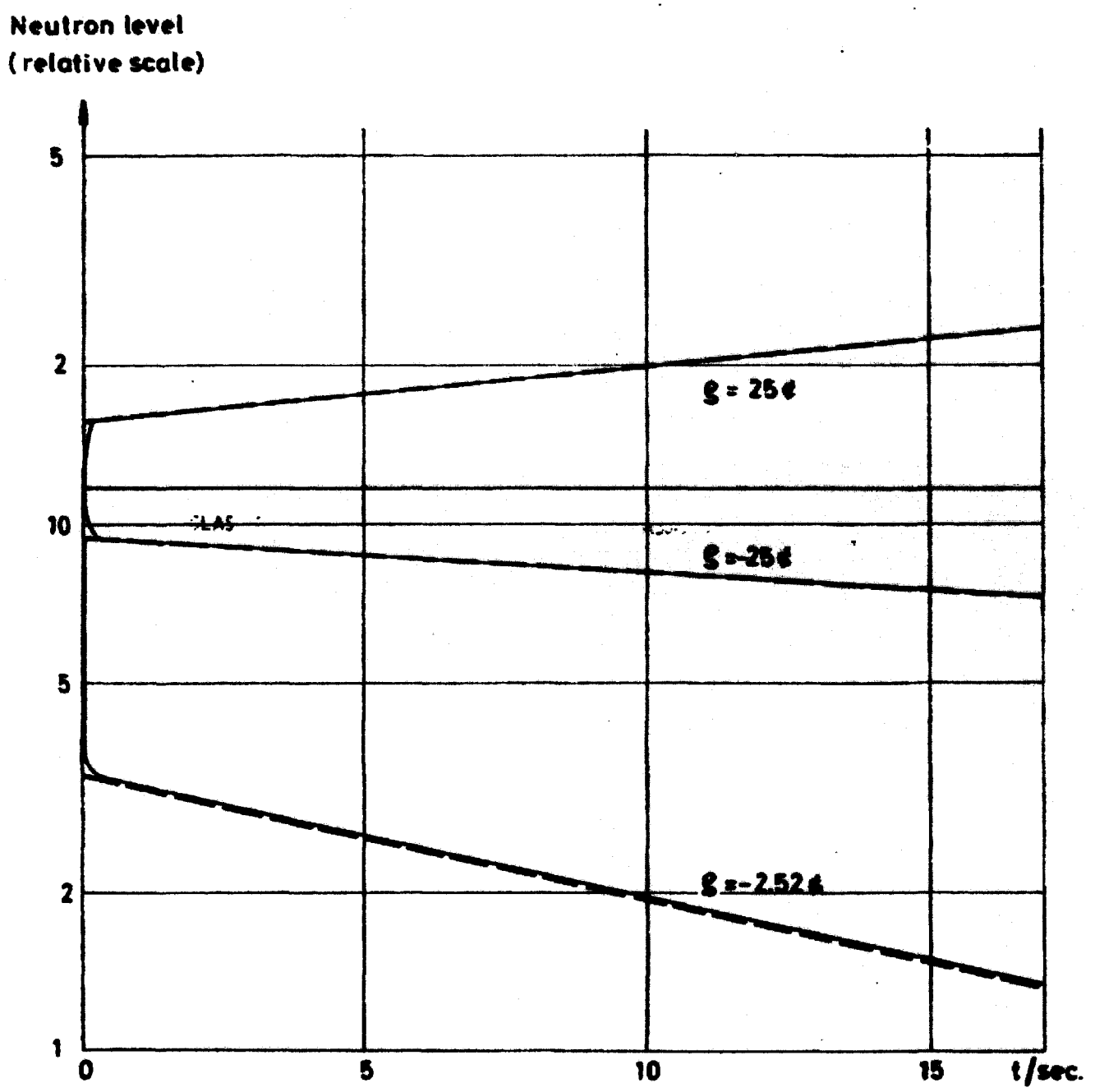
One delayed group theory
Computer results
Neutron level
(relative scale)
5
2
10
5
2
1
0
5
10
15
t/sec.
ρ = 25¢
ρ = -25¢
ρ = -2.52¢

Fig.6

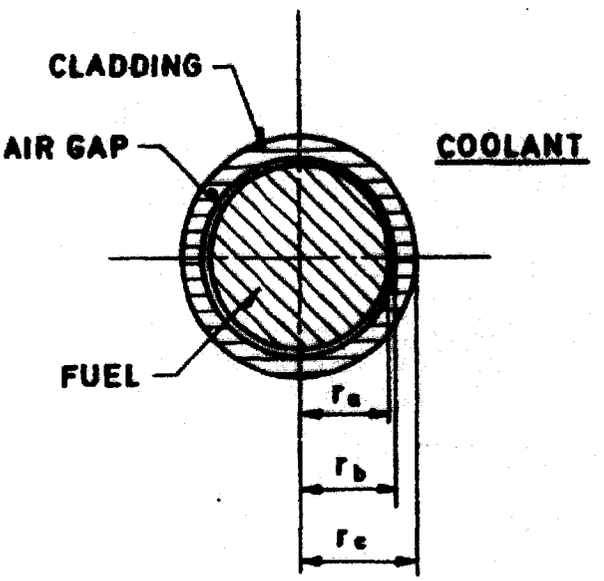

CROSS SECTION OF THE SYSTEM

Fig. 7

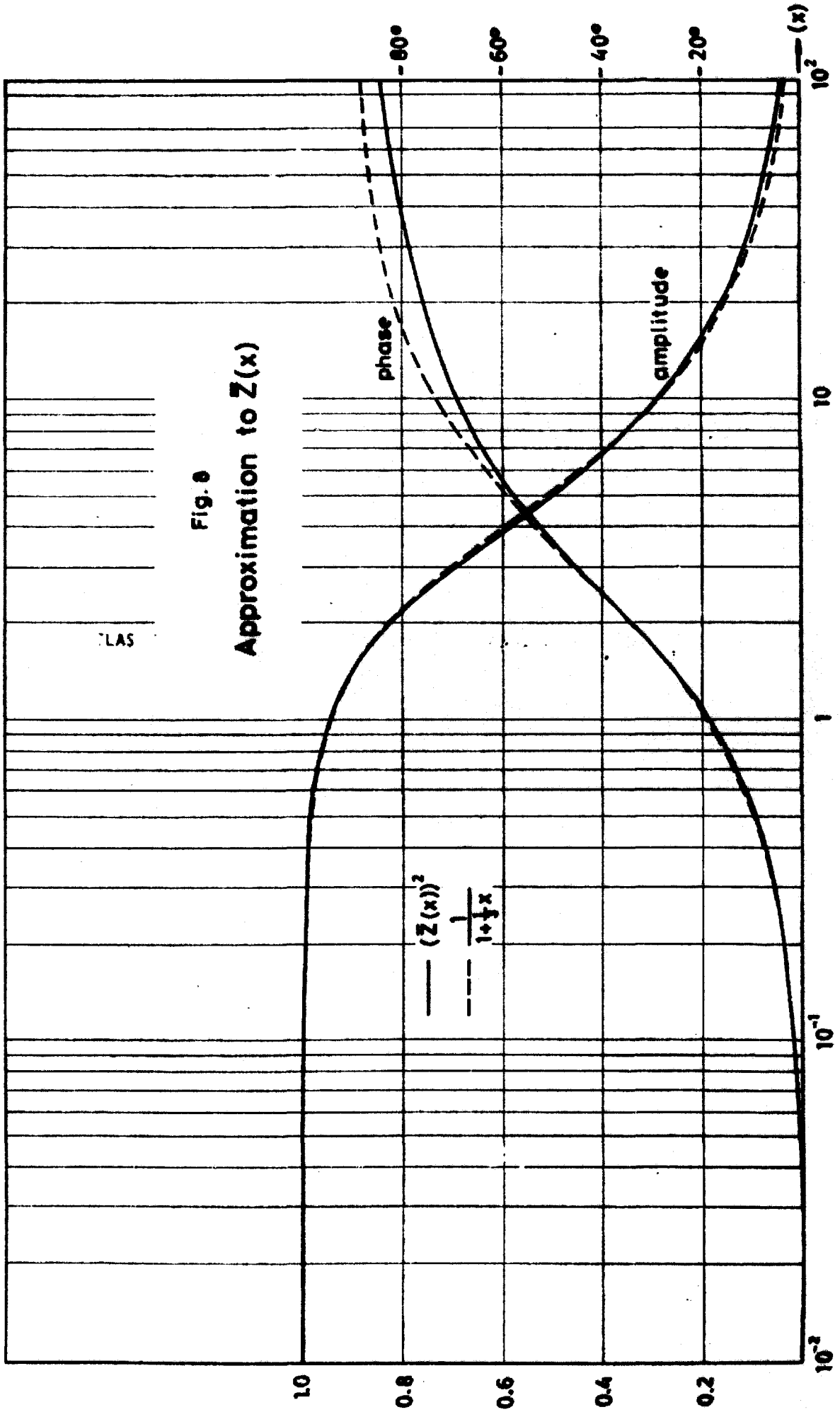
Approximation to Z(x)
phase
amplitude
-80°
-60°
-40°
-20°
10
1
1.0
0.8
0.6
0.4
0.2

Fig. 8

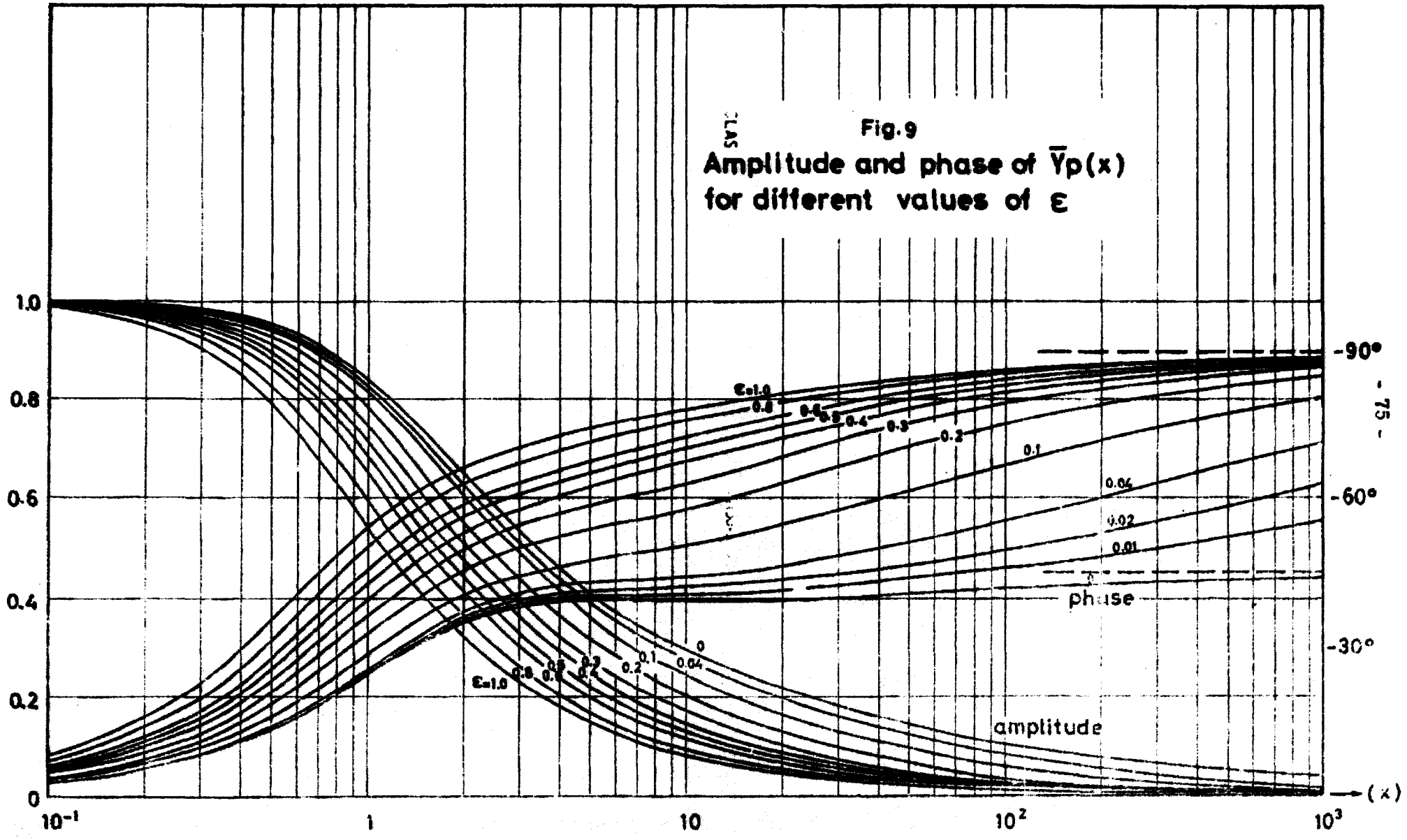
Fig. 9
Amplitude and phase of $\bar{Y}p(x)$
for different values of ε
1.0
0.8
0.6
0.4
0.2
0
10^{-1}
1
10
10^2
10^3
(x)
-90°
-60°
-30°
phase
amplitude
ε=1.0
0.8
0.6
0.5
0.4
0.3
0.2
0.1
0.04
0.02
0.01
0

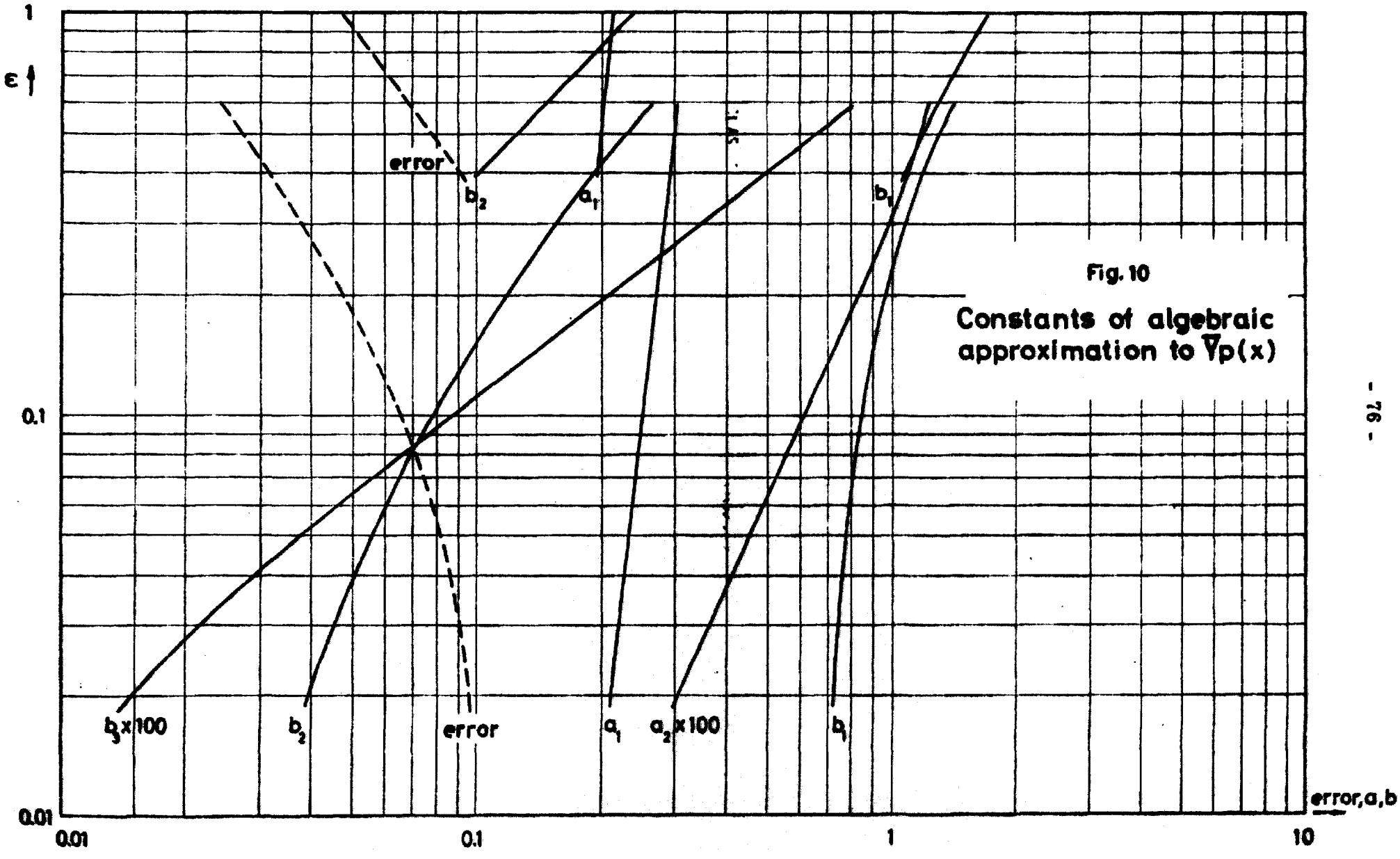

Fig. 10

Constants of algebraic approximation to $\nabla p(x)$

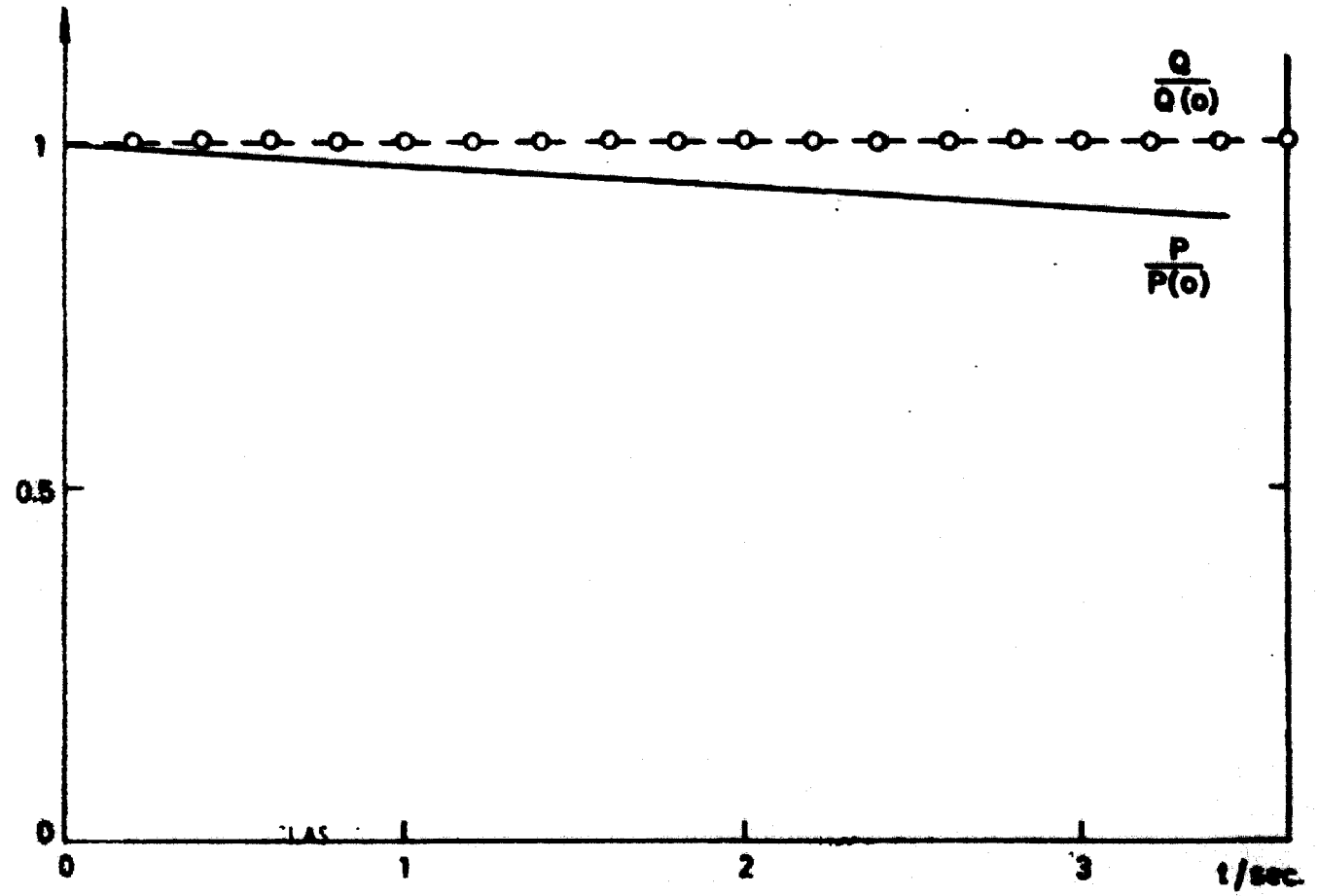
Power density
and heat flux
(relative scale)
Q/Q(o)
P/P(o)
1
0.5
0
0
1
2
3
t/sec.

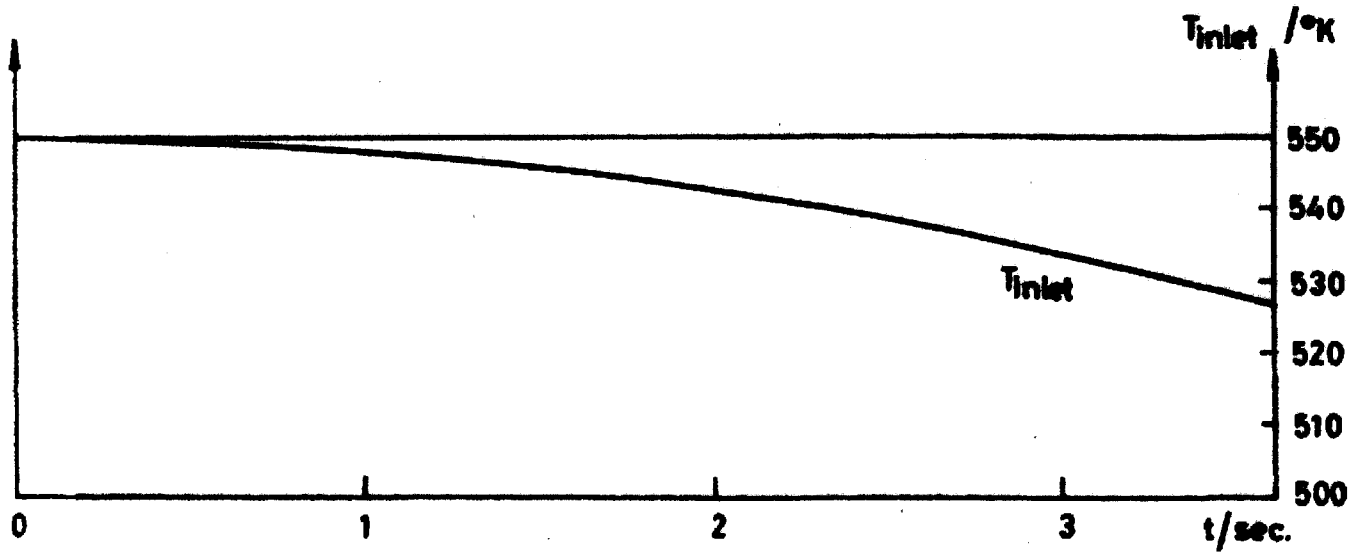
T inlet /°K
550
540
530
520
510
500
T inlet
0
1
2
3
t/sec.

Fig. 11

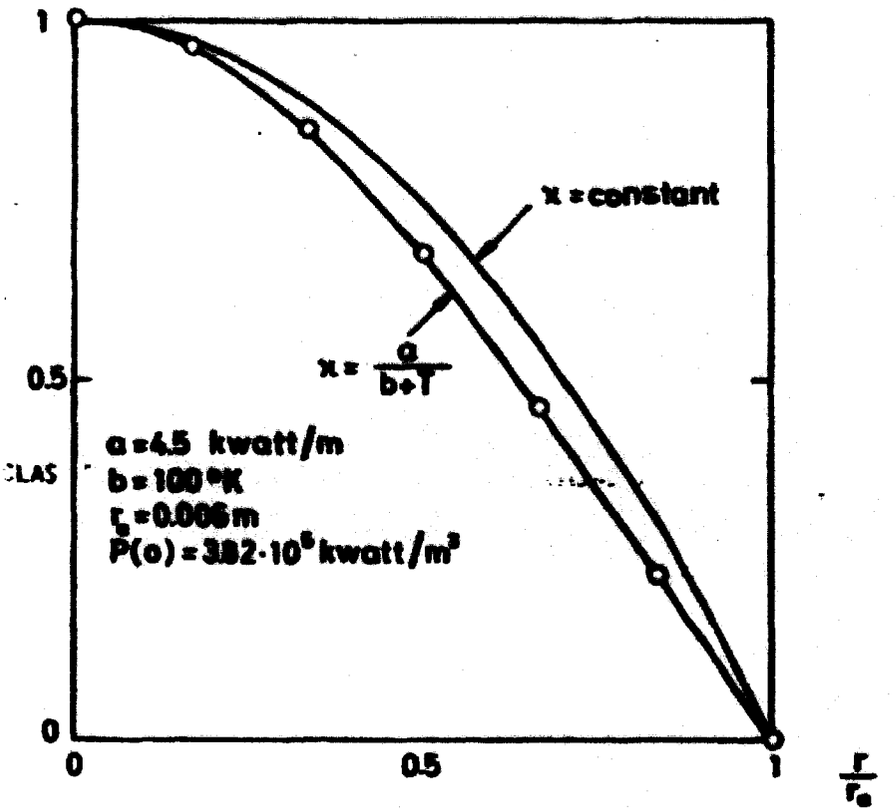

o Computer results

——— Theoretical curves

Fig.12

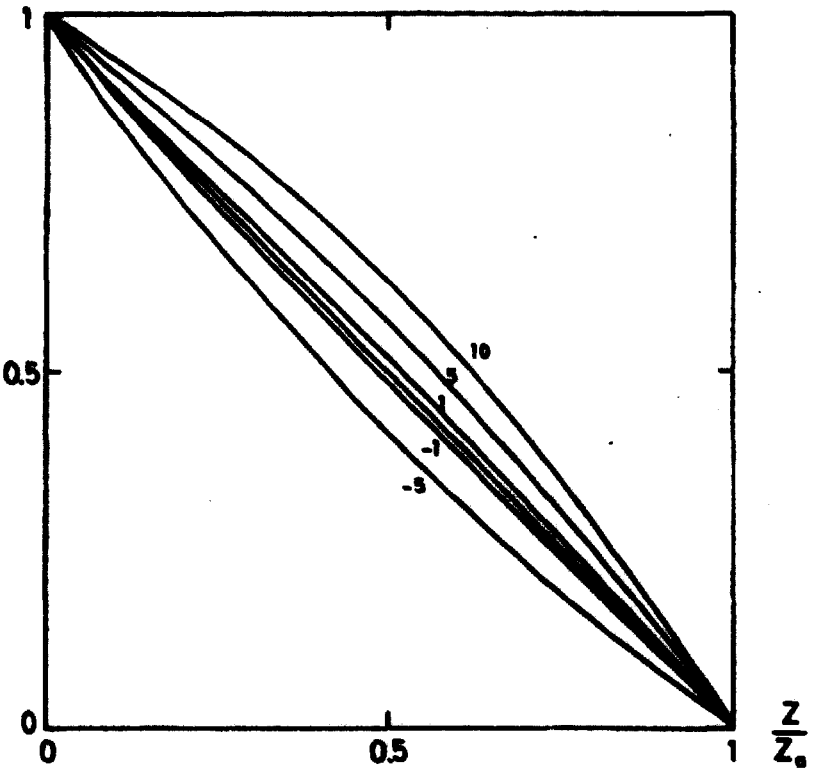

$\frac{\theta(Z, Z_a)}{\theta(o)}$ for different values of Z_a

CLAS

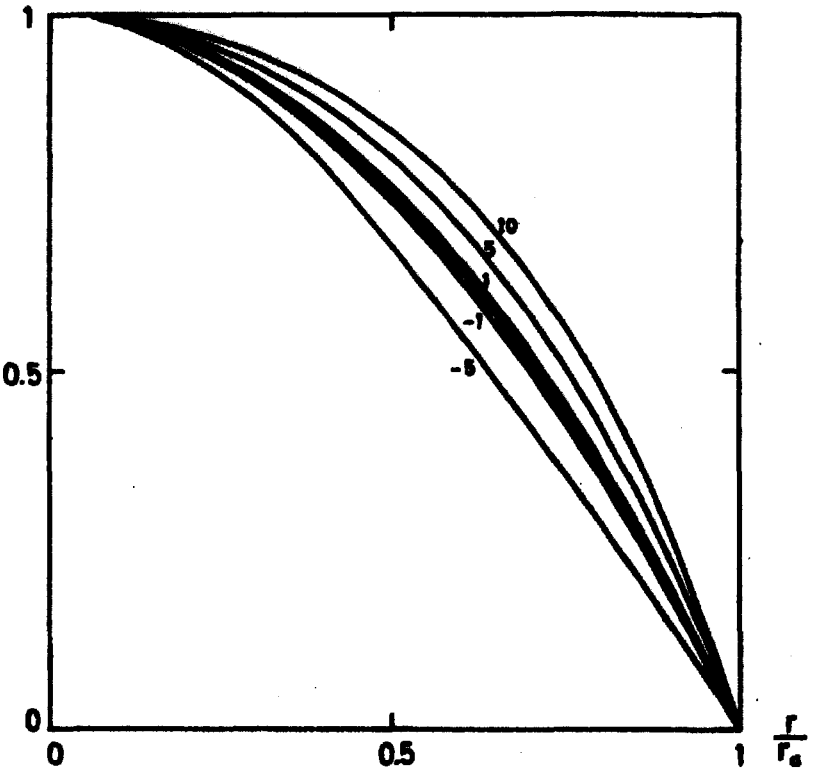

$\frac{\theta(r, Z_a)}{\theta(o)}$ for different values of Z_a

Fig.13

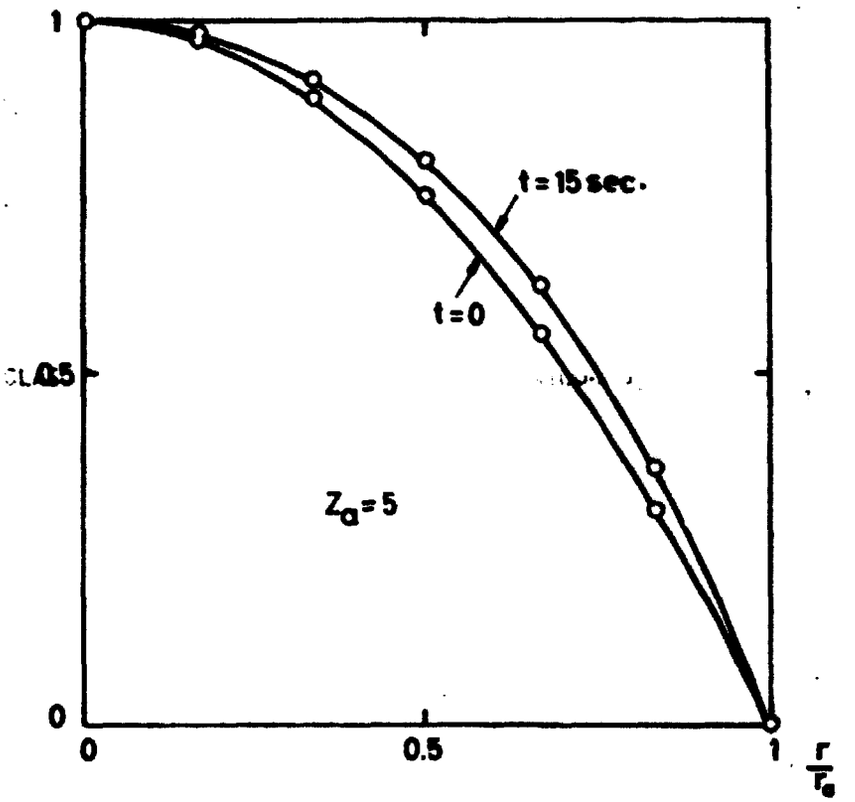

○ Computer results

—— Theoretical curves

Fig.14

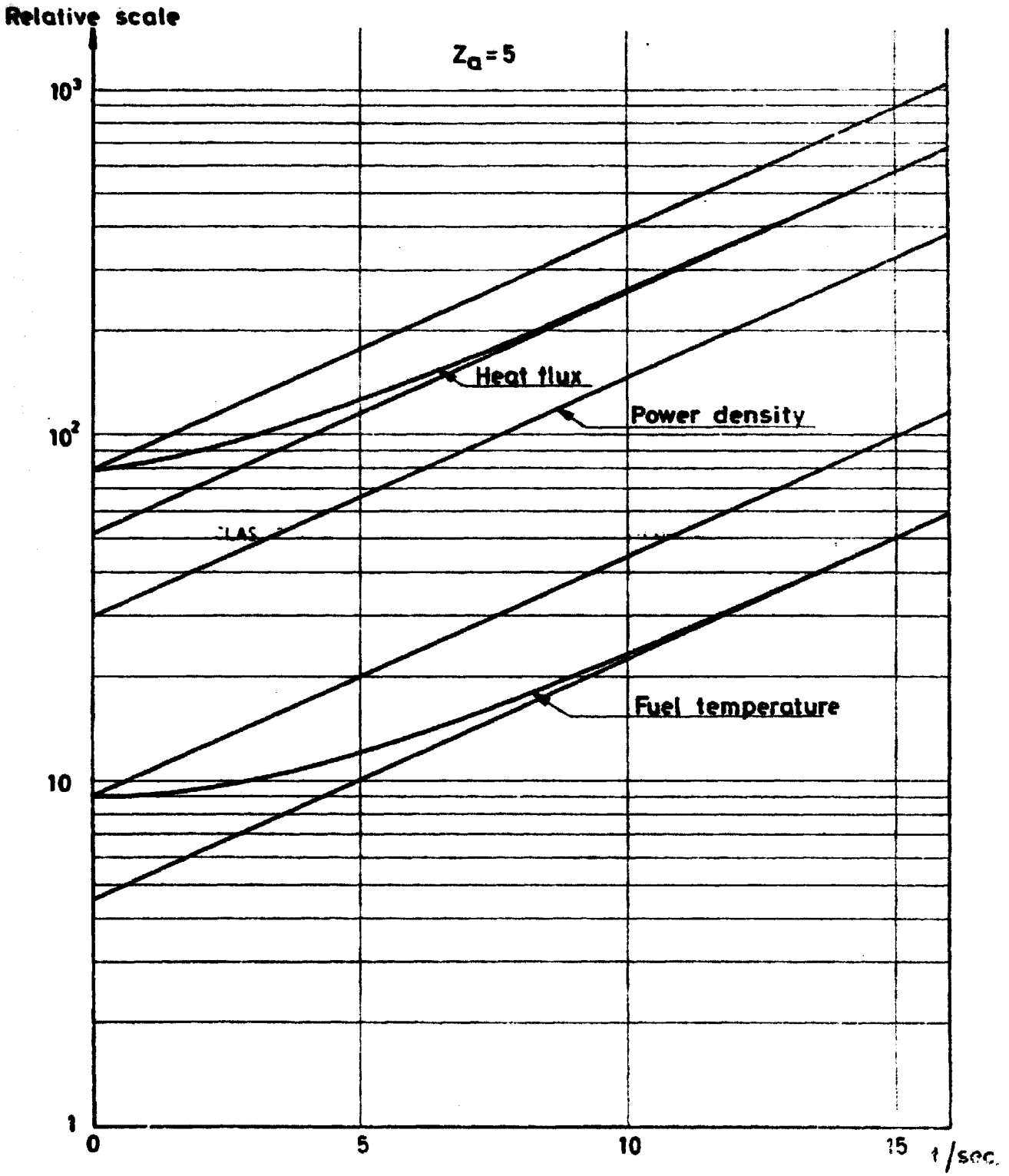
Relative scale
$Z_a = 5$
10^3
10^2
10
1
Heat flux
Power density
Fuel temperature
0
5
10
15
t/sec.

Fig. 15

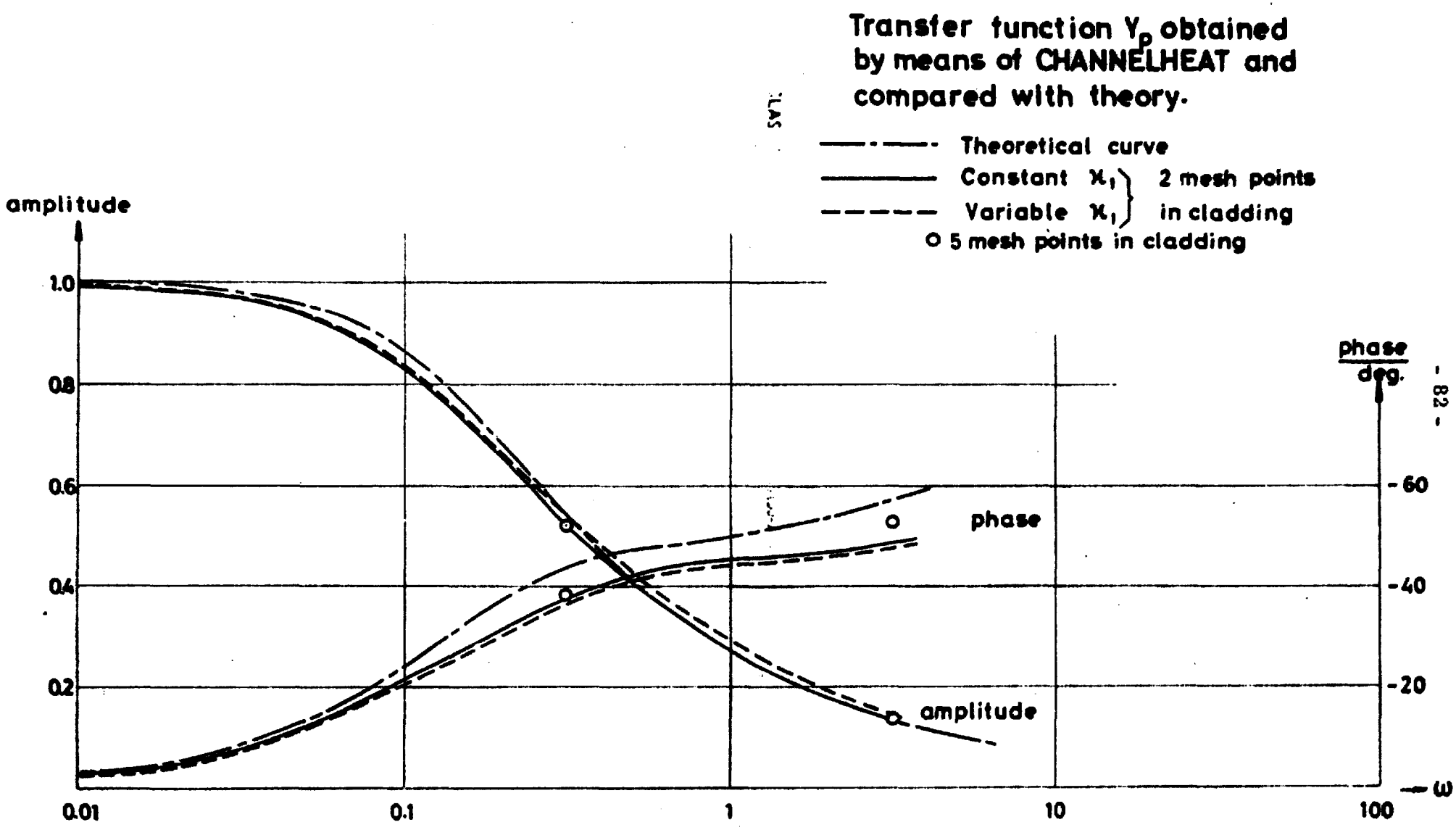
Transfer function Y_p obtained by means of CHANNELHEAT and compared with theory.
Theoretical curve
Constant χ_1 } 2 mesh points
Variable χ_1 } in cladding
5 mesh points in cladding
amplitude
phase
deg.
1.0
0.8
0.6
0.4
0.2
-60
-40
-20
0.01
0.1
1
10
100
phase
amplitude
ω

Fig.16

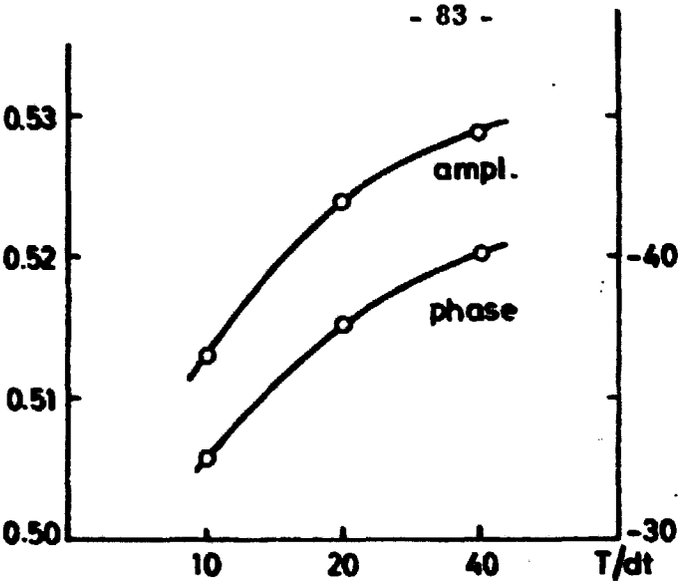

$\omega = 0.314$ sec.$^{-1}$

2 mesh points in cladding

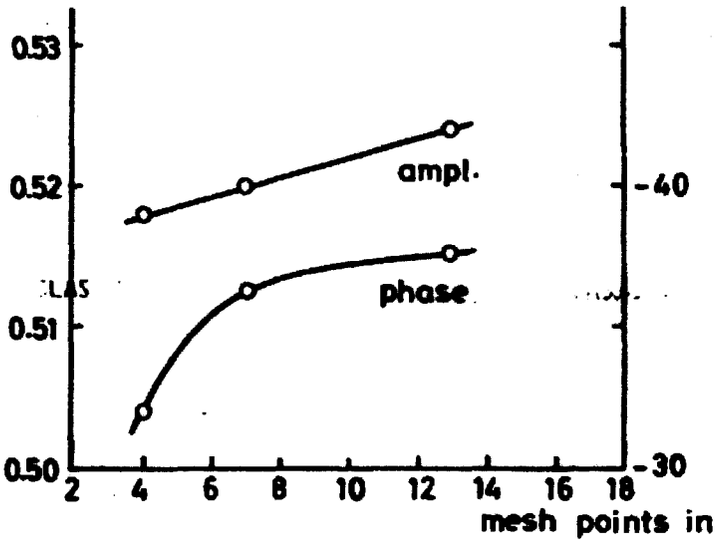

$\omega = 0.314$ sec.$^{-1}$

2 mesh points in cladding

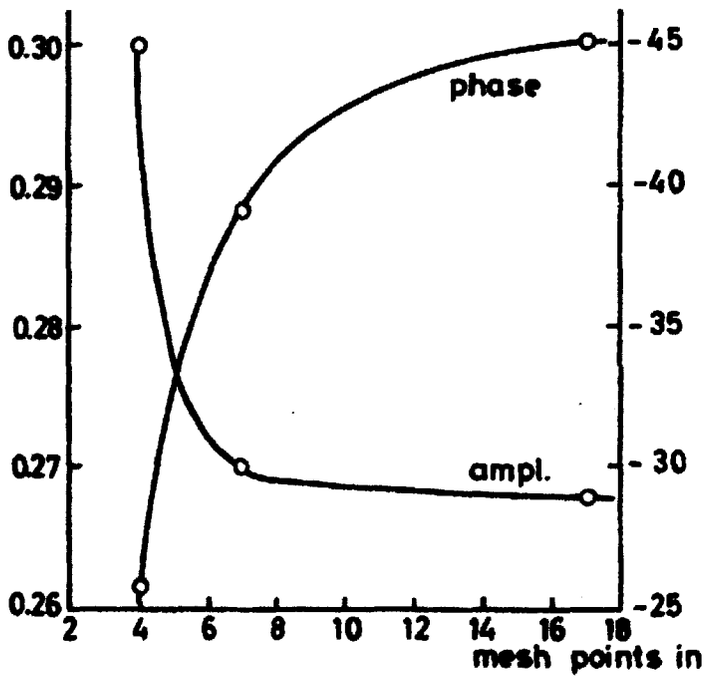

$\omega = 1.048$ sec^{-1}

2 mesh points in cladding

Fig.17

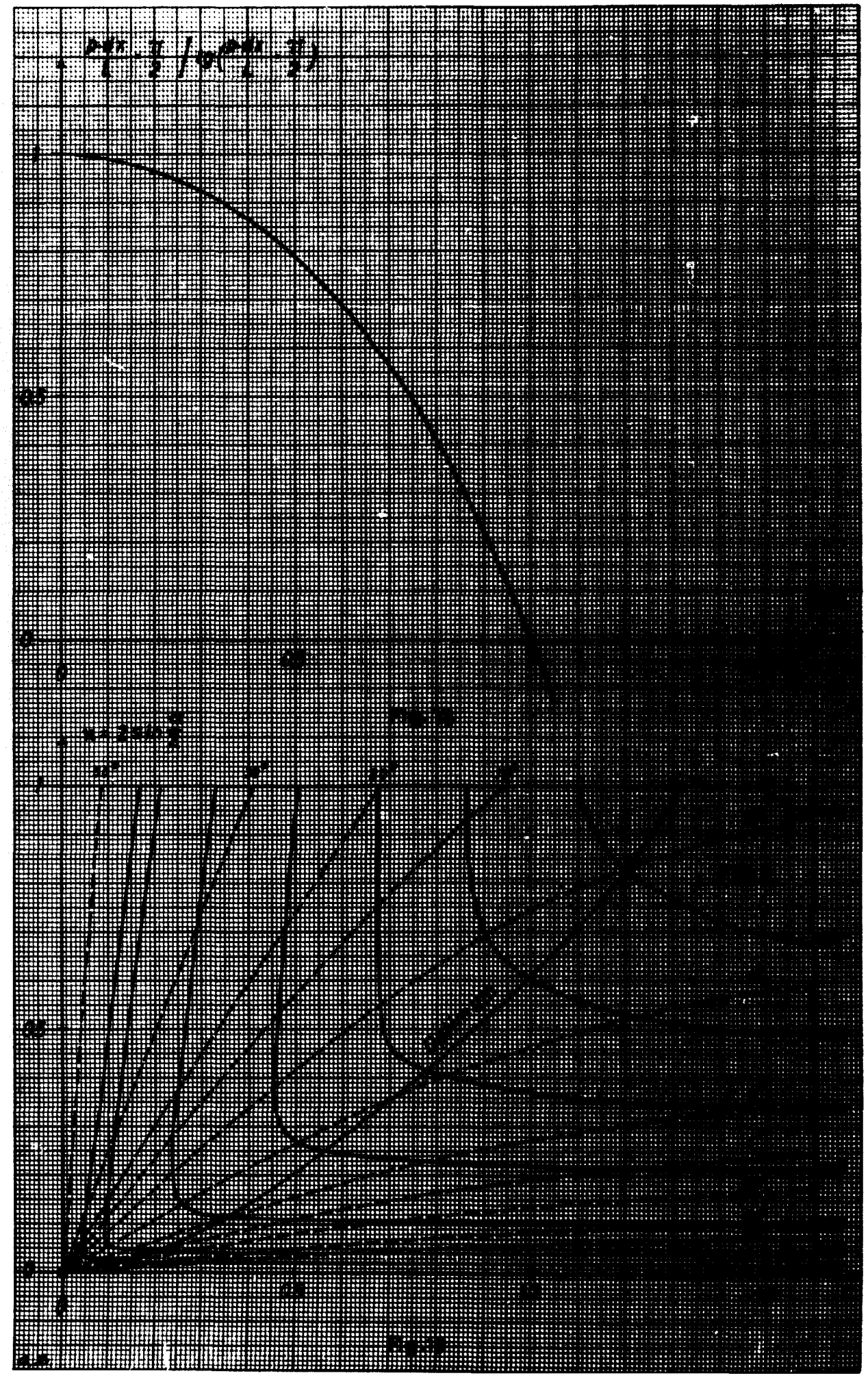

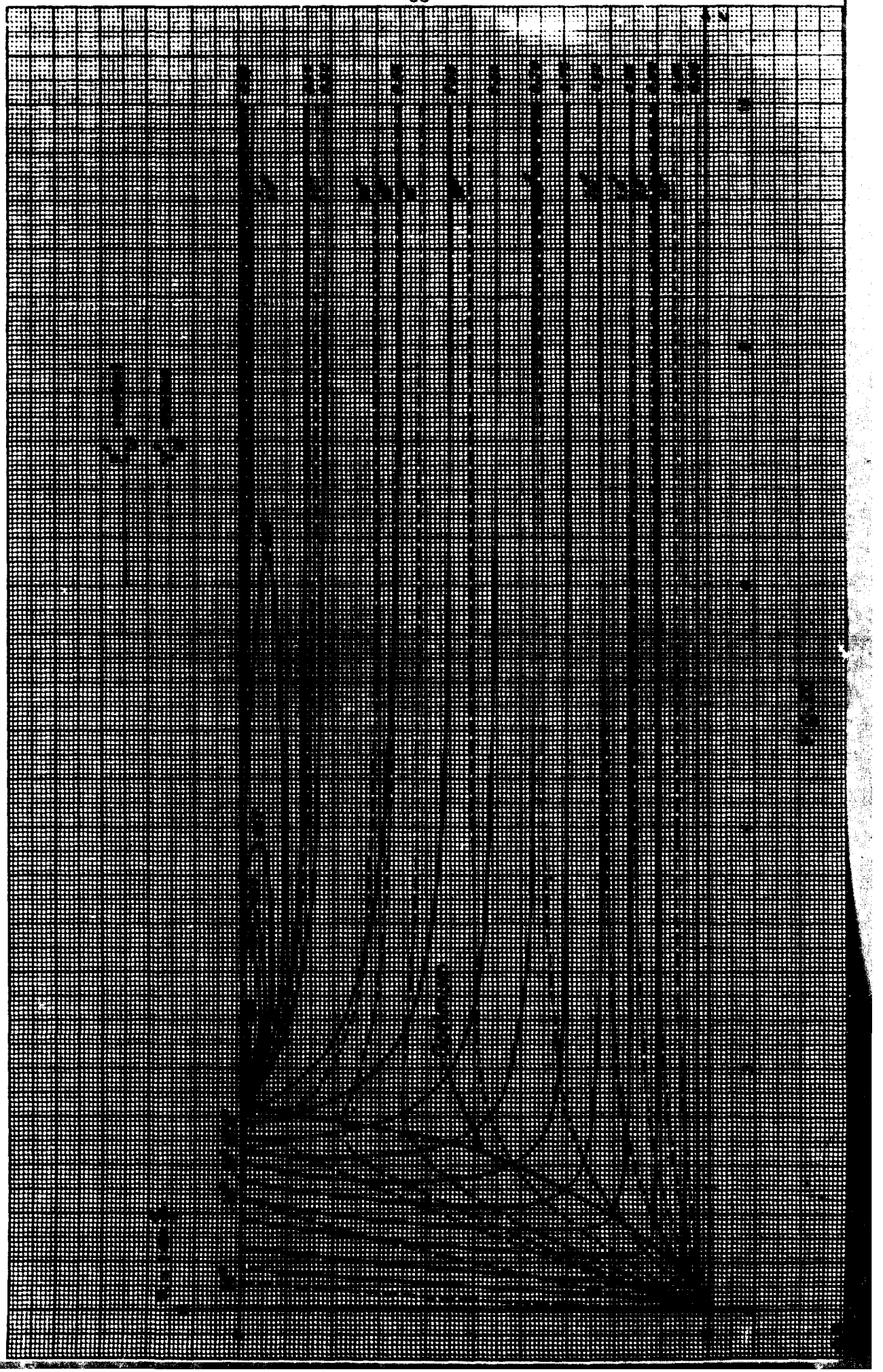

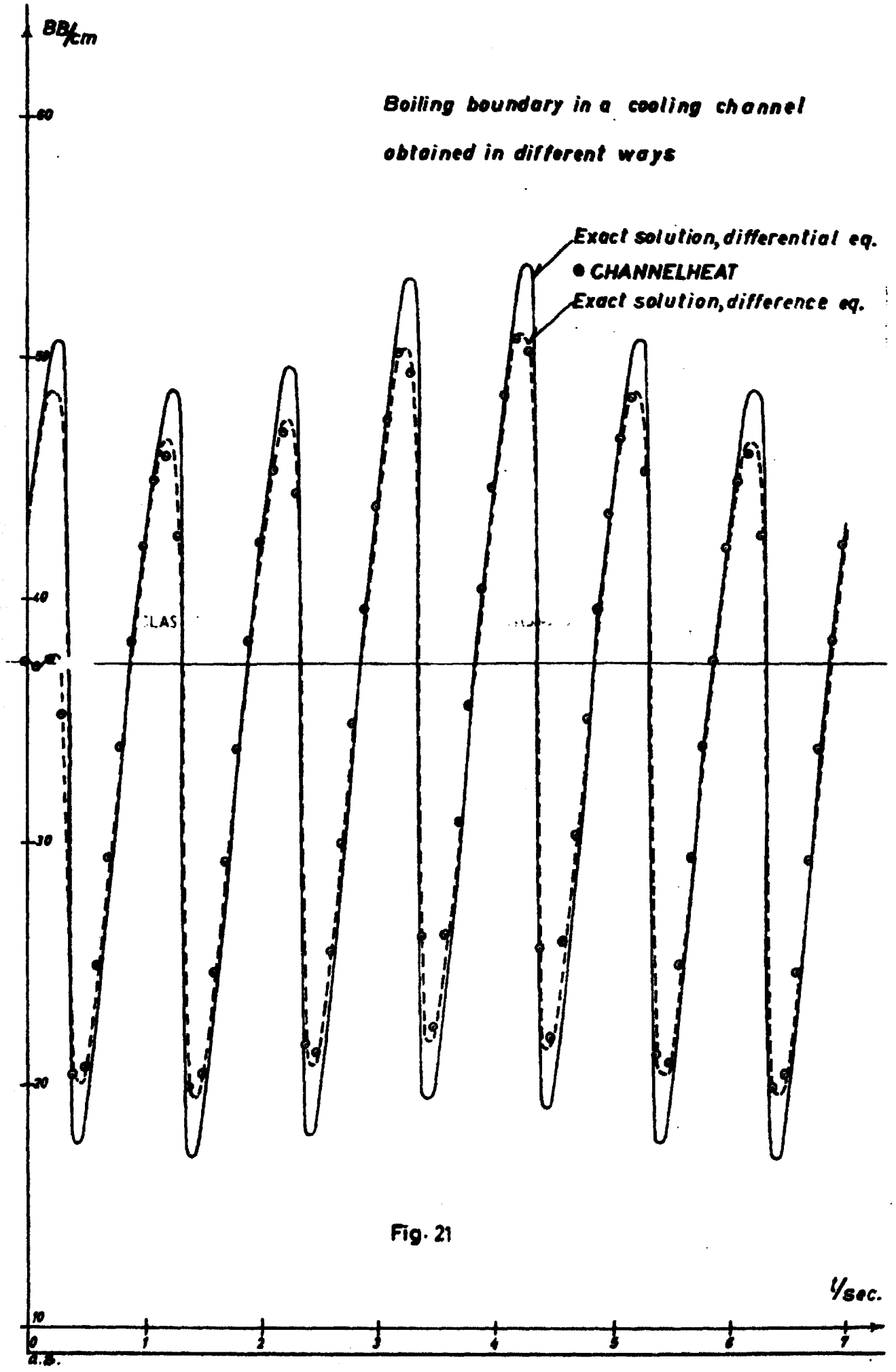
BB/cm
Boiling boundary in a cooling channel
obtained in different ways
Exact solution, differential eq.
● CHANNELHEAT
Exact solution, difference eq.
60
40
30
20
1/sec.
0
1
2
3
4
5
6
7

Fig. 21

Appendix 1

Derivation of Two-Group Diffusion Parameters

1. Main Features of the Computational Method

Like the code TATAR[3], this method is based on the four-factor formula and the Westcott cross-section concept. The main difference between the method used and TATAR is the fact that no flux calculations at all are made in the former, while the latter works with a rather advanced collision-probability flux calculation. This accounts for a gain in computing speed of a factor of approximately 50. Instead of flux calculations a fitted expression for the thermal flux depression in the interior of the fuel zone of the element is used.

The calculation is divided into two parts:

(1) The initial calculation, in which the information about the lattice is stored and subjected to a basic treatment resulting in some key quantities, which are stored in the computer.

(2) The final calculation, in which the two-group parameters are calculated in a rather simple way from the key quantities of the initial calculation.

When a new calculation is desired for the same lattice, but with other temperatures of moderator, coolant and fuel and other densities of coolant and moderator (the case occurring currently in BRENDA), only the final calculation has to be repeated.

2. Survey of Formulae

In this section a few comments on the formulae used are made with proper references.

(a) Neutron temperatures and Westcott r-factor

$$T_{n,m} = T_m\left(1 + C\,\frac{\sum_f V_i \Sigma_{ai}^{2200}}{\sum_c V_i \frac{\Sigma_{si}}{A_i}}\,\sqrt{\frac{293}{T_m}}\right) \qquad (1)$$

$$T_{n,f} = T_{n,m} + \frac{\sum_f V_i(\xi\Sigma_s)_i}{\sum_c V_i(\xi\Sigma_s)_i} \left(T_c\left(1 + \alpha \frac{\sum_f V_i \Sigma_{ai}^{2200}}{\sum_f V_i(\xi\Sigma_s)_i}\right) \frac{\sqrt{293}}{T_c} - T_{n,m}\right)$$

(2)

$$+ K \frac{\sum_f V_i \Sigma_{ai}^{2200}}{V_f} R_f \sqrt{\frac{293}{T_{n,m}}}$$

$$r_f = P \frac{\sqrt{\pi}}{2} \frac{\sum_f V_i \Sigma_{ai}^{2200} \sqrt{\frac{293}{T_{n,f}}}}{\sum_c V_i(\xi\Sigma_s)_i + \frac{2}{\sqrt{\mu}} \sum_f V_i \Sigma_{ai}^{2200} \sqrt{\frac{293}{T_{n,f}}}} \quad . \qquad (3)$$

In these formulae, $T_{n,m}$ and $T_{n,f}$ are the neutron temperatures of moderator and fuel, while T_m and T_c are the physical temperatures of moderator and coolant. f and c, as indicators of limits of the summation over index i, refer to the region of the cell within the shroud (not included) and the whole cell, respectively. V_i indicates the volume (i.e. cross-sectional area) in which the i'th material is present. V_f and R_f are the volume (cross-sectional area) and the radius, respectively, of the f region. Σ_{ai} and Σ_{si} are macroscopic cross sections of the i'th material computed locally in the region V_i. Σ_a^{2200} refers to the value at 2200 m/sec neutron speed. r_f is the Westcott r-factor. C, α, K, P, and μ are constants fitted experimentally. The following values may be used:

C = 0.66, α = 0.5 (for D_2O coolant),

K = 93 oK, P = 0.97, μ = 5 (for D_2O moderator).

Formulae (1), (2) and (3) are presented in ref. 2.

(b) Resonance integral

The resonance integral is computed by means of the formulae

$$RI = \frac{1}{2N_f R_f} \lambda_f(1-P(\lambda_f)) \left\{ \frac{\alpha a}{\sigma_n^1} RI(\sigma_n^1) + \frac{(1-\alpha)b}{\sigma_n^2} RI(\sigma_n^2) \right\}$$

$$+ RI(\sigma_n^1) \frac{\sigma_n^1 - \sigma_p}{\sigma_n^1} \left\{ \sigma^2 \frac{\sigma_k^1}{\sigma_n^1 - \sigma_k^1} + \alpha(1-\alpha) \frac{\sigma_k^2}{\sigma_n^1 - \sigma_k^2} \right\}$$

$$+ \; RI(\sigma_n^2) \; \frac{\sigma_n^2 - \sigma_p}{\sigma_n^2} \left\{ (1-a)^2 \; \frac{\sigma_k^2}{\sigma_n^2 - \sigma_k^2} + a(1-a) \; \frac{\sigma_k^1}{\sigma_n^1 - \sigma_k^1} \right\}$$

$$- \; RI(\sigma_k^1) \; (\sigma_k^1 - \sigma_p) \left\{ a(1-a) \frac{1}{\sigma_n^2 - \sigma_k^1} + a^2 \; \frac{1}{\sigma_n^1 - \sigma_k^1} \right\}$$

$$- \; RI(\sigma_k^2) \; (\sigma_k^2 - \sigma_p) \left\{ a(1-a) \; \frac{1}{\sigma_n^1 - \sigma_k^2} + (1-a)^2 \frac{1}{\sigma_n^2 - \sigma_k^2} \right\} \qquad (4)$$

$$\lambda_f^{LAS} = 4 \; \frac{\Sigma_c \; \Sigma_{si} \; V_i - \Sigma_f \; \Sigma_{si} \; V_i}{2\pi \; R_f} \qquad (5)$$

$$P(\lambda) = \frac{a\lambda}{a+\lambda} + \frac{(1-a)\lambda}{b+\lambda} \qquad (6)$$

$$RI(\sigma) = \sqrt{D(\sigma - \sigma_a) + E} \qquad (7)$$

$$D = 6.904 + 3.351 \; 10^{-3} \; t - 1.682 \; 10^{-6} \; t^2 + 7.750 \; 10^{-10} \; t^3 - 1.463 \; 10^{-13} \; t^4 \qquad (8)$$

$$E = 8.447 + 1.535 \; 10^{-3} \; t - 1.842 \; 10^{-6} \; t^2 + 3.637 \; 10^{-10} \; t^3 \qquad (9)$$

$$t = T_f - 273 \tag{10}$$

$$\sigma_n^1 = \frac{1}{2N_f R_f}\, a\lambda_f(1 - P(\lambda_f)) + \sigma_p \tag{11}$$

$$\sigma_n^2 = \frac{1}{2N_f R_f}\, b\,\lambda_f(1 - P(\lambda_f)) + \sigma_p \tag{12}$$

$$\sigma_k^1 = \frac{F}{2N_u R_u}\, a\lambda_u\,(1 - P(\lambda_u)) + \sigma_{so} \tag{13}$$

$$\sigma_k^2 = \frac{F}{2N_u R_u}\, b\,\lambda_u\,(1 - P(\lambda_u)) + \sigma_{so} \tag{14}$$

$$\lambda_u = 4\,\frac{\sum_f \Sigma_{si} V_i - \sum_u \Sigma_{si} V_i}{2\pi R_u \overline{nr}} \tag{15}$$

$$F = \frac{1}{1 + N_f R_f RI} \tag{16}$$

$$\sigma_p = \frac{\sum_f \Sigma_{si} V_i}{N_f V_f} \tag{17}$$

$$\sigma_{so} = \frac{\sum_u \Sigma_{si} V_i}{N_u V_u} \quad . \tag{18}$$

Here RI denotes the resonance integral. a, a and b are fitted parameters with the values 2, 1.707 and 2.414 respectively. u, as indicator of the limit of the summation over index i, refers to the fuel rods. V_u and R_u are the volume (cross-sectional area) and radius, respectively, of a fuel rod. N_f and N_u are the densities of U 238 atoms in the f and the u zone respectively.

From formulae (16), (13) and (14) it is seen that the resonance integral to be calculated also appears on the right-hand side of the expres-

sion (4), namely through σ_k^1 and σ_k^2. This means that an iterative procedure is required. The number of necessary iterations, however, is small and has been fixed at 3 (starting with F = 1).

The above formulae can be found in ref. 2 except for F as appearing in expression (4). The present way of introducing F is in accordance with ref. 3.

(c) Fast-fission factor

The fast-fission factor ε is calculated from the formula

$$\varepsilon = 1 + \frac{(\nu_f - 1)\,\Sigma_f - \Sigma_c}{\Sigma_t - (\nu_f \Sigma_f + \Sigma_s)P}\,P \quad . \tag{19}$$

Here ν_f is the number of neutrons produced per fast fission, Σ_f, Σ_c, Σ_s, and Σ_t are the macroscopic cross sections of fast fission, fast radiative capture, fast elastic scattering, and total fast interaction. The last-mentioned is equal to $\Sigma_f + \Sigma_c + \Sigma_s + \Sigma_{in}$, where Σ_{in} denotes the macroscopic fast inelastic scattering cross section.

P is the probability of a new-born neutron colliding in the fuel region before escaping. Formula (19) is applied to the fuel-rod cluster considered as a whole. Then P is calculated from

$$P = \frac{2R_f \Sigma_t}{1 + 2R_f \Sigma_t} \qquad \text{(Wigner approximation)} . \tag{20}$$

Formula (19) and its derivation can be found in ref. 4, p. 696. A similar expression is used in ref. 2, but here a quantity h (p. 14, formulae 4.2 and 4.4) accounts for the fact that only 61% of the neutrons are born with energies above the fast-fission threshold. Further it is somewhat doubtful what values should be assigned to the microscopic fast cross sections of formula (19). It is believed that those of ref. 2 are most relevant and should be chosen. Allowance for the factor h is recommended to be made by way of the library.

(d) Fermi age

The Fermi age τ is calculated from the expressions

$$\tau = \tau_o\left(1 - \frac{\Sigma_{in}}{\Sigma_t}P\right) + \tau_{in}\frac{\Sigma_{in}}{\Sigma_t}P \tag{21}$$

$$\tau_o = \tau_{o,\,Mod}\ \frac{\Sigma^t_{Mod}\,(\xi\Sigma_s)_{Mod}\,(V_c - V_f)}{\sum\limits_c \Sigma^t_i\,V_i\ \sum\limits_c (\xi\Sigma_s)_i\,V_i} \tag{22}$$

$$\tau_{in} = \tau_o\ \frac{\tau_{in,\,Mod}}{\tau_{o,\,Mod}}\ . \tag{23}$$

Here P is the same quantity as in (c), $\tau_{o,\,Mod}$ and $\tau_{in,\,Mod}$ are the Fermi ages of the pure moderator for all scattering being elastic and inelastic respectively, measured at a moderator density of 1.1 g/cm^3. Σ^t_i and Σ^t_{Mod} denote the macroscopic transport cross sections for fast neutrons for the i'th material and the pure moderator respectively.

The formulae originate from ref. 2

(e) Resonance escape probability

The resonance escape probability is calculated from the expression

$$p = \exp\left(-\frac{N_f V_f R I}{\sum\limits_c (\xi\Sigma_s)_i\,V_i}\left\{\exp\left(-\frac{V_c}{4\pi\beta\tau}\right)+\frac{V_c}{4\pi\beta\tau}\exp\left(-1.5\frac{V_f}{4\pi\beta\tau}\right)\right\}\right); \tag{24}$$

β is a parameter which should be put equal to 0.54 for heavy water (ref. 2).

(f) Fast-diffusion constant and slowing-down cross section

The fast-diffusion constant D_1 and the macroscopic slowing-down cross section Σ_{r1} are calculated from the expressions

$$D_1 = \frac{V_c}{3\ \sum\limits_c \Sigma^t_i\,V_i} \tag{25}$$

$$\Sigma_{r1} = \frac{D_1}{\tau}\ . \tag{26}$$

(g) Thermal-flux depression and thermal cross sections

If we define the thermal-flux depression factor as the ratio of the thermal flux in the fuel zone to that in the moderator zone, the following expressions can be obtained:

$$\Sigma_F = \Sigma_{f(25)}^{2200} \frac{V_u}{V_c} \frac{\sqrt{\pi}}{2} (g_{(25)f} + r_f \cdot s_{(25)f}) \sqrt{\frac{293}{T_{n,f}}} \cdot F \qquad (27)$$

$$\Sigma_{AF} = \frac{1}{V_c} (\Sigma_{a(28)}^{2200} V_u g_{(28)a} + \Sigma_{a(25)}^{2200} V_u (g_{(25)a} + r_f \cdot s_{(25)a})) \frac{\sqrt{\pi}}{2} \sqrt{\frac{293}{T_{n,f}}} F \qquad (28)$$

$$\Sigma_A = \Sigma_{AF} + \frac{1}{V_c} \sum_{f-u} \Sigma_{ai}^{2200} V_i \frac{\sqrt{\pi}}{2} \sqrt{\frac{293}{T_{n,f}}} F + \frac{1}{V_c} \sum_{c-f} \Sigma_{ai}^{2200} V_i \frac{\sqrt{\pi}}{2} \sqrt{\frac{293}{T_{n,m}}} \qquad (29)$$

$$\Sigma_{SM} = (\frac{1}{V_c} \sum_{u} (\Sigma_s (1-\mu))_i^{2200} V_i + \frac{1}{V_c} \sum_{f-u} (\Sigma_s (1-\mu))_i^{2200} V_i (1-a_c (1- \sqrt{\frac{293}{T_{n,f}}})))F$$

$$+ \frac{1}{V_c} \sum_{c-f} (\Sigma_s (1-\mu))_i^{2200} V_i (1-a_m (1- \sqrt{\frac{293}{T_{n,m}}})) \quad . \qquad (30)$$

Here Σ_F, Σ_A and Σ_{SM} denote the macroscopic cross sections of fission, absorption and transport scattering for the cell. Σ_f^{2200}, Σ_a^{2200} and $\Sigma_s(1-\mu)^{2200}$ correspondingly denote these quantities for the individual materials, (28) denotes U 238, (25) denotes U 235, while other materials are identified by a number i. The summation limit indications f-u and c-f refer to coolant and moderator regions respectively.

The factors $(g_f + r_f \times s_f)$ and $(g_a + r_j \times s_a)$ are the Westcott correction factors for fission and absorption cross sections respectively. It is noted that only U 235 and U 238 cross sections are Westcott corrected as all other materials are considered 1/v - absorbers. For U 238 the s-factor is neglected since the epithermal absorption is already considered through the resonance integral. The parameters a_c and a_m in formula (30) are characteristic of the coolant and moderator media respectively. For heavy water, a is equal to 0.360[2].

The flux depression factor F has been fitted by the expression

$$F = \frac{1}{1 + (0.92 + 2.62\ R_f\ \Sigma_{AF}) R_f\ \Sigma_{AF}} \sqrt[4]{\frac{R_f}{R_c}} \quad . \tag{31}$$

where R_c denotes the radius of the whole cell.

This was done by comparison with results from the code TATAR.

(h) Thermal-diffusion constant, thermal-diffusion length and thermal-neutron velocity

The thermal-diffusion constant D_2 and the thermal-diffusion length squared, L, are calculated by means of the formulae

$$D_2 = \frac{1}{3(\Sigma_A + \Sigma_{SM})} \tag{32}$$

$$L^2 = \frac{D_2}{\Sigma_A} \quad . \tag{33}$$

The thermal-neutron velocity is calculated as

$$V = 2200\ \text{m/sec} \sqrt{\frac{T_{n,m}}{293}} \quad . \tag{34}$$

Appendix 2

Data Sheet for BRENDA

Library-tape identification number: _____

Number of mesh points in axial direction, n: _____

Number of mesh points in radial direction, fuel region, p: _____

Number of mesh points in radial direction, cladding, q: _____

Step size in acial direction, dx: _____ (m)

Step size in radial direction, fuel region, dr: _____ (m)

Step size in radial direction, cladding, drc: _____ (m)

Time step, dt: _____ (sec)

Pressure index: _____ . Printing index: _____

Maximum flux: _____ ($n/cm^2/sec$)

error T: LAS (deg.); error v: _____ ; error Q: _____

error T eff: _____ (deg.); error phi: _____; erfeul: _____

error my: _____ ; error P: _____

Radius of fuel rod, ra: _____ (cm)

Inner radius of cladding, rb: _____ (cm)

Outer radius of cladding, rc: _____ (cm)

Radius of lattice cell, rch: _____ (cm)

Reflector saving at bottom, Hl: _____ (cm)

Reflector saving at top, Hn: _____ (cm)

Core extrapolated radius, R: _____ (cm)

Inner radius of shroud, ri: _____ (cm)

Outer radius of shroud, ro: _____ (cm)

Rubber-band radius, rbr: _____ (cm)

Enrichment of fuel: _____

Number of materials in cell regions except region 5, nf: _____

Number of materials in region 5, nm: _____

Number of fuel rods per cell, nr: _____

Material reference numbers for all regions (nf+ nm quantities):

Region-type indicators (nf+nm quantities):

Region densities (nf+nm quantities):
(for coolant and moderator regions specify 1) (g/cm^3)

Region reference numbers (nf+nm quantities):

Weight fractions (nf+nm quantities):

Compound reference numbers (nf+nm quantities):

Distribution of control absorption cross section along axis:

(A5

Moderator-temperature distribution along axis:
(deg. Kelvin)

Inlet temperature of coolant: _____ (deg. Kelvin)

Inlet coolant velocity: _____ (m/sec)

System pressure: _____ (at)

{

Control parameter: _____

Moderator-temperature distribution:
(deg. Kelvin)

Inlet temperature of coolant: _____ (deg. Kelvin)

Inlet coolant velocity: _____ (m/sec)

System pressure: _____ (at)

}

The data group in braces corresponds to the first time step. A similar group should follow for each time step. The calculations are brought to an and when a group is followed by -1.

Appendix 3

Data Sheet for BRENDAPLOT

Number of print-outs from BRENDA to be treated, I: _____

Number of time points at which axial plots of heat inflow to coolant, power density in fuel, fuel temperature (radial average), coolant temperature, and void fraction are desired, ma: _____

Numbers assigned to these time points, number one being given to the steady-state case (ma quantities):

_____

Number of time points at which radial fuel temperature plots are desired, mr: _____

Total number of radial fuel temperature plots to be drawn, smra: _____

Number assigned to the first time point at which radial plots are desired: _____

Number of radial plots to be drawn at this time point, mra: _____

Numbers assigned to the axial mesh points at which these radial plots are desired (mra quantities):

_____

.
.
.

Group similar to that in brackets for each time point at which radial plots are desired (mr groups)

.
.
.

Number of time points at which printing of all available information is desired, mp: _____

Numbers assigned to these time points (mp quantities):

_____

If plots of the time variation of axial averages of heat inflow, power density, fuel temperature, coolant temperature, and void fraction together with system pressure, inlet velocity, inlet temperature, boiling boundary, and control-rod reactivity are desired, write 1, if not, write 0: _____

(The information required for calibrating the time plots will be punched out, and the user is recommended to transfer it immediately to the plots by hand.)

Appendix 4

Derivation of Heat-Release Transfer Functions

Stepwise derivation of exact solution, referring to chapter II, subsection 3(a)

On introduction of

$$\tau \equiv T - T_a$$

(1) may be rewritten

$$\nabla^2 \tau - \frac{\varrho_1 c_1}{\varkappa_1} \frac{\partial T}{\partial t} = - \frac{P - \varrho_1 c_1 \frac{\partial T_a}{\partial t}}{\varkappa_1} .$$

Laplace transformation yields

$$\nabla^2_{LAP} \overline{\delta\tau}\ (s) - \frac{s \varrho_1 c_1}{\varkappa_1} \overline{\delta\tau}\ (s) = - \frac{\overline{\delta P}(s)}{\varkappa_1} + \frac{s \varrho_1 c_1}{\varkappa_1} \overline{\delta T}_a(s)$$

$$\nabla^2 \left\{ \overline{\delta\tau}\ (s) + \overline{\delta T}_a(s) - \frac{\overline{\delta P}(s)}{s \varrho_1 c_1} \right\} - \frac{s \varrho_1 c_1}{\varkappa_1} \left\{ \overline{\delta\tau}(s) + \overline{\delta T}_a(s) - \frac{\overline{\delta P}(s)}{s \varrho_1 c_1} \right\} = 0 .$$

This is a standard form the solution of which may be found e. g. in ref. 7:

$$\overline{\delta\tau}\ (s) + \overline{\delta T}_a(s) - \frac{\overline{\delta P}(s)}{s \varrho_1 c_1} = C \frac{J_o\left(\sqrt{- \frac{\varrho_1 c_1}{\varkappa_1}}\, s r \right)}{J_o\left(\sqrt{- \frac{\varrho_1 c_1}{\varkappa_1}}\, s r_a \right)} .$$

$r = r_a$ yields $C = \overline{\delta T}_a(s) - \frac{\overline{\delta P}(s)}{s \varrho_1 c_1}$, whence

$$\overline{\delta\tau}\ (s) = \left(\delta T_a(s) - \frac{\overline{\delta P}(s)}{s \varrho_1 c_1} \right) \left\{ \frac{J_o\left(\sqrt{- \frac{\varrho_1 c_1}{\varkappa_1}}\, s r \right)}{J_o\left(\sqrt{- \frac{\varrho_1 c_1}{\varkappa_1}}\, s r_a \right)} - 1 \right\} .$$

By differentiation we obtain

$$\overline{\delta Q}_a(s) = - \varkappa_1 \left(\frac{\partial}{\partial r} \overline{\delta\tau}(s)\right)_{r=r_a}$$

$$= \left(\overline{\delta T}_a(s) - \frac{\overline{\delta P}(s)}{s \varrho_1 c_1} \right) \sqrt{- \varrho_1 c_1 \varkappa_1 s} \, \frac{J_1\left(\sqrt{- \frac{\varrho_1 c_1}{\varkappa_1}} s r_a \right)}{J_o\left(\sqrt{- \frac{\varrho_1 c_1}{\varkappa_1}} s r_a \right)} \quad . \tag{A1}$$

Further

$$\overline{\delta T}_f(s) - \overline{\delta T}_a(s) = \frac{1}{\pi r_a^2} \int_o^{r_a} 2\pi \, r \, \overline{\delta\tau}(s) \, dr$$

$$= \left(\overline{\delta T}_a(s) - \frac{\overline{\delta P}(s)}{s \varrho_1 c_1} \frac{2}{r_a^2} \left\{ \frac{r J_1\left(\sqrt{- \frac{\varrho_1 c_1}{\varkappa_1}} s r\right) - \frac{1}{2} \sqrt{- \frac{\varrho_1 c_1}{\varkappa_1}} s r^2 J_o\left(\sqrt{- \frac{\varrho_1 c_1}{\varkappa_1}} s r\right)}{\sqrt{- \frac{\varrho_1 c_1}{\varkappa_1}} s \; J_o\left(\sqrt{- \frac{\varrho_1 c_1}{\varkappa_1}} s r_a\right)} \right\}_o^{r_a}\right.$$

$$= \left(\overline{\delta T}_a(s) - \frac{\overline{\delta P}(s)}{s \varrho_1 c_1} \right) \frac{1}{4} \sqrt{- \frac{\varrho_1 c_1}{\varkappa_1}} s r_a \, \frac{J_1\left(\sqrt{- \frac{\varrho_1 c_1}{\varkappa_1}} s r_a\right)}{J_o\left(\sqrt{- \frac{\varrho_1 c_1}{\varkappa_1}} s r_a\right)} \, \overline{Z}(s) \quad ,$$

where the definitions of T_f and $\overline{Z}(s)$ from eqs. (7) and (15) have been used. By means of (A1) the expression is reduced to

$$\overline{\delta T}_f(s) - \overline{\delta T}_a(s) = \frac{1}{4} \frac{r_a}{\varkappa_1} \overline{Z}(s) \; \overline{\delta Q}_a(s) \quad . \tag{A2}$$

Eliminating $\overline{\delta T}_a(s)$ between (A1) and (A2) and using (15), we obtain

$$\overline{\delta Q}_a(s) = \frac{1}{2} r_a \left\{ \overline{\delta P}(s) - \varrho_1 c_1 s \quad \overline{\delta T}_f(s) \right\} \quad . \tag{A3}$$

On introduction of

$$\tau \equiv T - T_c$$

(2) may be rewritten

$$\nabla^2 \tau - \frac{\varrho_2 c_2}{\varkappa_2} \frac{\partial \tau}{\partial t} = \frac{\varrho_2 c_2}{\varkappa_2} \frac{\partial T_c}{\partial t} \quad .$$

Laplace transformation yields

$$\nabla^2 \overline{\delta \tau}\ (s) - \frac{s \varrho_2 c_2}{\varkappa_2} \overline{\delta \tau}\ (s) = \frac{s \varrho_2 c_2}{\varkappa_2} \overline{\delta T}_c(s)$$

$$\nabla^2 \left\{ \overline{\delta \tau}\ (s) + \overline{\delta T}_c(s) \right\} - \frac{s \varrho_2 c_2}{\varkappa_2} \left\{ \overline{\delta \tau}\ (s) + \overline{\delta T}_c(s) \right\} = 0 \quad .$$

As the centre line is not included in the area considered, the standard solution takes the form

$$\overline{\delta \tau}\ (s) + \overline{\delta T}_c(s) = A J_o\left(\sqrt{-\frac{\varrho_2 c_2}{\varkappa_2}} s\, r \right) + B N_o\left(\sqrt{-\frac{\varrho_2 c_2}{\varkappa_2}} s\, r \right) \quad . \tag{A4}$$

Differentiation yields

$$\frac{\partial}{\partial r} \overline{\delta \tau}\ (s) = - \sqrt{-\frac{\varrho_2 c_2}{\varkappa_2}} s \left\{ A J_1\left(\sqrt{-\frac{\varrho_2 c_2}{\varkappa_2}} s\, r \right) + B N_1\left(\sqrt{-\frac{\varrho_2 c_2}{\varkappa_2}} s\, r \right) \right\} . \tag{A5}$$

$r = r_c$ gives, by (A4) and (A5),

$$A = \frac{1}{J_o^c} \left\{ \overline{\delta T}_c(s) - B N_o^c \right\} \tag{A6}$$

$$B = \frac{-J_o^c}{N_o^c J_1^c - N_1^c J_o^c} \left\{ \frac{\overline{\delta Q}_c(s)}{\sqrt{-\varrho_2 c_2 \varkappa_2 s}} - \frac{J_1^c}{J_o^c} \overline{\delta T}_c(s) \right\} . \qquad \text{(A7)}$$

Now, putting $r = r_b$, we have by means of (A5), (A6) and (A7)

$$\overline{\delta Q}_b(s) = \sqrt{-\varrho_2 c_2 \varkappa_2 s} \left\{ \frac{J_1^b}{J_o^c} \overline{\delta T}_c(s) \right.$$

$$\left. + \left(\frac{J_1^b}{J_o^c} N_o^c - N_1^b \right) \frac{J_o^c}{N_o^c J_1^c - N_1^c J_o^c} \left(\frac{\overline{\delta Q}_c(s)}{\sqrt{-\varrho_2 c_2 \varkappa_2 s}} - \frac{J_1^c}{J_o^c} \overline{\delta T}_c(s) \right) \right\}$$

$$\overline{\delta Q}_b(s) = X_{o1}^{bc} \overline{\delta Q}_c(s) + \alpha \overline{\delta T}_c(s) \qquad \text{(A8)}$$

and, by means of (A4), (A6) and (A7)

$$\overline{\delta T}_b(s) = \frac{J_o^b}{J_o^c} \overline{\delta T}_c(s)$$

$$+ \left(\frac{N_o^c}{J_o^c} J_o^b - N_o^b \right) \frac{J_o^c}{N_o^c J_1^c - N_1^c J_o^c} \left\{ \frac{\overline{\delta Q}_c(s)}{\sqrt{-\varrho_2 c_2 \varkappa_2 s}} - \frac{J_1^c}{J_o^c} \overline{\delta T}_c(s) \right\}$$

$$\overline{\delta T}_b(s) = \frac{X_{oo}^{bc}}{\sqrt{-\varrho_2 c_2 \varkappa_2 s}} \overline{\delta Q}_c(s) + \beta \overline{\delta T}_c(s) . \qquad \text{(A9)}$$

The Laplace transforms of eqs. (3), (4) and (5) can be written

$$\overline{\delta Q}_a(s) = \frac{r_b}{r_a} \overline{\delta Q}_c(s) \qquad \text{(A10)}$$

$$\overline{\delta T}_a(s) = \overline{\delta T}_b(s) + \eta \overline{\delta Q}_b(s) \qquad \text{(A11)}$$

$$\overline{\delta T}_c(s) = \overline{\delta T}_o(s) + \frac{1}{k} \overline{\delta Q}_c(s) . \qquad \text{(A12)}$$

Now eqs. (A2), (A3), (A8), (A9), (A10), (A11), and (A12) form a system of seven linear equations from which any of the Laplace transforms $\overline{\delta P}(s)$, $\overline{\delta T}_c(s)$, $\overline{\delta T}_f(s)$, $\overline{\delta T}_a(s)$, $\overline{\delta T}_b(s)$, $\overline{\delta T}_c(s)$, $\overline{\delta Q}_a(s)$, $\overline{\delta Q}_b(s)$ and $\overline{\delta Q}_c(s)$ can be determined when two of them are specified.

Next, this system is reduced to a system of two equations involving $\overline{\delta P}(s)$, $\overline{\delta T}_o(s)$, $\overline{\delta T}_f(s)$, and $\overline{\delta Q}_c(s)$:

Eqs. (A8), (A9), (A10), (A11), and (A12) immediately yield

$$\overline{\delta Q}_a(s) = \frac{r_b}{r_a}\left\{ \left(X_{o1}^{bc} + \frac{a}{k}\right) \overline{\delta Q}_c(s) + a\ \overline{\delta T}_o(s) \right\} \tag{A13}$$

$$\overline{\delta T}_a(s) = \left\{\eta\left(X_{o1}^{bc} + \frac{a}{k}\right) + \frac{\beta}{k} + \frac{X_{oo}^{bc}}{\sqrt{-\varrho_2 c_2 \varkappa_2 s}}\right\}\overline{\delta Q}_c(s) + (\eta\ a + \beta)\ \overline{\delta T}_o(s) \quad . \tag{A14}$$

Eqs. (A2), (A13) and (A14) now give

$$\overline{\delta T}_f(s) = \left\{ \left(\eta + \frac{1}{4}\frac{r_b}{\varkappa_1}\overline{Z}(s)\right)\left(X_{o1}^{bc} + \frac{a}{k}\right) + \frac{\beta}{k} + \frac{X_{oo}^{bc}}{\sqrt{-\varrho_2 c_2 \varkappa_2 s}}\right\}\overline{\delta Q}_c(s) \tag{A15}$$

$$+ \left\{ \left(\eta + \frac{1}{4}\frac{r_b}{\varkappa_1}\ \overline{Z}(s)\right) a + \beta \right\}\ \overline{\delta T}_o(s) \quad .$$

Eqs. (A3) and (A13) yield

$$\left(X_{o1}^{bc} + \frac{a}{k}\right)\ \overline{\delta Q}_c(s) = \frac{1}{2}\frac{r_a^2}{r_b}\ \overline{\delta P}(s) - \frac{1}{2}\frac{r_a^2}{r_b}\ \varrho_1 c_1 s\ \overline{\delta T}_f(s) - a\ \overline{\delta T}_o(s) \quad . \tag{A16}$$

Elimination of $\overline{\delta T}_o(s)$ between (A15) and (A16) yields

$$\frac{X_{o1}^{bc}\ \beta - \dfrac{X_{oo}^{bc}}{\sqrt{-\varrho_2 c_2 \varkappa_2 s}}\ a}{\left(\eta + \frac{1}{4}\frac{r_b}{\varkappa_1}\ \overline{Z}(s)\right) a + \beta}\ \overline{\delta Q}_c(s) = \frac{1}{2}\frac{r_a^2}{r_b}\ \overline{\delta P}(s) - \left\{\frac{1}{2}\frac{r_a^2}{r_b}\ \varrho_1 c_1 s \right. \tag{A17}$$

$$+ \left. \frac{a}{\left(\eta + \frac{1}{4}\,\frac{r_b}{w_1}\,\bar{Z}(s)\right)\alpha+\beta} \right\} \overline{\delta T}_f(s) \quad .$$

Eqs. (A15) and (A17) are identical with (8) and (9).

References

1. A. N. Nahavandi and Richard F. von Hollen, A Digital Computer Solution for Space-Dependent Neutron Kinetics Equations. Nucl. Sci. and Eng. 18, 335-350 (1964).

2. O. Kalnæs, H. Neltrup and P. L. Ølgaard, A Recipe for Heavy-Water Lattice Calculations. Risö Report No. 81 (1964).

3. O. Kalnæs, TATAR, Program No. 158 (GIER-Computer Library, Danish Atomic Energy Commission Research Establishment Risö, 1964).

4. R. V. Meghreblian and D. K. Holmes, Reactor Analysis (McGraw-Hill, London, 1960).

5. M. A. Schultz, Control of Nuclear Reactors and Power Plants (McGraw-Hill, London, 1961).

6. M. Ash, Nuclear Reactor Kinetics (McGraw-Hill, London, 1965).

7. N. W. McLachlan, Bessel Functions for Engineers (Clarendon Press, Oxford, 1955).

8. E. Jahnke and F. Emde, Tables of Functions (Dover Publications, New York, 1945).

9. Modesto Iriarte, jr., An Accurate Transfer Function for the Dynamic Analysis of Temperature and Heat Release in Cylindrical Fuel Elements. Nucl. Sci. and Eng. 7, 26-32 (1960).

10. N. Kjær-Pedersen, COMPFIT, Algol-algorithm SA-65. GIER Computer Library, Danish Atomic Energy Commission Research Establishment Risö.

11. N. Kjær-Pedersen, Dynamic Aspects of Boiling-Heavy-Water Nuclear Reactors, Part I. Risö Report No. 128 (1966).